Droplet Microfluidic Approaches for Single-Cell Proteolytic Functional Assay

JING TENGYANG

B. Eng. (Hons.), National University of Singapore

A THESIS SUBMITTED

FOR THE DEGREE OF DOCTOR OF PHILOSOPHY

DEPARTMENT OF BIOMEDICAL ENGINEERING

NATIONAL UNIVERSITY OF SINGAPORE

2016

DECLARATION

I hereby declare that the thesis is my original work and it has been written by me in its entirety. I have duly acknowledged all the sources of information which have been used in the thesis.

This thesis has also not been submitted for any degree in any university previously.

_____

Jing Tengyang

July 2016

ACKNOWLEDGEMENTS

First of all, I would like to thank my main supervisor Prof. Lim Chwee Teck for the wise pointers and advice throughout my pursuit in this research path. He always gave me the freedom to search for creative solutions and allowed me to learn from my numerous mistakes, meanwhile providing insightful suggestions and substantial supports whenever I needed it. More importantly, I am grateful for his trust in me and my PhD work.

I would also like to thank my co-supervisor Prof Jongyoon Han for continuously providing constructive suggestions on technical issues and sharing holistic views on research projects. His strategic vision has encouraged me to move beyond my comfort zone and embrace new knowledges. Besides, his great knowledge and experience has been my vane directing me to impactful research direction.

I also express my gratitude to another co-advisor Dr. Chen Chia-Hung for teaching me all the microfluidic techniques and his supervision through my PhD journey. His great attention on details has trained my analytical skills and logical reasoning.

At Singapore-MIT Alliance for Research and Technology (SMART), I want to appreciate Dr. Khoo Bee Luan, Dr. Majid E. Warkiani, and Dr. Yin Lu for supervising me and offering me helps in different projects. Thanks to their help, my research progress could move forward at a right pace. I am also grateful to other colleagues at SMART for their resourceful supports and great friendships, especially Dr. Balasubramanian, Averil, Aoli, Bena, Evan, Guofeng, Sang, Yan Teck, Yasaman, Zhangxing and Zhen Yang. It was a pleasure to work with such a cheerful group of individuals.

At Singapore Institute for Neurotechnology (SINAPSE), I would like to thank Dr. Ramesh Ramji and Ng Ee Xien for doing experiments together with me in my first two years of PhD. With their company, spending countless nights in the

cold lab did not seem that miserable. Also, I feel grateful to other colleagues, especially Dr. Luo Rongcong and Wang Ming, for their help from time to time

At MechanoBioEngineering Laboratory and Mechanobiology Institute (MBI), I would like thank Kenry and Parthiv for the great friendship and supports both inside and outside lab. I appreciate the necessary fabrication help from Ashraf, Gianluca, Mona and Sree. In addition, I would also like to extend my sincere regards to other colleagues, such as Joo Chuan, Yeong Yuh and Han Wei, for all helpful discussions and valuable suggestions.

In Massachusetts Institute of Technology (MIT), I feel appreciative to all members of Micro/Nanofluidic BioMEMS group for hospitably hosting me during my exchange period. Dr. Wu Lidan, in particular, provided me supervision and guidance over my entire stay and has become a great friend afterwards.

Last but not least, I would like to thank my loved ones for their unconditional love and thorough care throughout my PhD journey. I would like to thank my parents and parents-in-law for encouraging me to pursue my passion on research. Also I would like to thank my wife Zhou Yi for always believing in me and being supportive. She has never given up on me although sometimes I have appeared stubborn, irrational and idiotic. Indeed, it has been a long journey and I am extremely thankful for all support.

With regards, I sincerely acknowledge National University of Singapore and Singapore-MIT Alliance for Research and Technology for providing me the prestigious scholarship for my PhD study and the funding for my research work.

LIST OF PUBLICATIONS AND PRESENTATIONS

Journal Publications:

1. T. Jing, Z. Lai, L. Wu, J. Han, C. T. Lim, & C. Chen, Single cell analysis of leukocyte protease activity using integrated continuous-flow microfluidics. *Analytical Chemistry, In press* (2016)

2. B. L. Khoo, G. Grenci, T. Jing, Y. B. Lim, S. C. Lee, J. P. Thiery, J. Han & C. T. Lim, Liquid biopsy and therapeutic response: circulating tumor cell cultures for evaluation of anti-cancer treatment. *Science Advances*, **2** (7) (2016)

3. P. K. Chaudhuri, M. E. Warkiani, T. Jing, Kenry & C. T. Lim, Microfluidics for Research and Applications in Oncology. *Analyst*, **141**, 504-524 (2016)

4. T. Jing, R. Ramji, M. E. Warkiani, J. Han, C. T. Lim & C. Chen, Jetting microfluidics with size-sorting capability for single-cell protease detection. *Biosensors and Bioelectronics*, **66**, 19-23 (2015)

Conference Presentations:

1. T. Jing *et al*, High-throughput single cell protease analysis on human circulating tumor cells, 19th International Conference on Miniaturized System for Chemistry and Life Sciences (MicroTAS), Korea (2015), (Poster)

2. T. Jing *et al*, An integrated microfluidics device for single cell encapsulation and cellular enzymatic assay, 15th International Conference on Biomedical Engineering (ICBME), Singapore (2013), (Oral)

3. T. Jing *et al*, High throughput single cancer cell encapsulation and self-sorting for protease assay by using jetting microfluidics, 17th International Conference on Miniaturized System for Chemistry and Life Sciences (MicroTAS), Germany (2013), (Poster)

TABLE OF CONTENTS

ABSTRACT

Every cell has its distinct phenotype, behavior and function. However, conventional biological analytical assays, such as western blot and enzyme-linked immunosorbent assay, adopt ensemble measurements to extract the average information from non-homogeneous cell populations without taking into account the critical details of individual cells. Such simplistic methods could generate misleading results from highly heterogeneous cells, like cancer and immune cells. In order to accurately and effectively study functional heterogeneity of single cancer and immune cells, we developed a series of microfluidic droplet platforms. We first developed a novel and label-free droplet system to enhance single-cell encapsulation efficiency by incorporating jetting and size-based sorting. The device consistently achieved above 70% single-cell efficiency for a wide range of input cell concentrations, which broke the Poisson prediction on random encapsulation process. Next, we applied the droplet microfluidics to study single-cell matrix metalloproteinase activity of various breast cancer cell lines and patient-derived circulating tumor cells. It was discovered that the proteolytic activity level was positively correlated with invasiveness and metastatic potential of cultured cell lines. The assay results of in-vitro cultured circulating tumor cells revealed great cellular heterogeneity, reflecting diverse treatment responses on patients undergoing the same type of treatment. Lastly, we developed a new droplet microfluidic system to study

matrix metalloproteinase of single leukocytes with solving the pre-encapsulation contamination issue, which was a serious problem for single leukocyte study. By integrating a cell washing channel in front of a droplet generator, we successfully suppressed the background signals of empty droplets and accurately detected the proteolytic activity of individual leukocytes under naïve and drug-treated conditions. Overall, we managed to use droplet microfluidics to probe the proteolytic activity of cancer and immune cells at the single-cell level. The acquired proteolytic profile could facilitate diagnosis of diseases, surveillance of drug responses and development of treatment strategies. The droplet technology holds a great potential in personalized medicine to provide point-of-care in various healthcare applications.

LIST OF FIGURES

LIST OF TABLES

LIST OF ACRONYMS

a.u.: Arbitrary Unit

AFM: Atomic Force Microscopy

CSC: Cancer Stem Cell

CTC: Circulating Tumor Cell

CK: Cytokeratin

DEP: Dielectrophoresis

DLD: Deterministic Lateral Displacement

DNA: Deoxyribonucleic Acid

DRIE: Deep Reactive Ion Etching

ECM: Extra Cellular Matrix

ELISA: Enzyme-Linked Immunosorbent Assay

EMT: Epithelial-to-mesenchymal Transition

FACS: Fluorescence Activated Cell Sorting

FBS: Fetal Bovine Serum

FSC: Forward Scattering Light

FITC: Fluorescein Isothiocyanate

FRET: Fluorescent Resonance Energy Transfer

IPA: Isopropyl alcohol

LOC: Lab on a Chip

MMP: Matrix Metalloproteinase

PBS: Phosphate Buffer Saline (solution)

PCR: Polymerase Chain Reaction

PDMS: Polydimethylsiloxane

PMA: Phorbol 12-Myristate 13-Acetate

PFF: Pinch Flow Fractionation

PI: Propidium Iodide

OT: Optical Tweezer

RBC: Red Blood Cell

SAW: Surface Acoustic Wave

SCA: Single-Cell Analysis

SSC: Side Scattering Light

WBC: White Blood Cells

2D: Two Dimensional

mL: milliliter

µL: microliter

nL: nanoliter

pL: picoliter

CHAPTER 1. Introduction

1.1 Overview

Nature has never been known to make any exact duplicates. Gottfried Wilhelm Leibniz, a German philosopher and mathematician, stated any two distinct things cannot have all their properties in common. In the Principle of Identity of Indiscernibles, he suggested that if two entities are alike in every aspect, they are essentially the same object. Leibniz elaborated on this rule using leaves, claiming there are no two leaves exactly alike.

Likewise, the same principle also applies to the fundamental building blocks of our body – cells. No two cells are exactly identical. Each cell has its distinct phenotype, behavior and function even when compared to other cells from the same lineage or sharing the same gene. The collaborative efforts of different cells contribute to a comprehensive list of tissue functions and help to maintain the healthy status of the human body.

Researchers today are increasingly aware of the importance of heterogeneity in cell samples, especially for clinical applications. Heterogeneous diseased cells are difficult to be specifically targeted all at once by a single drug. Furthermore, heterogeneous drug responses make treatment efficacy vary dramatically across different patients. Research in characterizing cellular heterogeneity allows a better understanding of disease status, leading towards more reliable diagnostics and accurate therapeutics.

Despite the importance of cellular heterogeneity, technological limitations restrict conventional biological assays to adopt the simplistic method of extracting averaged properties from non-homogeneous cell populations. Thousands, if not millions, of cells are studied together in an ensemble manner using tools such as western blot and enzyme-linked immunosorbent assay (ELISA). For many decades, life scientists have acquired significant biological knowledge relying on such technology by studying seemingly identical cells.

Genetic patterns and protein expression can explain cellular behavior to a large extent based on assaying a population of cells. However, the ensemble characteristics of a cell population may not represent the characteristics of any individual cell, especially for highly heterogeneous cell types such as cancer and immune cells. These cells usually have a diverse composition with many subpopulations present together.

In order to study cellular heterogeneity, new technology must be developed to study the behavior of individual cells by isolating them from complex multi-cellular organisms. This newly-established research area is known as single cell analysis (SCA). Indeed, some single-cell analysis methods have been readily available in the market. However, their functionality, throughput and cost-effectiveness are still largely constrained by various technological limitations.

Due to the recent advancement of microfabrication technology, many microfluidic devices, also known as lab-on-a-chip (LOC), have been developed to perform various biological assays at micro-meter scale. Microfluidics has

gained unique research interest in single-cell analysis because it requires small volume of sample and reagent (usually in micro-liter (μL) scale), reduces process and response time, and increases assay sensitivity as well as accuracy. The essential approach adopted in microfluidic single-cell analysis is to create cell compartments to isolate individual cells so that assays at single-cell resolution can be achieved. Till now, many of the single-cell microfluidic approaches have been developed using four main compartmentalization techniques: hydrodynamic trap, microwell, valve-assisted microchamber, and droplet system.

Compared with various single-cell microfluidic technologies, the droplet-based system is fit for study of metabolism and biomolecule secretion at single-cell level. This method suspends cells in water-in-oil emulsions, effectively preventing contamination across droplets. Cells trapped in droplets are completely isolated from other cells and ambient environment. Meanwhile, the metabolites and biomolecules produced by cells are confined within pico-liter-volume droplets and can accumulate to high concentrations for downstream analysis. It is hence evident that droplet-based technology holds a great potential to study functional heterogeneity of cell samples, particularly minute amounts of clinical samples.

This PhD project aims to explore how to accurately and effectively perform droplet-based single-cell functional analysis on proteolytic activity, especially matrix metalloproteinase (MMP) activity. Proteolytic activity of cells plays a

significant role in cell migration, tissue remodeling and immune response [1, 2]. It has broad clinical implications in fetal development, wound healing, cancers, inflammation, etc. A series of droplet-based microfluidic devices have been developed and exploited to probe cell-to-cell variation of single-cell proteolytic activity (e.g. matrix metalloproteinases activity). The assay targets of this entire PhD work include cultured cancer cell lines, patient-derived cultured circulating tumor cells (CTCs) and freshly-retrieved white blood cells (WBCs). The obtained single-cell proteolytic information could be helpful in evaluating proteolytic heterogeneity of cell populations and contribute to disease diagnosis and surveillance. With further development on throughput and detection sensitivity, the droplet-based single-cell assay technique could become a versatile and powerful tool to examine primary patients' samples and provide critical information on proteolytic and other cellular functions at the single-cell level. I believe this technique would play a great role in personalized medicine as well as fundamental life science research in a short future.

1.2 The motivation and hypothesis

We would like to apply droplet-based microfluidics to perform proteolytic functional study on living single cancer cells and leukocytes. New functions would be built on top of the existing technology in order to resolve some current technological limitations: 1) low single-cell encapsulation rate and 2) high pre-encapsulation contamination. Additionally, patient-derived cancer cell samples

would be investigated using droplet microfluidics as a proof-of-concept for clinical application.

With this aim in mind, we focus on verifying three hypotheses in the PhD dissertation:

Hypothesis 1: size-based droplet sorting can be utilized to enhance single-cell encapsulation rate for samples with low cell concentration.

> We will apply jetting technique to create a size difference between empty and cell-containing droplets before using size-based sorting to remove empty ones.

Hypothesis 2: droplet-based single-cell assay could be used to detect matrix metalloproteinase (MMP) activity of cultured cancer cell lines and cultured circulating tumor cells (CTCs), which could be correlated to metastatic potential.

> We will first develop an in-vitro CTC culture device and then encapsulate the cultured CTCs obtained from different patients into droplets to perform single-cell functional MMP assay.

Hypothesis 3: cell washing can be implemented before cell encapsulation to purify target cells from soluble contaminants that are secreted by the target cells prior to the assay, resulting in more accurate downstream analysis.

> We will adopt size-based sorting design to achieve cell purification under laminar flows. Subsequently, the washing function will be integrated with a droplet generator to encapsulate each purified cell into

a droplet for downstream MMP analysis.

1.3 Scope of work

The scope of the dissertation is confined to the use of droplet microfluidic system to perform single-cell proteolytic analysis. The proteolytic activity of human cells will be studied using the developed droplet platforms as suggested in the hypothesis. The measured activity at single-cell level will provide important insights of cellular heterogeneity which in turn aids in accurate cell behavior evaluation and precise personalized medicine. Both cancer cells and leukocytes will be used in the project to prove the concept and application for medical diagnostics.

1.4 Summary of chapters

Following this introduction is a chapter on literature review. It first gives an overview of cellular heterogeneity, including the cause and significance. Recent research on both cancer and immune heterogeneity, the two foci of this dissertation, is then summarized. Based on the clinical implications of cancer and immune heterogeneity, the importance of performing single-cell analysis (SCA) on cancerous cells and immune cells is highlighted. Conventional macro-scale single-cell analysis technologies, including their working principles and inescapable limitations, are briefly discussed. Subsequently, various

microfluidic single-cell technologies will be discussed to provide a comprehensive review on this emerging research area. Eventually, we would elaborate the reasons why we have selected droplet technology to fulfill the task of single-cell functional analysis.

Chapter 3 next focuses on how to increase single-cell encapsulation efficiency using passive droplet sorting. We created size difference between cell-containing droplets and empty droplets using jetting. Empty droplets were next separated out in the deterministic lateral displacement (DLD) isolation array for effective downstream analysis. As passive size-based sorting was implemented, no external power source was necessary to conduct the sorting function. More importantly, original cell status was preserved since no immunochemical labeling was required in this system. The enrichment performance on single-cell encapsulation efficiency was independent of input cell concentration, which is largely favorable for clinical applications because clinical samples are usually low in cell count. The droplet device was applied to study proteolytic function of cultured cancer cell lines and conduct single-cell drug screening.

However, the first-generation of droplet device still had some drawbacks to perform accurate functional assay on rare patient-derived samples. Therefore, in chapter 4 in-vitro CTC culture was utilized to expand the cell population to a desirable level for droplet-based assay. Several breast epithelial cell lines, originated from breast cancerous and healthy tissues, were analyzed using droplet technology. The proteolytic activity acquired from single breast cells

revealed that metastatic cancer cells had a more intensive proteolytic activity profile than non-invasive cancer cells and healthy epithelial cells. Next, cultured CTCs derived from breast cancer patients and lung cancer patients were carefully studied in the functional assay, revealing the huge heterogeneity in the cultured CTC samples.

When studying cultured CTC samples, we always found some leukocytes present with cultured CTCs and they had similar proteolytic activity levels. Therefore, in chapter 5 we conducted a comprehensive MMP study on single leukocytes. Unlike cancer cells, leukocytes are highly active in protease production due to their duty in immune defense. Consequently, direct assay on leukocytes encountered a big challenge on pre-encapsulation contamination. To solve this problem, we developed a cell-washing channel to purify target cells before they were encapsulated into droplets. By incorporating the on-chip washing function with droplet generator, clean signals of single leukocytes were successfully detected from droplets. Excellent signal-to-noise ratio enabled rigorous functional study on single leukocytes under naïve and PMA (phorbol 12-myristate 13-acetate)-mediated status. The results indicated that PMA treatment not only elevated the protease production but also stimulated the cell-to-cell variance.

Lastly, a summary of this dissertation is provided in the final chapter together with the outlook of future development. The outcomes of this dissertation have been presented in international and domestic conferences in the field of

microfluidic technology. Some of the chapters have also been published in or submitted to recognized peer-reviewed journals.

Chapter 2. Literature review

2.1 Cellular heterogeneity and need for single-cell analysis

Cellular heterogeneity describes the fact that any two cells can own distinct morphological and phenotypic profiles. People used to think isogenic cells that have uniform genetic make-up, such as cell lines, are identical in all aspects. However, after decades of probing and analyzing the behaviors of single cells, substantial evidences have shown that considerable heterogeneity can exist even within isogenic cell populations [3-5]. For example, monozygotic twins that stem from one split zygote still have some distinct features.

What is the reason for the occurrence of cell-to-cell difference within the same cell type? First of all, cell cycle can contribute to the cellular heterogeneity in many ways. Cell morphology, metabolism and protein expression of the same type of cell vary at different stages of cell cycle [6, 7]. For instance, the expression of proteins, implicated in cell cycle regulation and DNA replication, relatively increases at interphase stages in contrast to G_0 stage [8]. Apart from cell cycle, genetic drift can also increase the heterogeneity within a cell population [9]. When a cell is proliferating, variations in gene replication can occur randomly, which lead to a different daughter cell. This process is known as mutation. Furthermore, epigenetic modifications that functionally change

gene expression via DNA methylation and histone modification can lead to different phenotypes of cells that share the same DNA sequence [10].

Although phenotypic differences among cells are always present at a fine-enough resolution of investigation, population-averaging assays are still predominant tools in biology. This is because the average behavior of a cell population may be summarized by a mean value, revealing important biological information of all cells within the same cell type. Cell-to-cell differences in some cases may not have any functional significance, for example those due to biochemical noise or environment fluctuation [11, 12].

However, cell-to-cell differences can have functional consequences as observed in the random development of antibiotic resistance in the same strain of bacteria [13]. Subpopulation of stem-like cells was recently identified from human breast cancer cell lines to give rise to phenotypically diverse progeny and survive through a course of chemotherapy [14]. Therefore, models derived from a population average may yield misleading results because ensemble measurement does not account for critical details of individual cells as shown in figure 2.1.

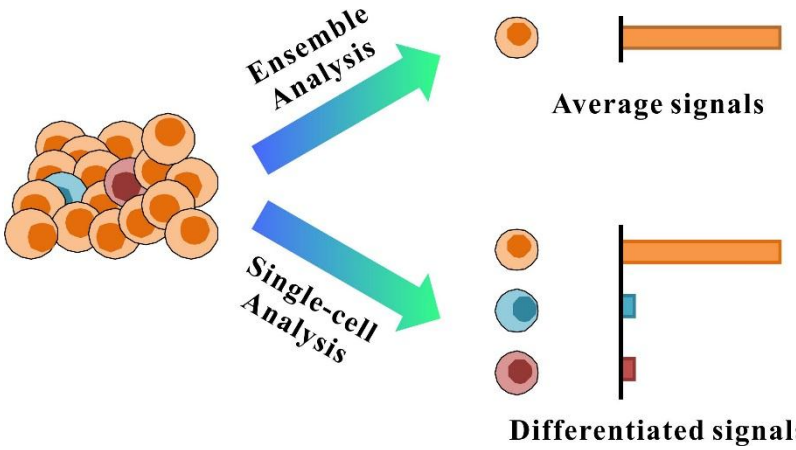

Figure 2.1 Comparison between ensemble analysis and single-cell analysis on a heterogeneous cell population. Ensemble analysis generates average signal based on the predominant cell population. However, single-cell analysis reveals precious details of minor cell subpopulations.

Capturing functional details of individual cells becomes increasingly critical in clinical applications. Unlike cultured cell lines, clinical samples are not homogeneous, consisting of multiple subpopulations. Mixed cell populations greatly increase cellular heterogeneity and cannot be accurately represented by population averages. The cell-to-cell variation is one of the keys to answer previously irresolvable questions in cancer research, stem cell biology, immunology, developmental biology, and neurology [15-17]. In order to acquire the details of cell-to-cell difference, single-cell analysis technology is essential to enable scientists to look at the world beneath population averages of seemingly identical cells.

2.2 Cancer and its heterogeneity

Cancer is one of the world's deadliest human diseases. This disease stems from

cell lesions that enable abnormal cell growth with the potential to spread to distant organs in the body. Cancer has created huge economic and healthcare burdens to the society. In 2012, there were 14.1 million new cases of cancer and 8.2 million deaths from cancer in the world [18]. The incidence rate is about 185 new cancer cases for every 100,000 people and the mortality rate is about 105 cancer death for every 100,000 cancer patients [19].The number of cancer-related deaths is now increasing at a rapid rate due to the extended life expectancy of our aging population, unhealthy lifestyles and obesity [20].

Normal cells always run through an orderly process of growth and proliferation. When they grow old or become damaged, they undergo apoptosis and new cells take their place. Certain mutations in cells may lead to the upregulation of oncogene or downregulation of tumor suppressor gene. Consequently, old or damaged cells are able to escape from programmed death by growing and dividing uncontrollably, eventually forming a cancerous tissue also known as a tumor.

Cancer presents significant heterogeneity both between tumors (inter-tumor heterogeneity) and within tumors (intra-tumor heterogeneity) [21]. Cancer occurring at the same organ differs among patients with distinct mutations. Cancer cells within one tumor site show different phenotypic characteristics due to different microenvironment influence and accumulation of different mutations as shown in Figure 2.2.

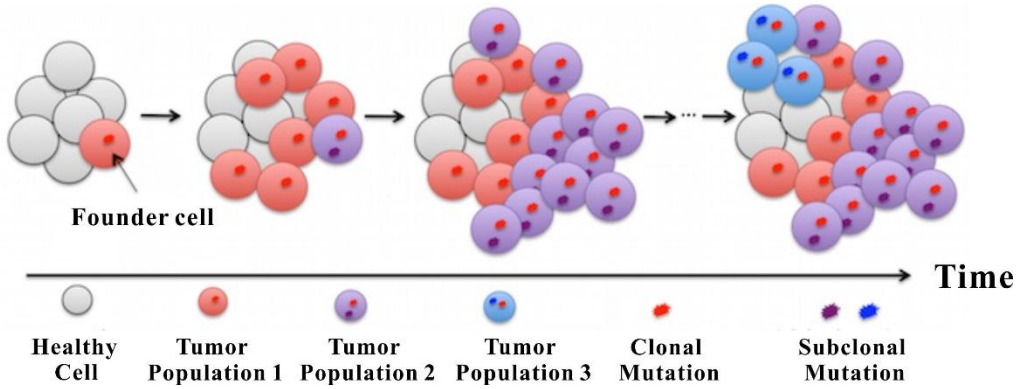

Figure 2.2 Illustration of the development of intra-tumor heterogeneity. Subclonal tumor cell populations carry diverse mutations that might be different from the initial tumor cell population. (Adopted from Layla Oesper's website from Carleton College)

As tumor cells proliferate, their DNA tends to accumulate more mutations. Some of the mutations enhance the invasiveness of tumor cells and turn benign tumors to malignant. Such mutations enable cancerous cells to break off from the primary tumor site and spread into distant tissues to form secondary tumors. The dissemination of malignant tumor cells is known as cancer metastasis [22]. These self-renewal tumorigenic cells leading to metastasis is known as cancer stem cells (CSCs) [23].

Many therapeutic methods have been developed to stop cancer cells from growing and metastasizing to other organs. However, the heterogeneity of tumor cells imposes significant challenges in finding effective treatment approaches. When treated with cancer drugs, some resilient tumor cells can develop bypass mechanism to counter the inhibitory effect of the drug, resulting in treatment failure and cancer relapse [24].

Research into investigating and characterizing tumor heterogeneity can provide

a better understanding of disease status. In turn, the knowledge of cancer heterogeneity can guide the creation of diagnosis and treatment strategies with better accuracy and higher efficacy. In order to effectively analyze tumor heterogeneity, the resolution of biological assay must be improved to single-cell level to differentiate the cell-to-cell variation and identify the aggressive subpopulation of cancer cells from other non-tumorigenic cells.

2.3 Leukocyte and its heterogeneity

Apart from cancer cells, leukocytes, also known as white blood cells, are also highly heterogeneous and clinically important. Leukocytes are one of the hematological cells that circulate throughout the human body. Unlike the other two hematological cells, erythrocytes (red blood cells) and platelets, all leukocytes have nuclei. The normal concentration range of leukocytes is 5 to 10 million per milliliter of blood. They make up approximately 1% of the total blood volume in a healthy adult, substantially less than erythrocytes at 40 to 45%. The size of a leukocyte varies from 10 to 30 μm.

Leukocytes can be divided into different classes including neutrophils, eosinophils, basophils, lymphocytes and monocytes based on their morphological and functional characteristics (figure 2.3). Additionally, neutrophils, eosinophils and basophils are grouped as granulocytes because of the presence of granules and lobed nuclei. Among all subclasses, neutrophils are the most abundant cells accounting for approximately 60% of the total

leukocytes, followed by lymphocytes at approximately 30%.

Leukocytes are the cells of the immune system that are involved in protecting body against invaders such as bacteria and virus. As the frontline of immune defense, leukocytes play multiple roles in immune response and host protection. Neutrophils primarily defend against bacterial and fungal infection as the first responder in the innate immune system. Eosinophils mainly fight against parasitic infections while basophils are predominantly responsible for allergic response. T and B lymphocytes play key roles in the adaptive immune system. Last but not least, monocytes chiefly eliminate debris and pathogens.

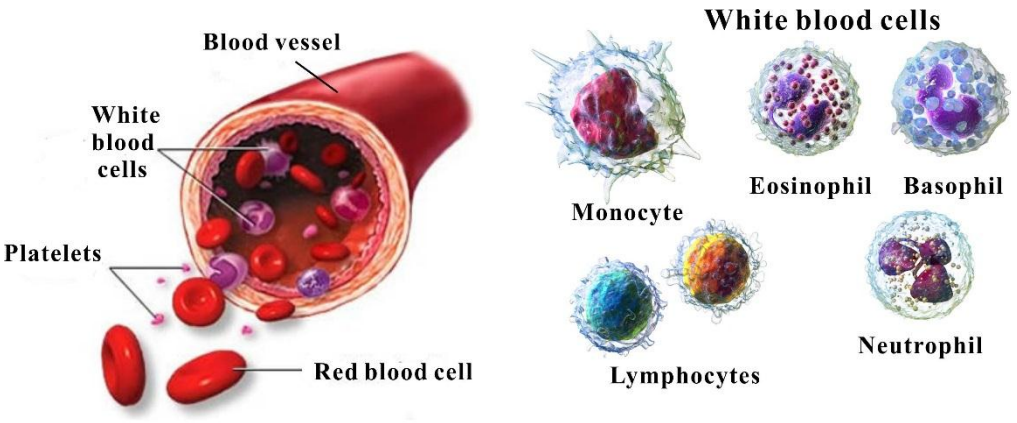

Figure 2.3 (Left) Illustration of blood composition. Hematological cells include red blood cells, white blood cells and platelets. (Right) Subpopulations of white blood cells based on their different morphologies and functionalities (adopted from Wikipedia).

Without doubt, cellular heterogeneity is present among various subtypes of leukocytes. Different subgroups of leukocytes have been associated with inflammatory response, autoimmune disease and cancer progression [25-27]. Functional heterogeneity has also been observed within the same subtype of

leukocytes. Differential priming effects of pro-inflammatory cytokines on neutrophil were detected in response to bacterial N-formyl peptide [28]. Varied oxidative responses of subpopulation of neutrophils were demonstrated between healthy subjects and patients with rheumatoid arthritis [29]. More recently, different pro- and anti-inflammatory roles of leukocyte subsets were investigated in models of tumor microenvironment [30].

Characterization of individual leukocyte secretion profiles, such as the protease profile, is important to reveal the functionality of the immune system and provide insights into personal physiological conditions for precision medicine. For example, protease MMP-8 produced by neutrophils has been shown to promote leukocyte recruitment to fight against bacteria in sepsis [31]. Protease MMP-9 from leukocytes has been found to facilitate basal membrane degradation and promote cancer development [32]. Moreover, several autoimmune diseases such as asthma and rheumatoid arthritis, have been associated with abnormal protease secretion [33, 34].

Diverse functionalities of leukocytes suggest different treatment strategies must be developed in order to optimize immune response and enhance drug efficacy [35]. Therefore, single-cell analysis technology is in a great demand to probe the cell-to-cell variance in term of heterogeneous leukocyte functionalities for battling against both acute and chronic diseases.

2.4 Conventional methods for single-cell analysis

As the awareness of biological significance of cellular heterogeneity increases, the need of single-cell analytical methods becomes urgent. The easiest method of doing single-cell assay is to pipette single cells into a microwell plate (e.g. 96 well plate) with proper dilution. In this way, single cells are spatially confined into individual wells and ready for any downstream analysis. However, this technique has many practical issues including uncontrollable single cell dispersion and limited detection sensitivity due to dilution.

To realize experiments at the single-cell level, many analytical technologies have been developed to manipulate and analyze one cell at a time. Some force cells to pass through a narrow channel so that single-cell observation resolution can be achieved. Others miniaturize the manipulation tools to micrometer scale so that they can directly handle single cells. Here, we classify these conventional macro-scale technologies into two groups according to the cell properties to be measured, namely biochemical and biophysical analytical methods.

2.4.1 Biochemical single-cell analytical method

Flow cytometry, first invented in 1953, is one of the most popular single-cell analytical tools that has been routinely used in the diagnosis of blood disorders and fundamental biological research [36]. The flow cytometer mainly measures the expression of biochemical markers on the surface of individual cells (figure 2.4(A)). It consists of a cell dispersion module and a light detection module.

Before loading into the flow cytometer, the cell sample is immunochemically stained with antibodies conjugated with different fluorophores. The labeled cell sample passes into a narrow cell dispersion channel together with sheath flow, which allows only one cell to pass through the detection point at one time. Based on the fluorescence intensity detected by photo sensors, the expression level of certain surface biomarkers can be analyzed quantitatively.

The measured expression results can assist in identifying unknown cells, discovering new biomarkers for specific cell types and correlating with phenotypic characteristics. For example, researchers identified CD44+/CD24-/Lin- breast cancer cells to have significantly improved tumor forming ability in NOD/SCID mice compared with CD44+/CD24+/Lin- cells [37] using flow cytometry. Moreover, using the same tool, a subset of neutrophils with CD11c+/CD62L-/CD11b+/CD16+ expression was reported to have the ability to inhibit T cell response to macrophage integrin MAC-1 in systemic inflammation [38].

Although flow cytometry is a high-throughput technique to monitor multiple characteristics of single cells spontaneously, its major limitations include 1) poor cell viability, 2) limited detection targets due to overlapped fluorescent spectrum, 3) high equipment and maintenance cost due to complicated system design, and 4) incapability of acquiring functional information and monitoring cell behaviors, apart from surface marker expression.

Mass spectrometry is another powerful analytical technique to analyze biomolecules that can be applied for single-cell analysis. Unlike flow cytometry measuring optic signals, a mass spectrometer measures the mass-to-charge ratio of ionized biochemical species such as proteins and peptides (figure 2.4(B)) [39]. Since different biomolecules possess distinct mass-to-charge signatures, the abundance of target molecules present in the sample can be quantitatively determined. Usually, mass spectrometry is used to analyze biological specimen obtained from a population of cells, for instance the lysate from a group of cells.

With appropriate modifications, a mass spectrometer can also be used to analyze protein expression and metabolism at single cell level. Nemes's group has demonstrated that single-cell electrophoresis-electrospray ionization mass spectrometry can be used to identify 40 metabolites from single embryonic cells [40]. The differential concentration of some metabolites leads to different tissue fate in the embryonic development revealing the metabolome affects cell phenotypes in the embryo [40]. In another study, live single cell mass spectrometry has been reported for the analysis of large numbers metabolites to disclose dynamic molecular mechanisms [41]. A high resolution mass spectrometer was even able to measure 20ng of protein content in single embryonic cells [42].

Mass spectrometry is a powerful analytical technique with high detection resolution on small volume of sample, but it has limited applications beyond

basic research. The main constraints include 1) complicated system with high cost, 2) low throughput due to purification process such as liquid chromatography and electrophoresis, and 3) incapability of recovering cell due to cell destruction during the sampling process.

Apart from using flow cytometry and mass spectrometry separately, researchers can also combine both techniques to develop mass cytometry with improved single-cell analysis function. The limitation on fluorescent spectrum can be overcome by replacing the fluorescent labeling with isotope labeled antibodies. The number of distinguishable labels can be increased beyond 30 which means more than 30 kinds of biomolecules can be monitored at one time, far more than normal cytometry [43]. This combined technique has been implemented on bone marrow and cancer studies with superior resolution [44, 45].

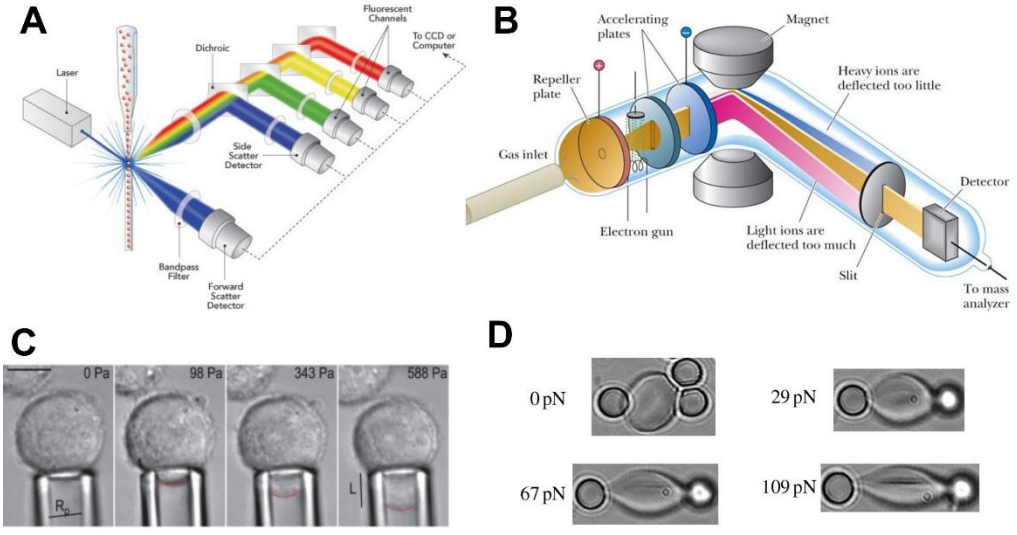

Figure 2.4 (A) Scheme of flow cytometry where single cells are detected based on their light scattering signals and fluorescent labelling (adopted from Semrock website) (B) Scheme of mass spectrometry to study proteins and metabolites produced by single cells (adopted from slideplayer.com). (C) A series of images showing micropipette aspiration of a cancer cell to study cell stiffness [46]. (D) A series of images showing single RBC stiffness measurement using optical

tweezers [47].

2.4.2 Biophysical single-cell analytical method

Biophysical, or biomechanical, property of cells often refers to cell stiffness and is mainly attributed by actin filament and cytoskeleton [48]. The biophysical characteristics of cells have drawn research attention in the recent years because many studies suggested the stiffness of cells has significant implications in physiological and pathological conditions. Softer breast cancer cells are deemed to be more invasive as they can remodel their morphology and squeeze through tissue membrane and blood vessels easily [49]. Therefore, many techniques have been developed to specifically study biophysical properties at single-cell level. The common ones include micropipette aspiration, atomic force microscopy (AFM) and optical tweezers (OT).

Micropipette aspiration is an analytical method to study mechanical properties of single cells in which the surface of a cell is aspirated into a small glass tube while the deformation of the cell surface is monitored (figure 2.4(C)) [46]. Based on the membrane deformation, single cell stiffness could be derived using Law of Laplace. Scientists have used micropipette aspiration technique to study the correlation between cancer cell stiffness and invasiveness [50].

Atomic force microscopy (AFM) is a versatile scanning probe microscopic technique with nanometer scale resolution. AFM has a spring-like cantilever with fine tip fixed to its free end. A beam of laser shines at the back the cantilever

and a photo detector records its reflection, indirectly monitoring the motion of the cantilever. By touching the sample surface, topographic image of the sample surface can be acquired [51]. Apart from imaging, AFM can also be used to perform force measurements. In force measurements, a spherical bead is usually attached at the AFM tip to indent cells [52]. The local stiffness of a single cell at various cell locations (i.e. near nucleus) can be quantified by measuring the indentation depth and force exerted on the cantilever.

Optical tweezers (OT) is another scientific instrument to manipulate single biological cells and perform biophysical characterizations. Unlike micropipette and AFM, OT applies non-contact force for cell manipulation by creating an optical gradient trap [53]. In biophysical characterization, silica beads are attached to the target cells. The single-cell stiffness can be induced by exerting different optical force to stretch the cell and measuring the cell elongation (figure 2.4(D)) [47].

The conventional analytical techniques for single-cell biophysical assay are dedicated to study basic cellular biology and have limited applications at current stage. This is mainly because the equipment for single-cell biophysical study is bulky and expensive. Furthermore, the current assay time for one single cell can reach up to one hour. The single-cell detection process still needs be improved in order to achieve high throughput operation.

Overall, the macro-scale conventional single-cell techniques play a big part in basic biological research to examine certain properties of cells, such as surface marker expression and stiffness. However, their clinical application has been constrained by high system cost, low assay throughput, low detection sensitivity and high sample consumption. There is a tremendous need of simple but versatile tool probing functional difference on the basis of single cells. Microfluidic single-cell analytic techniques have emerged to meet this need.

2.5 Microfluidic methods for single-cell analysis

The rapid development of microfluidics has enabled accurate and high-throughput single-cell analysis. Unlike conventional macro-scale techniques that rely on sophisticated equipment to manipulate individual cells one at a time, most of the microfluidic platforms aim to create parallelized micro-scale cell compartment to facilitate single-cell biological assays. Cells are isolated from each other so that the behavior of individual cells can be monitored and studied separately, which is impossible for ensemble measurements [54]. The resolution and sensitivity of microfluidic single-cell assay are also dramatically enhanced as unnecessary dilution of target molecules and contamination across different cells are prevented. Additionally, miniaturization of single-cell compartment systems largely reduces reagent consumption and sample requirement without comprising the assay accuracy, thus cutting the cost of single-cell analysis.

To date, a lot of microfluidic designs have been developed for various

downstream single-cell analysis using four main compartmentalization techniques: hydrodynamic trap, microwell, microchamber, and droplet encapsulation. Here, the working principles of these techniques are explained together with their advantages and disadvantages.

2.5.1 Hydrodynamic trap

Hydrodynamic trap, one of the earliest microfluidic designs, uses barriers to capture single cells suspended in fluid. Cells are brought to microfluidic traps by flow. Once a trap site is occupied by a cell, new incoming cells will have to bypass the occupied trap and be captured by following empty traps as shown in Figure 2.5(A). As cells are trapped at different positions, single-cell phenotype and behavior can be easily monitored. Di Carlo developed a trap device to capture single HeLa cells and observe how these cells proliferated and divided [55]. Kobel and his coworkers designed a microfluidic chip that comprised of 2048 single-cell traps to study non-adherent stem cells [56]. The trap dimension and shape could be easily customized for different assay purposes. For example, Lee and Liu designed an array of single-cell traps with 8 μm openings. They used this device to study single cell stiffness, mimicking micropipette aspiration, but in a high-throughput manner [57]. Voldman's group has used a U-shaped trap to create two-cell pairs and observe lymphocyte interactions at single-cell level [58].

Hence, hydrodynamic trap is a simple technique to obtain spatially isolated

single cells for single-cell long-term culture and other applications. However, comprehensive biochemical single-cell assay cannot be achieved using simple trap design. This is because cells at neighboring capture sites are still not completely isolated from each other. Biomolecules produced from one cell can diffuse to neighboring cells in the trap chamber. Consequently, precise biochemical assays, such as measuring single-cell secretion and metabolism, is difficult to achieve in a hydrodynamic trap system.

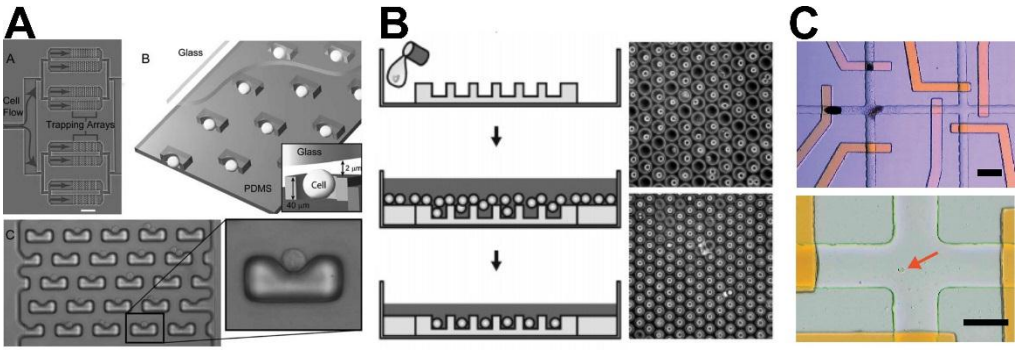

Figure 2.5 (A) Device schematics of hydrodynamic trap for single-cell capture with an enlarged image showing single cell sitting at the center of a capture site [55]. (B) Illustration of operation of microwell-based single-cell device with two phase-contrast images showing cells falling in microwell matrix [59]. (C) (Above) image of valve-based microchamber device where yellow channels control the on-off of the beneath cell channel. (Below) image of a cell trapped in the enclosed microchamber [60].

2.5.2 Microwell

Microwell devices are similar to the commonly-used 96 well plate but with nanoliter well volume. Cells are first seeded on top of the microwell before they enter individual wells by gravitational sedimentation or centrifugation. Cells that fail to enter microwells are washed away and only single cells falling in the

microwells are used for subsequent analysis as shown in figure 2.5(B) [59]. The probability of capturing a single cell in microwell depends on the microwell size. Rettig and Folch demonstrated the single-cell capture rate of microwell device ranged from 92.2% for 20 μm (well diameter) design to 25% for 35 μm design using fibroblast cells [59]. High-throughput quantitative analysis on single yeast response to mating pheromone was conducted on a microwell device on real-time and time-lapse basis [61]. Compared with hydrodynamic trap, the microwell design provides better spatial confinement for cells. Therefore, microwell device has improved assay accuracy and operation reliability.

Nevertheless, microwell device does not provide a completely isolated environment for single cells. Cell solution still flows above the microwell structure to provide nutrients and remove metabolic waste for better long-term survival. As a result, cells in neighboring wells can still "contaminate" each other via diffusion of biomolecules, hindering the acquisition of a pure signal from a single cell. In order to improve on the single-cell isolation, a lid membrane can be added on top of the microwell device. After cells enter microwells, the membrane can be pushed against the microwell layer to close every microwell. Wu and her colleagues deployed this design to study enzymatic activity of single cancer cells in microwells under drug treatments [62]. However, adding the membrane layer could complicate system design and operation. Besides, the pressure inside microwells would increase when closing the lid membrane. The effect of high pressure on single-cell behaviors is still

unknown.

2.5.3 Valve-assisted microchamber technique

Rather than closing the entire microwells with a large lid, better control can be achieved in valve-assisted microchamber system. A microchamber device consists of multiple layers of channel structures. Gas control channels lie above sample channels with a thin membrane in between of them. By controlling the pressure in gas channel, the membrane can be locally deformed to open/close the sample channel, similar to the "on/off" function of a switch as shown in figure 2.5(C) [60]. Precise fluid control can be achieved with the help of gas valves. Therefore, complex biological assays such as single-cell PCR and DNA sequencing can be performed using the microchamber system. For example, Quake's group used an integrated microchamber technique to conduct single-cell gene expression analysis (i.e. RT-PCR analysis) with off-chip electrophoresis analysis [63]. A similar design was also used to study gene expression of single human embryonic stem cells [64]. Fluidigm, the famous microfluidic company founded by Quake, commercialized this valve-assisted microchamber to perform single-cell genetic studies. Microchamber systems can be scaled up to perform high-throughput single cell genetic expression analysis. Hansen's group developed a microchamber system that could perform 300 parallel RT-qPCR assays in a run and execute all steps of single-cell capture,

lysis, reverse transcription and qPCR [65].

It is evident that valve-assisted microchamber system is capable of performing complex single-cell analysis with precise control of fluid. Despite its advantages, the equipment cost is rather high because accurate gas control system is needed. Also, this technology is hard to scale up beyond 1000 capture sites because the fabrication needs to be extremely precise as the microfluidic device goes beyond 3-layers PDMS structure.

2.5.4 Droplet technique

Unlike the first three platforms where cells are captured at fixed trap sites, droplet-based system uses oil and aqueous solutions to create floating water-in-oil emulsions for single-cell isolation. In the microfluidic droplet generator (either cross-flow or T-junction), the aqueous solution is pinched by continuous oil flow and breaks into small droplets due to Plateau-Rayleigh instability [66]. Cell encapsulation can be achieved during droplet generation. The number of cells encapsulated in each droplet follows a Poisson distribution, where the key determining factors include droplet volume and cell concentration [67]. Cells are usually encapsulated with various reagents and/or drugs in order to conduct biological assays on the basis of single cells [68]. Comprehensive droplet operations, such as droplet generation, merging, mixing, incubation and detection, have been successfully integrated in a device as shown in figure 2.6(A)

[69].

As cell-containing droplets are surrounded by oil solution, biomolecules produced by cells are well-confined within droplets and can accumulate to relatively high concentrations. Hence, the cross-contamination issue is resolved and the detection sensitivity is greatly enhanced. Drug screening, PCR, measurement of cytokine production and metabolism as well as selective evolution have been successfully achieved using droplet-based platform (figure 2.6) [70-73]. Recently, several modified forms of droplet technology, such as hanging droplet and stationary droplet array, have emerged to improve the spatial resolution of individual droplets [74, 75].

Apart from these advantages, the droplet-based single-cell assay is primarily limited by the uncontrolled encapsulation process. Many empty droplets or multi-cell droplets (~ 70%) are generated, as modelled by Poisson statics, which unavoidably reduces the utility of downstream analysis. Moreover, droplet-based platform is intrinsically difficult for liquid addition and removal because of the droplet integrity. Therefore, antibody-based detection that requires addition of secondary antibody and washing is generally hard to be realized using the droplet platform. Although pico-injector [76], magnetic-controlled droplet manipulation [77] and droplet gelling [78] have been developed to solve this issue, these applications are still limited by their sophisticated operation.

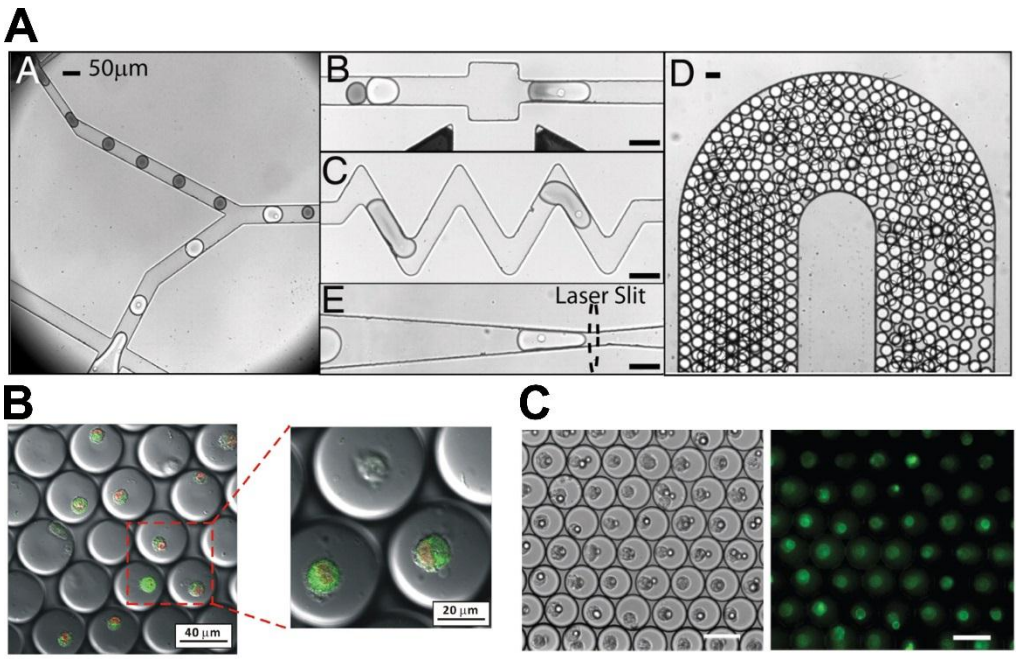

Figure 2.6 (A) A series of images demonstrating droplet generation, droplet merging, droplet mixing, droplet incubation and droplet-based single-cell detection for drug screening [69]. (B) Encapsulated cancer cells in droplets showing phosphorylation of kinase [70].(C) Encapsulated cells and beads in droplets showing active antibody production [73].

Overall, microfluidics offers a versatile solution to perform comprehensive biological assays at the single-cell level. Compared with macro-scale analytic tools, microfluidic single-cell platforms possess many advantages: low device cost, small reagent consumption, simple fluid control, easy to scale up, high sensitivity and fast reaction rate. So far, various single-cell compartment strategies have been developed and customized for different downstream applications. The features of the four main microfluidic single-cell techniques are summarized in the following table for comparison.

Table 2-1. Comparison of several microfluidic approaches for single-cell analysis

Technology	Design	Throughput	Cross contamination	Cell viability
Hydrodynamic trap	Simple	High	High	High
Microwell	Simple	High	High	High
Valve-assisted microchamber	Complex	Low	Low	High
Droplet	Simple	High	Low	High

2.6 Selection of droplet as SCA platform to test the hypotheses

Droplet microfluidics is chosen to perform single-cell functional analysis in this PhD project. Firstly, droplet-based platform has low cross-contamination which is critical for accurate long-term observations. Secondly, cells in droplets are not subjected to any physical stress which guarantees the cell viability and reliability of single-cell assay. Droplet microfluidic systems are also fast and easy to fabricate due to its one-layer structure. Last but not least, this technology can be scaled-up in terms of droplet generation and detection for high throughput study of cell samples.

Chapter 3. Jetting-based droplet microfluidics for high single cell encapsulation

3.1 Introduction

Based on the literature review in Chapter 2, microfluidic droplet approach has been selected to study single cells because of its high-throughput cell encapsulation (up to 10^3 droplets per second), simple fluidic control, high detection sensitivity and low contamination across neighbouring droplets [69, 78]. Despite these advantages, microfluidic droplet system has an intrinsic drawback – low single-cell encapsulation rate, limiting the efficiency of downstream biological assay. Although some approaches have been proposed to enhance the single-cell efficiency, those approaches either require high cell concentration or need active droplet sorting based on cell labelling. These additional requirements largely restrict the clinical applications of droplet technology since clinical samples are usually low in cell abundance and original cell status must be preserved. In this chapter, we discuss the novel usage of jetting and size-based sorting for passive enhancement of single-cell encapsulation efficiency regardless of input cell concentration. We demonstrate the downstream application on single-cell protease assay and drug test.

3.1.1 Poisson distribution: limitation on single-cell analysis

Droplet microfluidics has been extensively applied for single-cell analysis.

Continuous cell solution is broken into small droplets by oil sheath flow as shown in Figure 3.1(A). Cells randomly suspended in the solution are encapsulated into droplets in an uncontrolled manner, which leads to generation of undesirable empty droplets. In fact, the probability of number of cells per droplet in the random encapsulation process could be predicted by Poisson statistics as shown below,

$$P(\lambda; k) = \frac{\lambda^k \ exp\ (-\lambda)}{k!} \tag{3.1}$$

where P stands for probability of getting certain type of droplet, k is the desired number of cells in the droplet and λ is the average number of cells per droplet [67]. The average number of cells per droplet λ is defined as the total number of cells in 1mL of cell solution divided by the total number of droplets produced from 1mL cell solution. To estimate the probability of getting single cells inside droplets, k is set to 1. As a result, the probability depends on the λ value, which is predominantly determined by the concentration of cell solution and the droplet volume.

Based on the formula, the theoretical maximum single-cell rate is around 36% when λ is equal to 1. That is to say, the number of cells in solution need to match with the number of droplets generated from the solution in order to reach the optimal single-cell encapsulation rate. For example, when 1 million cells in 1mL solution are encapsulated into 1 million droplets (e.g. 1nL per droplet), the single-cell encapsulation rate reaches maximum value in theory.

For most microfluidic droplet platforms, the droplet size is in the range of 10 to 100 μm in diameter, corresponding to 0.5 picoliter to 0.5 nanoliter in volume. The cell concentration has to be more than one million of cells per milliliter in order to achieve above 30% single-cell encapsulation efficiency, which is practically difficult for most of cell samples. Therefore, the realistic single-cell encapsulation efficiency is generally lower than the optimal efficiency, especially under low cell concentration condition as demonstrated in Table 3-1 and Figure 3.1(B).

Table 3-1. The predicted cell encapsulation percentage under different cell concentrations and droplet sizes based on the Poisson distribution

Cell Concentration	**25 μm droplet**			**50 μm droplet**		
	0 cell	1 cell	1+ cell	0 cell	1 cell	1+ cell
20 k cells per mL	99.98%	**0.02%**	0.00%	99.87%	**0.13%**	0.00%
200 k cells per mL	99.84%	**0.16%**	0.00%	98.70%	**1.29%**	0.01%
2 M cells per mL	98.38%	**1.61%**	0.01%	87.73%	**11.48%**	0.79%
20 M cells per mL	84.91%	**13.89%**	1.20%	27.01%	**35.35%**	37.64%

3.1.2 State-of-the-art for enhancement of single-cell encapsulation

High encapsulation rate enables effective detection of single cells in downstream biological assays. Different microfluidic approaches have been developed to overcome the Poisson limitation encountered in the random encapsulation process. These approaches can be classified into three categories based on the enhancement principle, including inertial cell ordering, active droplet selection and hydrodynamic droplet sorting.

Inertial cell ordering can be deployed before droplet formation in order to improve single-cell encapsulation efficiency. Cells can be ordered along the microchannel under sufficiently high flow rates to form an equally spaced "cell train" due to the net effect of inertial force and wall lift force [79]. Droplet generation frequency can be synchronized with the distance between cells so that the cell train can be broken into uniform droplets with single cells inside as shown in Figure 3.1(C). The single-cell encapsulation efficiency has been improved to 80% by coupling a straight (~5 cm) or spiral channel (~1 cm) with a droplet generator [79, 80]. The original status of cells can be retained when using this approach because fluorescent labelling is unnecessary. However, inertial ordering method requires extremely high cell densities (10^6 ~10^7 cells/mL) to prevent the generation of empty space in the cell train, which deteriorates the cell encapsulation efficiency [70, 81]. This requirement on cell concentration largely limits the single-cell assay application on samples with low cell abundance.

The active droplet selection approach is another way to improve single-cell encapsulation efficiency. The system consists of two critical elements: a detector to detect presence of single cells in droplets based on fluorescence labelling, and a sorter to manipulate droplets relying on external force or field. Many microfluidic sorting techniques have been successfully applied on droplet application, such as gas-controlled valve [82], dielectrophoresis (DEP) force [83], and surface acoustic wave (SAW) [84]. Ideally, single-cell encapsulation

efficiency can be enhanced to 100% using active selection method, by removing all empty droplets as shown in Figure 3.1(D). However, fluorescent labelling, which is essential to distinguish empty and cell-containing droplets, might alter the cell function, leading to incorrect cell assay results [85, 86]. More recently, image processing method has been developed to detect cells inside droplet without the aid of fluorescent labelling [87]. Nevertheless, this method is computationally expensive at current stage as thousands of images captured by high speed camera must be analysed in a short time frame. Therefore, the processing throughput is limited to 10Hz. Apart from these drawbacks, active droplet selection system is usually expensive to construct due to optical components and control systems.

Moreover, hydrodynamic droplet sorting has been demonstrated to improve single-cell encapsulation rate by separating droplets of different sizes when input cell concentration is high (~10^7 cells/mL). Passive droplet sorting was applied in single-cell study with achieving above 60% single cell ratio [88]. However, hydrodynamic sorting, such as pinch flow fractionation (PFF), is not a favourable method to sort water droplets in oil environment. This is because flow control in viscous oil is much more difficult than in normal aqueous fluid, imposing challenges on experiment operation and sorting accuracy.

All three techniques do not provide a comprehensive solution for single-cell encapsulation enhancement. Hence, in order to effectively study single cells using droplet microfluidics for rapid screening, new integrated method, which

takes low cell centration and avoidance of labelling into consideration, is required.

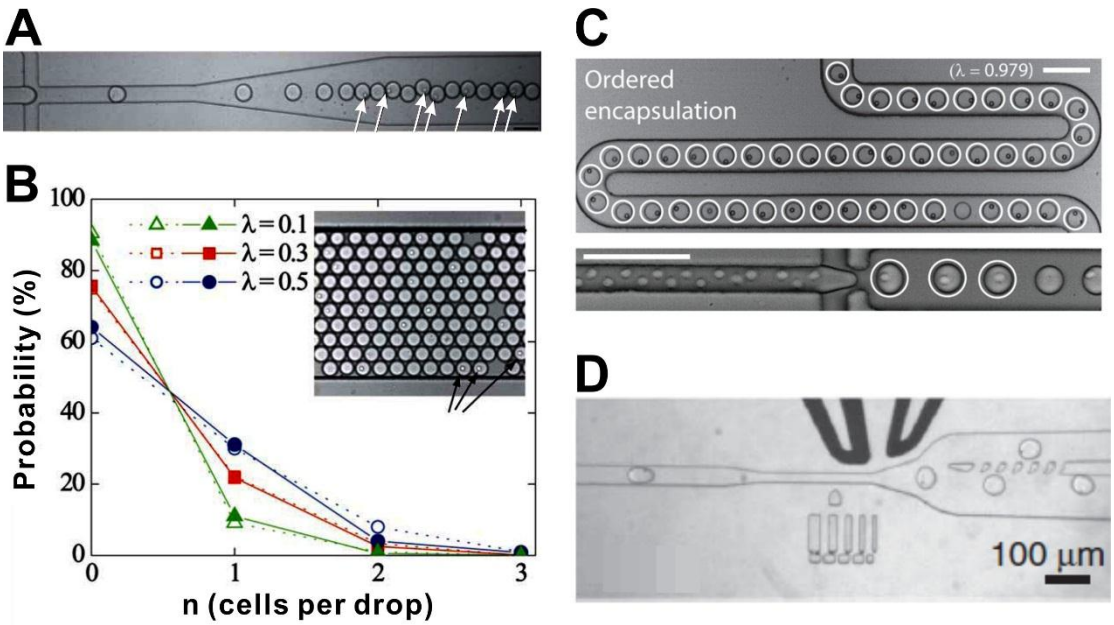

Figure 3.1 (A) Image of a flow-focusing droplet generator producing cell encapsulated droplets. The white arrows point to the cells inside droplets. Many of droplets remain empty [67]. (B) Comparison between experimental results (dotted lines with open dot) and theoretical model of Poisson distribution (solid lines with filled dot) shows a good agreement. 60% to 90% of droplets are empty. Inset showing hundreds of droplets with 3 droplets containing single cells [67]. (C) *Above* good single-cell encapsulation achieved by cell ordering. *Below* image of the droplet generator where cells are first ordered in a long straight channel to form an equally spaced "cell train" [79]. (D) Dielectrophoresis (DEP)-based droplet active sorting where the presence of cell is detected by fluorescent signal and the droplets are manipulated by positive DEP force [83].

3.1.3 Proposed techniques and hypothesis

Here, a novel droplet technique is proposed to take into account the low cell concentration and avoidance of fluorescent labelling by applying passive size-based droplet sorting. The microfluidic platform comprises a droplet jetting generator and a deterministic lateral displacement (DLD) size-sorting channel [89, 90]. Jetting creates size difference between cell-encapsulated and empty

droplets. Subsequently, DLD performs size-based sorting to isolate large cell-encapsulated droplets from small empty droplets in a robust and passive manner. We hypothesize that integration of droplet jetting and DLD sorting can increase single-cell encapsulation rate regardless of input cell concentration. By implementing the proposed technique, we are able to perform effective single-cell functional assay on samples with low cell abundance. We also hypothesize that protease secreted from single cancer cells can be assayed in individual droplets as protease concentration is accumulated to a rather high level in a picoliter droplet. From this, we will further study the heterogeneity of matrix metalloproteinase (MMP) secretion by cancer cells under normal and drug treated condition using the proposed platform in order to provide more understanding in cancer biology and disease management.

3.2 Material and Methods

3.2.1 Device design

The microfluidic device consisted of a flow-focusing droplet generator and a size-based droplet sorting array based on deterministic lateral displacement principle. In the flow-focusing droplet generator, the width of oil, cell solution and droplet channels was set 150 μm, 70 μm and 100 μm, respectively, as shown in Figure 3.2(A). The reason of having narrow channel for cell solution was to prevent oil backflow at high flow rate. For downstream matrix metalloproteinase (MMP) activity assay, a Y-shape junction was incorporated

into the droplet generator to mix the reagent with cell solution prior to encapsulation. As oil flowed into the junction point, it sheared aqueous solution (cell solution) from both sides to form water-in-oil droplets in a continuous manner. Size difference between cell-encapsulated droplets and empty droplets could be created by intentionally reducing the droplet size smaller than the average size of a cell.

Once droplets were generated, they flowed into a size-based sorter to separate the large cell-containing droplets from the small empty droplets. The sorter was essentially a DLD array of micropillars. When large droplets entered the sorting section, they collided with micropillar at every lateral position of the array and were gradually deflected to one side of the channel from the centre position while moving towards the outlet. In contrast, small droplets maintained their original moving trajectory without any lateral deflection while moving towards the channel end [90]. In this way, the droplets could be successfully separated at the bifurcation point of outlets, as shown in Figure 3.2(B).

Based on the principle of DLD design, the critical dimension of separation could be adjusted by tuning the micropillar diameter, gap and row shift distance. In order to separate large cell-containing droplets (~25 μm) and small empty droplets (<15 μm), the micropillar diameter was set 50 μm, the gap between micropillars was set 50 μm and the row shift distance was set 10 μm. The bifurcation point at the end of the sorting section was set 400 μm away from the left channel wall and 1600 μm away from the right channel wall, which led one

fifth of fluid to enter the cell-droplet outlet and the rest of fluid to enter the waste outlet. The width of the entire sorting section was set 2 mm in order to have good lateral resolution. The length of the sorting section was set 12 mm to guarantee large droplets can be sufficiently deflected to the cell-droplet outlet.

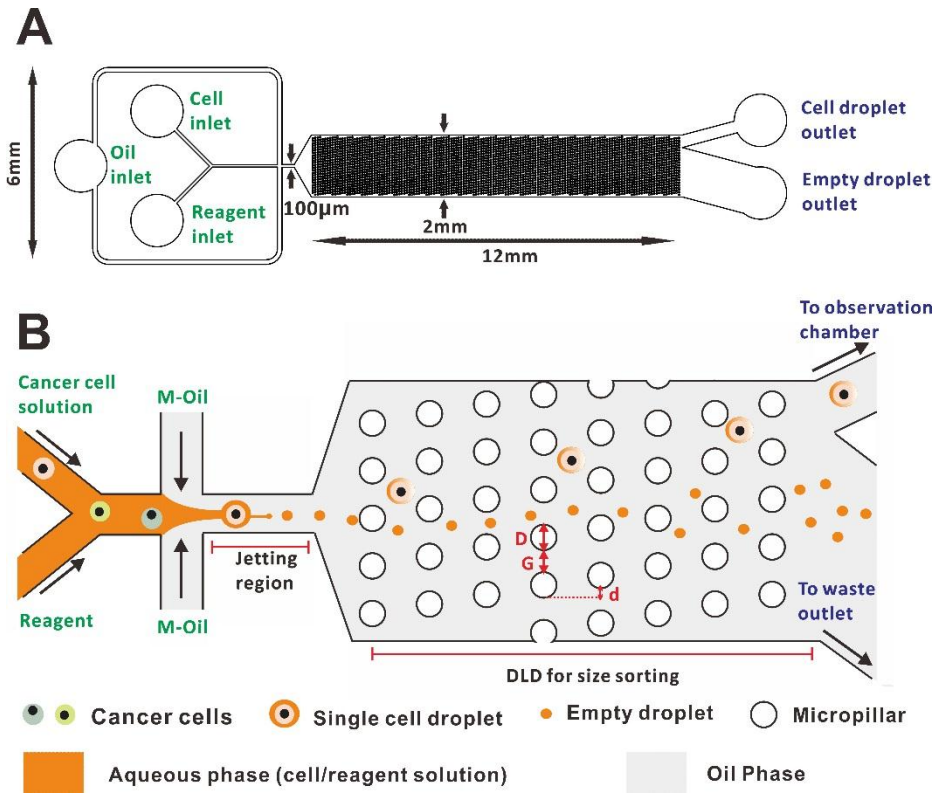

Figure 3.2 (A) Schematics of the microfluidic device for high single-cell encapsulation rate. The microfluidic design consists of a cross-flow droplet generator with a deterministic lateral displacement (DLD) micropillar array. (B) Illustration of the device operation. Cell solution is firstly mixed with reagent and then compartmentalized into small droplets at the jetting region. Cell-containing droplets appear bigger than empty droplets and can be deflected toward channel side wall in the DLD sorting channel.

3.2.2 Microfluidic device fabrication

The channel layouts were first designed using AutoCAD student version (AutoDesk, USA). After finishing, the design was sent to a mask shop (Infinite Graphics, Singapore) for mask fabrication. Then the microfluidic device was

created in Polydimethylsiloxane (PDMS) (Dow Corning, USA) using standard soft lithography method [91]. In brief, a 4-inch silicon wafer (Latech, Singapore) was first fabricated to produce a master mold based on the mask design using deep reactive ion etching (DRIE). The reason of choosing DRIE mold rather than simple SU-8 mold is to ensure good size and height uniformity of the micropillar pattern in the droplet separation array. The trenches were etched 50 μm in depth into the silicon wafer, which was essentially the microfluidic channel height. After etching, the silicon master wafer was silanized with trichloro (1H, 1H, 2H, 2H-perfluorooctyl) silane (Sigma Aldrich, USA) for 1 hour to prevent PDMS from sticking onto the silicon wafer surface. PDMS prepolymer mixed in 10:1 (w/w) ratio with curing agent was casted over the master mold to replicate the reverse pattern. After degassing in a vacuum desiccator for an hour, the PDMS was cured at 70 °C oven for 2 hours. The cured PDMS was cut out using surgical scalpel and peeled off from the master wafer. Inlet and outlet ports were produced using a 1.20 mm Harris Uni-Core puncher (Ted Pella, USA). After cleaning with isopropyl alcohol (IPA) (Sigma Aldrich, USA) and Scotch tape (3M, USA), the PDMS devices were irreversibly bonded to a PDMS-coated microscopic glass slide (Corning, USA) using an oxygen plasma machine (Femto Science, Korea). The hydrophobic channel surfaces are necessary to prevent aqueous solution from sticking to the channel wall. The PDMS-coated glass slides were produced by spin-coating a mixture of PDMS and hexane (Sigma Aldrich, USA) with a 1:1 (w/w) ratio at 1500 rpm.

After plasma bonding, the device was kept in the 70 °C oven overnight, forming strong bonding at interface as well as restoring PDMS surface hydrophobicity.

3.2.3 Cell culture

Human non-small lung cancer cell line PC-9 was a kind gift from Dr Daniel at National University Hospital. PC-9 cells were used to determine the single-cell encapsulation ratio and enzymatic activities at single-cell level. PC-9 cells were cultured in RPMI-1640 medium (ThermoFisher Scientific, Singapore) supplemented with 10% (v/v) fetal bovine serum (FBS) (Life technologies, Singapore) and 1% (v/v) penicillin-streptomycin (Life technologies, Singapore). The incubation environment was maintained at 37 ℃ in a humidified atmosphere with 5% CO_2. The cells were split every 3 days using 2x Trypsin-EDTA (Life technologies, Singapore) under sterile conditions. Green fluorescent calcein-AM live stain (Life technologies, Singapore) was used for cell viability evaluation and cell visualization in droplets.

Drug doxycycline (Sigma Aldrich, USA) was used in protease inhibition experiment [92]. Viable PC-9 cells were firstly harvested using trypsin and then re-suspended in fresh culture medium with 20 μg/mL doxycycline [93]. After 3-hour incubation in the 37 °C, treated PC-9 cells were loaded into a syringe for droplet-based single cell protease assay.

3.2.4 Droplet generation

Monodispersed water-in-oil emulsion was generated by jetting at a flow-

focusing junction. Aqueous fluids and mineral oil (M-oil, Sigma Aldrich, USA) were first loaded into separate plastic syringes (Terumo, Japan) and then introduced into the device using syringe pumps (Harvard Apparatus, USA). The microfluidic device and syringes were connected using micro polyethylene tubing (Scientific Commodities, USA) (0.38 mm inner diameter x 1.09 mm outer diameter). Non-ionic surfactants 3% (v/v) Span 80 (Sigma Aldrich, USA) and 2% (v/v) Abil EM90 (Evonik, Germany) was added into mineral oil to stabilize jetting formation and prevent droplet coalescence. In the cell experiment, biocompatible density gradient medium OptiPrep (Sigma Aldrich, USA) was mixed with cell solution (volume ratio 16:84) to minimize the effect of cell sedimentation.

3.2.5 Matrix Metalloproteinase Assay

A fluorescent resonance energy transfer (FRET)-based polypeptide matrix metalloproteinase (MMP) substrate (Biozyme Inc, USA) was used to measure the enzymatic activity of single cancer cells. The substrate basically consists of a fluorophore and a quencher. Both of them are connected by a polypeptide chain. The secreted MMPs from cancer cells could cleave the polypeptide and release fluorophores from quenchers, causing increase of droplet fluorescence signal. The MMP substrate solution was diluted to 40 μM concentration in 50 mM Tris buffer (pH 7.5, containing 150 mM NaCl, 2 mM $CaCl_2$, 5 μM $ZnSO_4$, and 0.01% Brij-35) (Sigma Aldrich, USA) before it was loaded into syringe. The final concentration of MMP substrate in each droplet was 20 μM after 1:1

dilution with cell solution at the Y-junction inlet. Before assaying cancer cells, pure MMP enzyme (Enzo Life Sciences, USA) was used to calibrate the droplet system. One thing to notice is that the MMP substrate used in the experiment is not specific to one kind of MMPs. It is especially sensitive to MMP-9 and MMP-13.

3.2.6 Optical Setup

The microfluidic devices were mounted on an inverted microscope (Nikon Eclipse Ti, Japan) for experiments. The process of droplet formation and sorting was observed and recorded using a high-speed camera (Phantom v7.3, USA). A fluorescence illumination microscopy system (CoolLED, UK) and digital CMOS camera (Hamamastu Orca Flash 4, Japan) were used to measure the single-cell encapsulation rate with fluorescence-labeled cells and perform automatic time lapse illumination for the single-cell assay experiment. The resulting fluorescent signals were analyzed using Image J® software (National Institutes of Health, USA).

3.3 Results and Discussion

3.3.1 Droplet generation using jetting and oil selection

When an aqueous phase fluid is shorn by an immiscible oil phase from both sides, it can be broken into droplets to form water-in-oil emulsions via two different mechanisms: dripping and jetting [89]. Under the dripping condition,

the aqueous phase is broken into droplets near the orifice due to pinch effect of the oil phase to form monodispersed emulsions. In this case, size of droplets is usually similar to or even larger than the microchannel dimension. By contrast, under the jetting condition, the aqueous phase extends a thin tip into the oil phase due to strong shearing effect of the oil phase. The thin tip eventually breaks into droplets away from the orifice because of Rayleigh-Plateau instability [94]. Under jetting, size of droplets is usually much smaller than the microchannel dimension. Hence, it is possible to produce uniform small droplets in a relatively large channel under jetting. Moreover, under jetting regime, droplet size can be precisely adjusted by controlling the flow rate of aqueous and oil solution.

Based on these droplet generation mechanisms, two designs were proposed to make droplets smaller than a cell size so that size difference can be created between empty droplets and cell-containing droplets. The first design was to reduce the dimension of droplet formation channel to 10 μm and then generate droplets using drippling. In this design, the channel was susceptible to clogging caused by cell clusters and PDMS debris. The second design was to keep channel dimension large and then use viscous oil to shear aqueous solution to form jetting. Compared with the first design, the second design is more resistant to channel clogging during the cell encapsulation process. Therefore, jetting is chosen to produce droplets in this project.

Previous studies have characterized the factors that determine either jetting or dripping to happen. They are the capillary number of the outer fluid and Weber number of the inner fluid. Their equations are shown as

$$C_{out} = \eta_{out} u_{out} / \ \gamma \tag{3.2}$$

$$W_{in} = \rho_{in} D_{orifice} u_{in}^2 / \gamma \tag{3.3}$$

where η_{out} is the viscosity of outer fluid, u_{out} and u_{in} are the mean velocities of outer and inner fluid respectively, γ is the surface tension, ρ_{in} is the density of inner fluid and $D_{orifice}$ is the dimension of orifice. Only when the sum of C_{out} and W_{in} is larger than one order of magnitude will jetting occur [95]. Otherwise, dripping with large droplet formation or continuous stream without droplet formation will occur.

High viscosity of outer oil and small surface tension is important for jetting formation. Eventually, mineral oil was selected because of its high viscosity (25.3 mPa s). The viscosity of water is about 1mPa s. Other oil candidates, such as hexadecane, fluorocarbon oil and silicon oil, are either too smooth to produce jetting or too viscous to be injected using syringe pump.

3.3.2 Selection of surfactants to prevent coalescence

Surfactants are compounds that lower the surface tension between two liquids. Surfactants are amphiphilic compounds, containing both hydrophobic groups (tails) and hydrophilic groups (heads). They can aggregate at oil-water interface

and promote the overall stability of bi-phase system. Surfactants are essential to droplet microfluidics because they prevent droplet coalescence. Without proper surfactant, water-in-oil droplets tend to merge with each other to minimize the overall system energy.

Surfactants can be divided into non-ionic, anionic, cationic and amphoteric groups based on the charge carried by hydrophilic heads. Ionic (anionic, cationic and amphoteric) surfactants can denature protein and lyse cells. As the water-in-oil droplets were used to encapsulate cancer cells and study protease activities, only non-ionic surfactants can be applied in our droplet system [96].

In literature, SPAN 80 and Abil EM90 are common non-ionic surfactants for mineral oil [96, 97]. To determine which surfactant to use, we investigated the effect of coalescence prevention and jetting stability of both surfactants. In the coalescence experiment, 5% SPAN 80 in mineral oil failed to prevent droplet from merging at stationary condition for 1 hour. Although 5% Abil EM90 provided a better droplet stability, it changed the surface tension between water and oil phase dramatically. As a result, jetting could no longer be formed.

Neither pure SPAN 80 nor Abil EM90 worked well with mineral oil. The mixture of SPAN 80 and Abil EM90 with mineral oil was utilized to leverage their advantages and compensate their disadvantages. Eventually, the combination of 3% SPAN 80 and 2% Abil EM90 demonstrated both good droplet and jetting stability and was used in the following experiment.

3.3.3 Droplet size characterization under different flow rate

Once jetting was established in the droplet generator, we started to investigate the relationship between flow rate and droplet size. Varied flow rates of oil and aqueous solutions were applied to form droplets of different sizes. The size of the droplets could be controlled within a range of 10 to 40 μm in diameter inside a 100-μm-wide flow-focusing channel. The measurement results revealed that the droplet size was linearly proportional to $(Q_{aqueous}/Q_{oil})^{0.5}$, as shown in Figure 3.3, where $Q_{aqueous}$ and Q_{oil} are the flow rates of the aqueous and oil solutions, respectively. When the ratio of $Q_{aqueous}$ to Q_{oil} was reduced by decreasing the aqueous flow rate or increasing the oil flow rate, the size of the droplets reduced correspondingly. When this flow ratio was greater than 0.4, the jetting tip became a thin stream and no more droplets could be generated.

Based on the characterized relationship, the optimal flow rates to produce size distinction between empty droplets and cell-containing droplets were 0.5 μL/min for the cell solution and 20 μL/min for the oil solution. The resulting diameter of empty droplets was 14.4 $\pm$ 0.7 μm (with relative standard deviation of 4.9%). The average size of cultured PC-9 cancer cells was 15.6 μm. When a cancer cell was encapsulated into a droplet, the droplet size could expand to 25 μm as shown in Figure 3.4(A). In this way, 10 μm size difference between empty and cell-containing droplet was created for downstream size-based sorting.

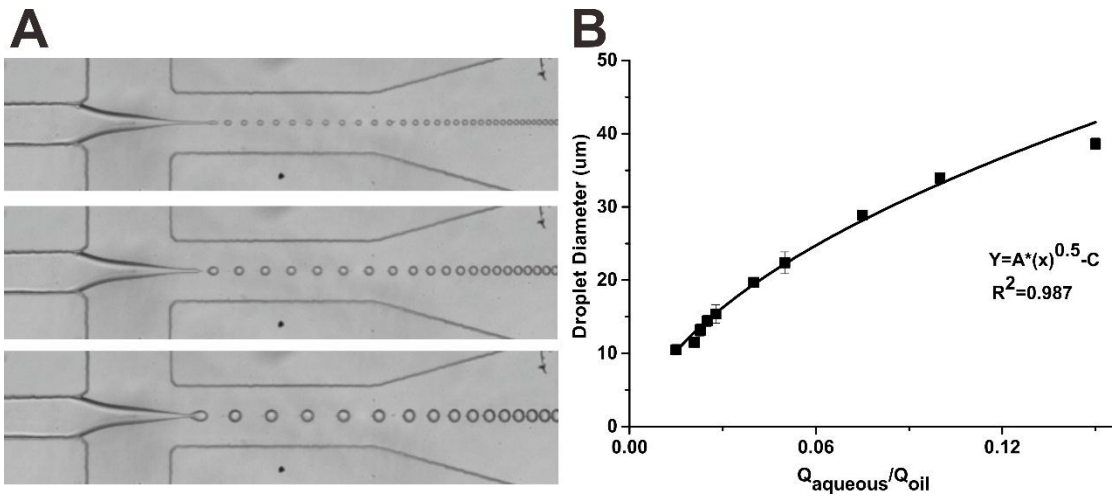

Figure 3.3 (A) Brightfield images of droplet jetting under various flow conditions. *Above*: oil flow rate 20μL/min, water flow rate 0.25 μL/min; *Middle:* oil flow rate 20μL/min, water flow rate 0.5 μL/min; *Lower:* oil flow rate 20μL/min, water flow rate 1 μL/min. The droplet size clearly increases as the water flow rate increases. (B) Quantified relationship between flow rate ratio and droplet size with a fitting model. The experimental results show a good agreement with Utada's model that the droplet size was linearly proportional to $(Q_{aqueous}/Q_{oil})^{0.5}$ [95].

3.3.4 Characterization of DLD based droplet separation

A deterministic lateral displacement (DLD) micropillar array was connected to the droplet jetting generator to sort the large droplets containing encapsulated cells from the small empty droplets for effective downstream single-cell measurement. There were two reasons to deploy DLD rather than other microfluidic separation methods to perform droplet sorting. Firstly, the separation principle of DLD design relies heavily on the geometric layout of micropillars, rather than fluidic conditions (such as Reynolds number). Hence, it can be easily adopted to any oil-ambient applications (such as water-in-oil droplet separation) [98]. Whereas, inertial microfluidic separation, one of the

most commonly-used particle separation approaches, can hardly work in the viscous oil environment due to limited Reynold's number. Most of inertial microfluidics requires a high flow rate to reach 50 ~ 100 Reynold's number [99]. Viscous oil effectively decreases the Reynold's number compared to water solution at the same flow rate, thus hindering the inertial based particle separation. Secondly, the DLD separation is independent of flow rate. Microfluidic droplet generation, in general, operates at low flow rate, ranging from 0.1 to 10 μL/min. This slow rate makes droplet generation incompatible to most of inertial microfluidic approach. However, DLD is able to achieve separation at such a low flow rate, and thus can be easily integrated to droplet generator to perform sorting directly.

Based on the aforementioned droplet size difference, the critical dimension of separation (D_C) was set at 20 μm according to the following formula

$$D_C = \frac{2\eta G d}{G+D} \tag{3.4}$$

where D is the micropillar diameter, 50 μm; G is the micropillar gap, 50 μm; d is the row shift distance, 10 μm; and η is a parabolic flow correction factor equal to 2, as shown in Figure 3.2(B) [100]. The optimized pillar diameter and gap design reduced the chance of droplet breakage when the droplets collided with pillars and passed through the gaps during the sorting process. The small empty droplets whose diameters were below the critical dimension of the DLD separation followed their original flowing direction inside the micropillar array, heading to the waste outlet. The droplets containing cells, whose diameters were

above the critical dimension, were deflected from their original direction toward the upper side wall and eventually entered an observation chamber as shown in Figure 3.4.

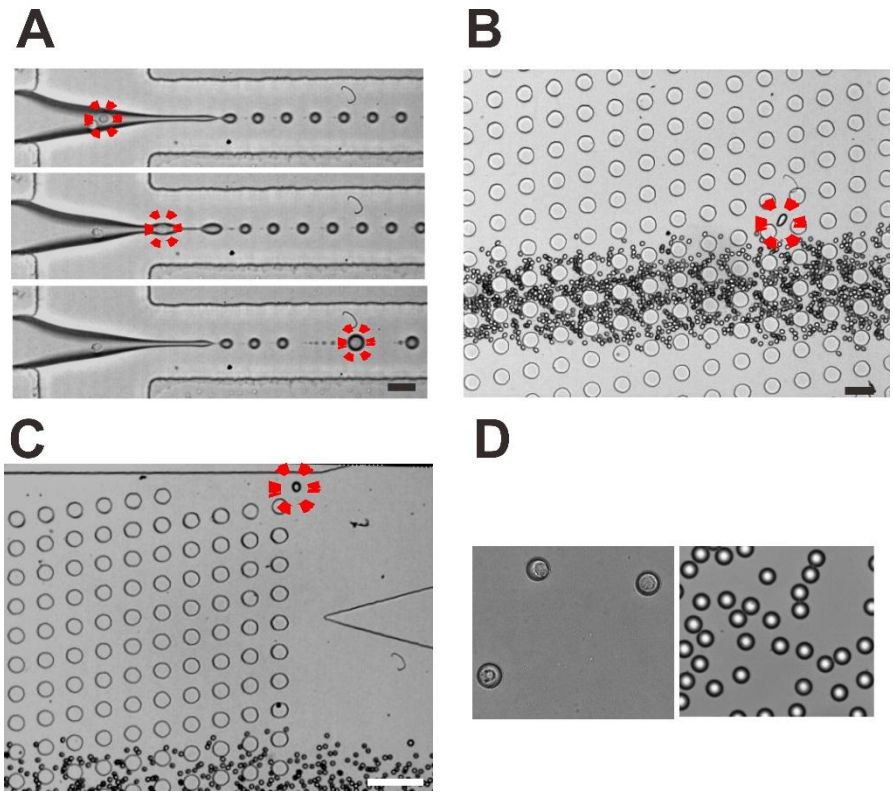

Figure 3.4 (A) A series of images showing the cell encapsulation process under jetting condition. Scale bar = 30 μm. (B) Image showing a cell-containing droplet gradually migrates away from the main stream of empty droplets. Scale bar = 60 μm (C) Image showing a cell-containing droplet is separated from other empty droplets and heading to observation chamber. Scale bar = 150 μm (D) Images of cell-containing droplets and empty droplets in the observation chamber.

3.3.5 Characterization of single-cell rate enhancement

In order to characterize the actual single-cell encapsulation rate of the combination of jetting and DLD sorting, freshly harvested cancer cells were first labelled using green fluorescent calcein-AM live stain and then injected into the developed device. Based on both bright-field and fluorescent images observed

under a fluorescence microscope (Figure 3.5(A) and 3.5(B)), the number of cells in individual droplets could be recorded to calculate the cell encapsulation rate.

Four different cell concentrations (2×10^4, 2×10^5, 2×10^6, and 2×10^7 cells/mL) were tested to prove that the integrated droplet device can overcome the Poisson limitation in terms of single-cell encapsulation rate at various cell concentrations. The experiment results revealed that high single-cell encapsulation efficiencies were obtained regardless of the cell concentrations in the sample solutions, yielding much better performance than that predicted by the Poisson model as illustrated in Figure 3.5(C). For instance, the single-cell rate of the random encapsulation process was as low as 0.02% for the cell solution with a concentration of 2×10^4/mL, whereas the developed device could achieve a single-cell rate of ~65%. When the cell concentration increased to 2×10^7/mL, the single-cell rate of the random encapsulation was approximately 13.9%, but still far below the enhanced rate of 70% achieved by the developed device. Therefore, a significant improvement in cell encapsulation rates was observed, particularly under low cell concentrations.

The single-cell encapsulation efficiency reached its maximum at 78% when the input cell concentration was 2×10^6 /mL. A slight decrease in the single-cell encapsulation rate was observed at both lower and higher cell concentrations, which might be due to empty droplets formed under flow fluctuations and multi-cell containing droplets generated from cell clusters formed during sample preparation. Further improvements in single-cell encapsulation performance

might be achieved by reducing the empty droplet size further to counter the effect of flow fluctuation and adding another DLD section to remove multi-cell containing droplets that are larger than 30 μm.

Additionally, we also characterized the false negative sorting rate, referring to the ratio of the cell-containing droplets entering the waste outlet, by monitoring fluorescent signals carried by cells at the bifurcation point. Only 2 out of 231 (~0.9%) cell-containing droplets entered the empty droplet outlet by mistake, corresponding to 0.9% false negative sorting rate. Small cells and cell debris could contribute to this false negative results.

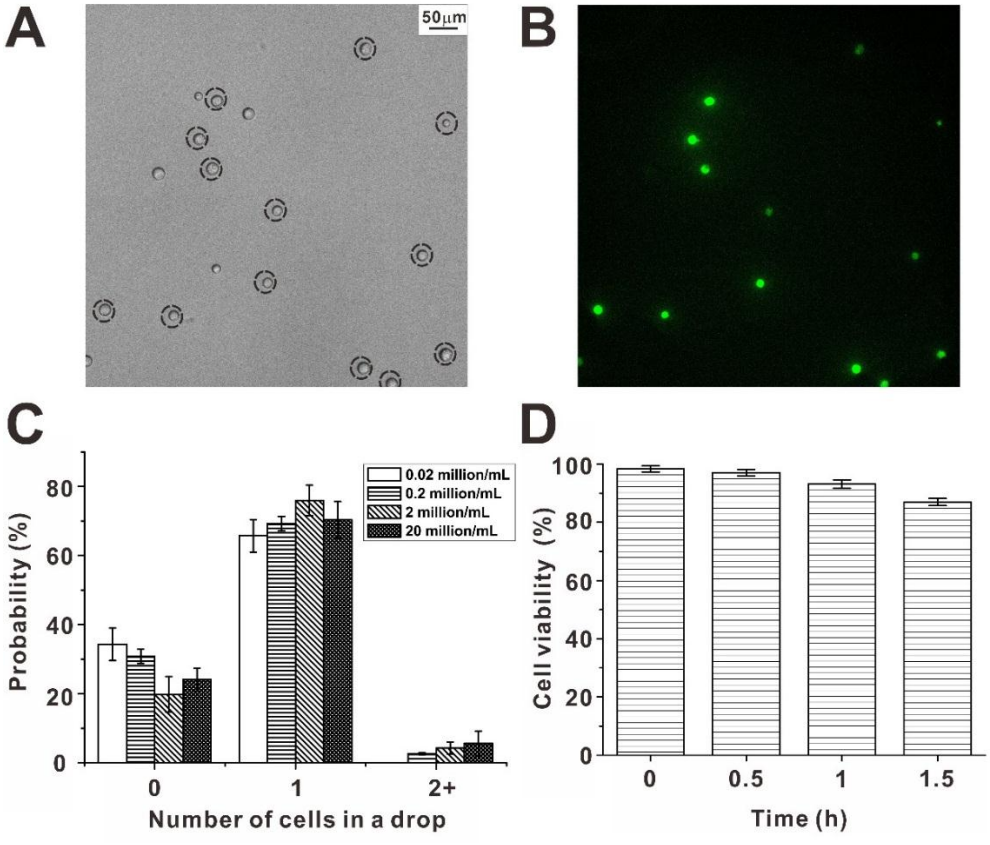

Figure 3.5 (A) A bright-field image of cell-containing droplets and (B) the corresponding fluorescent image showing 13 of 17 droplets (highlighted with black-dashed cycles in the bright-field image) with single cell inside. (C) The cell encapsulation efficiency was measured for different input cell

concentrations. Due to the usage of size-based sorting, high single-cell encapsulation efficiency (~70%) was achieved regardless of varied cell concentrations. Sample size = 537 droplets. (D) The survival rate of PC-9 cells inside droplets was measured for up to 1.5 hours. Sample size = 285 cells.

3.3.6 Viability test of cell in droplets

A cell viability test was also performed to characterize the cell survival rates inside the water droplets over time. All cancer cells were first stained with live/dead (Calcein AM @ 1 μM / Ethidium homodimer-1 @ 2 μM) stain reagent and then injected in the integrated device to produce cell-encapsulated droplets. The viability of cancer cells was evaluated every half an hour by counting the number of viable and dead cells acquired by fluorescence microscopy. Sometimes, a small group of cells displayed both live and dead fluorescent signals. These double positive cells were considered dead. This is because the live stain used here is to detect esterase within a cell, which might not be absolutely accurate. Some cells that were undergoing apoptosis may still have esterase accumulated and generate false "live" signal.

The overall viability ratios at different time points are reported in Figure 3.5(D). It gradually decreased from 98% to 85% over 1.5 hours due to shortage of nutrients and accumulation of metabolites. This result matched with previously reported cell viability in droplets of similar size [67]. In our system, the viability was approximately 90% after 1 hour of cell encapsulation. Therefore, the duration of the subsequent single-cell matrix metalloproteinase (MMP) assay experiments was controlled within 1 hour to minimize the false enzymatic

signal generated by unhealthy and dead cells.

3.3.7 Recombinant MMP test

Before conducting single cancer cell MMP assays, recombinant MMP-9 enzyme at various concentrations was first tested with the FRET-based polypeptide MMP substrate to correlate the MMP concentrations with the fluorescence signal read-out. The reasons to choose MMP-9 among the entire MMP group to do this calibration included: 1) MMP-9 has been proved a key enzyme produced by cancer cells to degrade ECM and promote tumor invasion; 2) the MMP substrate was sensitive to MMP-9 detection.

The flow rates of MMP with substrate solution and oil solution were set to 1 and 20 μL/min, respectively, to produce 20 μm droplets that were similar in size to cell-containing droplets. Each droplet contained 20 μM MMP substrate and a different concentration of MMP-9 (from 5 to 64 nM). The fluorescence intensity of these droplets was captured every 5 minute over 40 minutes as shown in Figure 3.6(A). Based on the increase in the fluorescent signal within the linear region, the corresponding reaction rate at various enzyme concentrations was obtained in units of a.u./min.

We observed very small fluorescence changes (~25 a.u.) over 40 minutes for the negative-control samples, which only contained MMP substrate without MMP-9. A linear increase in the reaction rate with increasing MMP concentration was observed (Figure 3.6 (B)). Notably, instead of total amount

of MMP, only a small fraction of pure recombinant MMP can actively cleave MMP substrate. The ratio of active enzyme in the pure MMP sample was estimated according to the PrAMA method, as described in the previous work [101]. After calibrating the fluorescence intensity of the droplets, the kinetic constant K_{cat}/K_m of 6.02×10^4 $M^{-1}s^{-1}$ was calculated by assuming Michaelis-Menten kinetics, consistent with previous study of the protease activity of the same type of MMP [102]. The kinetic constant K_{cat}/K_m was calculated using the following equation:

$$V_0 = S_0 \times K_{cat}/K_m \times E \tag{3.5}$$

where V_0 is the initial reaction rate normalized to the trypsin positive control, S_0 is the substrate concentration and E is the active MMP concentration, which is equal to the product of the MMP concentration and the active enzyme ratio (5%).

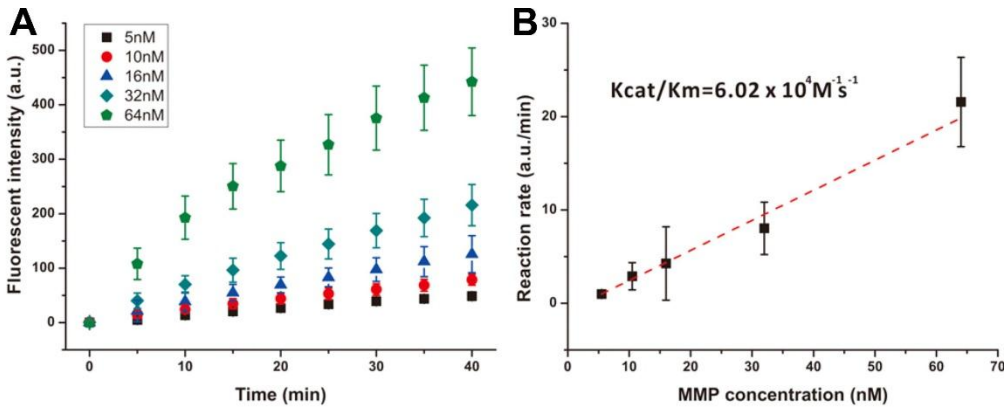

Figure 3.6 (A) The fluorescence intensity profiles of individual droplet groups containing various MMP concentrations (each droplet contained a certain concentration of pure MMP-9 and MMP substrate). Sample size = 97 droplets (B) The relationship between the reaction rate and MMP concentration in the droplets. Different concentrations were analysed to obtain the reaction kinetics constants.

3.3.8 Single-cell assay on protease secretion

After characterizing pure MMP recombinants, MMPs secreted from individual cancer cells were characterized by encapsulating the MMP substrate with cell solution into droplets. The secreted MMPs cleaved the substrate polypeptide to generate fluorescent signal that sigmoidally increased in intensity with reaction time, as shown in Figure 3.7. The fluorescence intensity increased at a slow rate in the beginning of the MMP assays and grew fast after some time, because the amount of MMPs accumulated gradually with the slow secretion process. The fluorescent signals eventually saturated at ~35 minutes due to the MMP substrate depletion. Based on the measured fluorescent intensities, cancer cell heterogeneity in the MMP activities could clearly be observed, with an increase in intensity from 400 to 800 a.u. (with mean value of 544.47 a.u. and standard deviation of 132.84 a.u.) over 35 minutes.

Based on the results obtained from pure MMP characterization, fluorescent signals from single cancer cells could be converted to MMP concentration. To do that, we only considered the fluorescent rate increase during the first 10 minutes, assuming a linear increase in the fluorescent signal during this time frame. For instance, the minimum and maximum fluorescent signal increasing rate of untreated PC-9 cells were 9.5 a.u./min and 20.3 a.u./min, respectively. The increasing rate of single-cell signals were then compared with the reaction rate that was determined from the pure MMP calibration. Based on the pure MMP calibration, these rates correspond to enzyme concentrations of

approximately 30 nM and 60 nM. Therefore, the range of ~1.5 to 3 nM active MMPs were secreted from individual live cancer cells in 35 minutes by assume 5% active enzyme ratio.

Notably, to ensure the consistency of the fluorescent-based assay, the time gap between droplet generation and start of assay was strictly controlled. The time period for a cell to travel from the reagent mixing area to the observation chip was about 30 seconds, and the time required to fill the observation chip was about 2 minutes; the summation of these durations was much shorter than the saturation time of fluorescent signal increase. Therefore, the readout time points for each cell-containing droplet were approximately the same, and the slopes of the fluorescence increases could be used to represent the MMP activities.

The inhibition of the MMP activities of individual cancer cells in response to the treatment with doxycycline was then analysed. The developed microfluidic device enabled continuous monitoring of the effects of doxycycline on individual cancer cells up to 1 hour. Different levels of suppression of MMP activities at the same dose of doxycycline were recorded, revealing heterogeneity in the resistance of cancer cells against doxycycline. In general, the MMP activities were greatly suppressed by doxycycline, as evidenced by the reduction in the increase in fluorescence exhibited by the droplet to 100 a.u. (with mean value of 81.29 a.u. and standard deviation of 46.06 a.u.) over 35 minutes (Figure 3.7(B)-red points). The MMP inhibitory effect observed in the single-cell droplets system was greater than that in conventional plate reader

assay where a batch of cancer cells were assay together in a 96-well plate. In the plate reader assay, the MMP activity of PC-9 cancer cells was reduced about 50% upon doxycycline treatment. However, the MMP activity of the same cell line was reduced more than 80% in the droplet-based single cell system. One possible explanation was that when in group, cancer cells might secrete cytokines and other biomolecules in order to support each other and enhance the drug resistance overall.

After signal conversion, the concentration of active MMPs secreted by individual doxycycline-treated cancer cells was reduced to a range of 0.2 to 0.5 nM. However, a few individual cancer cells retained some level of MMP activities under doxycycline treatment, which might suggest that a small group of cancer cells could quickly develop doxycycline resistance, even in the clonally cultured cancer cell line.

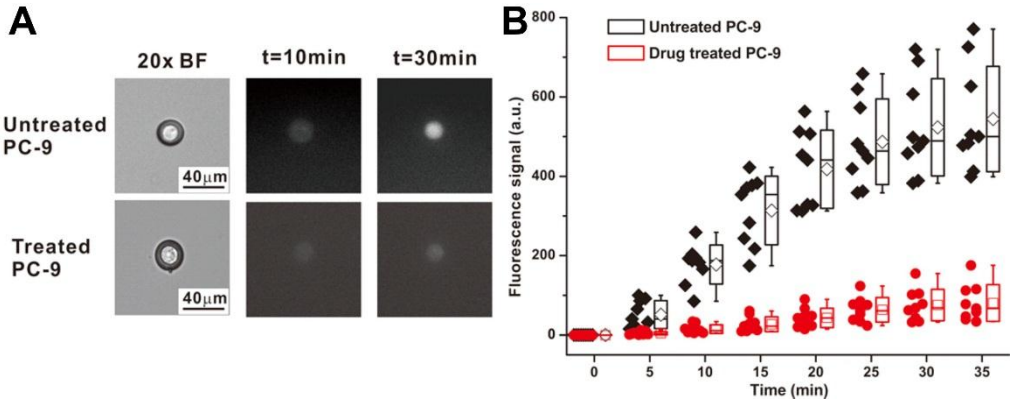

Figure 3.7 (A) Images of untreated and doxycycline-treated single cancer cells inside droplets, displaying suppressed MMP activity under the drug effect. (B) Quantified fluorescent signals from 9 untreated and 9 doxycycline-treated cancer cells, demonstrating the heterogeneity in MMP activities among cancer cells and the MMP inhibitory effect of doxycycline. Scattered points: original data points; box plots: mean, medium, standard deviation, minimum and maximum values. The signal of untreated PC-9 cells was 544.47 ± 132.84 a.u.

and the signal of treated PC-9 cells was 81.29 ± 46.06 a.u. after 35-minute incubation. The sample size was 18 cells (9 untreated, 9 treated PC-9 cells).

3.4 Conclusions

An integrated microfluidic device combining a droplet jetting component and a DLD sorting channel was developed for effective single-cell encapsulation, enabling assays of cell-secreted MMPs using minute quantities of reagents. The single-cell encapsulation rate was increased to 78% at an input cell concentration of 10^6 cells/mL, in contrast to the 1.6% rate predicted by the Poisson statistics. Single cancer cell protease assays were performed by measuring MMP secretion from the individual PC-9 cancer cells inside droplets. Heterogeneous MMP activities and various levels of drug resistance were observed at the single-cell level. The concentration of MMPs secreted from individual cells was in the range of 1.5 to 3 nM. After doxycycline treatment, the concentration of MMPs secreted by individual cells was suppressed to within 0.2 to 0.5 nM. We believe that our hybrid microfluidic system is ideal for the analysis of enzymatic activity at the single-cell level in samples with low cell concentrations (e.g. 10^4 cells/mL), because our method eliminates the need for immune-staining and active sorting. With further development on long-term stability and droplet size uniformity, this platform can be used for direct functional analysis of clinical samples with low cell concentrations for rapid diagnostics and customized therapeutics.

Chapter 4. Single cancer cell protease assay using droplet platform

4.1 Introduction

After developing the integrated droplet device to enhance single-cell encapsulation efficiency described in Chapter 3, we would like to conduct a comprehensive functional study on both cultured cancer cell lines and patient-derived circulating tumor cells (CTCs). As invasive cancer cells produce lots of matrix metalloproteinases (MMPs), especially MMP-2 and MMP-9, to degrade the extracellular matrix (ECM) and gain the ability to migrate, the activity level of matrix metalloproteinase has become a potential biomarker to evaluate the invasiveness of cancer cells [103, 104]. The MMP activity profiles at single-cell level can be utilized to search for aggressive cell subpopulation among a heterogeneous ensemble. Furthermore, single-cell proteolytic assay on patient-derived cancer cells sheds lights on the patients' disease status and can be further leveraged for customized treatment. In this chapter, we will explore how to use the droplet microfluidics to study matrix metalloproteinase activity of single live cancer cells in order to understand the biological and clinical relevance to cancer progression.

4.1.1 Cancer metastasis and circulating tumor cells

As reviewed in Chapter 2, cancer is one of the deadliest diseases imposing huge healthcare and economic burden on society. The predominant treatment

methods include surgical removal, chemotherapy and radiotherapy. Usually cancer patients go through a course of combinational treatments trying to kill malignant tumor cells. In most of the cases, although primary tumor is removed, cancer relapse could still take place at distant organs after years of treatment.

The reason for cancer relapse is mainly due to cancer metastasis. Cancer metastasis is a highly complex, multi-stage process which involves the dissemination of tumor cells from a primary site to other parts of the body via circulating blood stream and the development of secondary tumors as shown in Figure 4.1. In fact, more than 90% of cancer related deaths are caused by metastasis [105].

Circulating tumor cells (CTCs) play a very important role in cancer metastasis as they circulate freely in peripheral blood serving as seeds for secondary tumor [106]. Some scientists believe once tumorigenic CTCs find a proper microenvironment, they will extravasate from blood vessel, enter healthy tissue and start to grow into a secondary tumor [107]. Some research has suggested tumor tissue could release CTCs into blood stream even at the early stages of disease [108]. Many studies have demonstrated the detection of CTCs helps to predict the cancer progression in patients and evaluate the treatment efficacy. For example, the enumeration of CTCs negatively correlates with the overall survival rate of late-stage cancer patients [106]. Furthermore, CTC count evaluated at different time points during systemic treatment is a reliable surrogate marker of treatment response [109]. CTCs are believed to carry

relevant information about the primary tumor that they come from. CTCs are believed to carry relevant information about the primary tumor that they come from. Preliminary studies have suggested that selecting therapies based on molecular characteristics of CTCs may improve treatment outcomes in patients [110]. Hence, CTCs hold significant clinical potential for cancer diagnosis, disease monitoring and therapeutic applications.

4.1.2 Matrix metalloproteinase in tumor development

MMPs comprise a family of 23 zinc-dependent endopeptidases that are part of the metzincin family of enzymes and are generally active on or near the cell surface. Most MMPs are secreted molecules, with small exception of some membrane-type MMPs with transmembrane domain. As central regulators of extracellular matrix (ECM), MMPs are critical in microenvironment remodeling by degrading ECM. The cleavage of ECM can serve many purposes, such as creating space for cell migration and modifying the activity of signaling molecules [111].

In normal cases, the proteolytic activities of MMPs are carefully controlled and are only present when and where needed for tissue remodeling such as embryonic development, wound healing and modification of cell adhesion [112]. However, aberrant expression of MMPs has been implicated in pathological conditions for tumor development and cancer metastasis. In tumor development,

MMPs promote growth of cancer cells by cleaving insulin-growth-factor-binding protein, thereby liberating growth factors [113]. MMPs also promote angiogenesis by increasing the bioavailability of the pro-angiogenic growth factors such as vascular endothelial growth factor and fibroblast growth factor-2 [114]. In addition, MMPs promote migration and invasion of cancer cells by cleaving structural components of ECM, such as collagen type I and IV [113]. They help cancer cells intravasate and extravasate. Lastly, MMPs facilitate the epithelial-to-mesenchymal transition (EMT) — a transition that is associated with malignant behaviour — by cleaving the cell-adhesion molecule e-cadherin and by liberating transforming growth factor beta [115]. Therefore, it is important to study the MMP activity of heterogeneous tumor cells, including CTCs, in order to understand the aggressiveness and metastatic potential of the cancerous cells for better customized treatment.

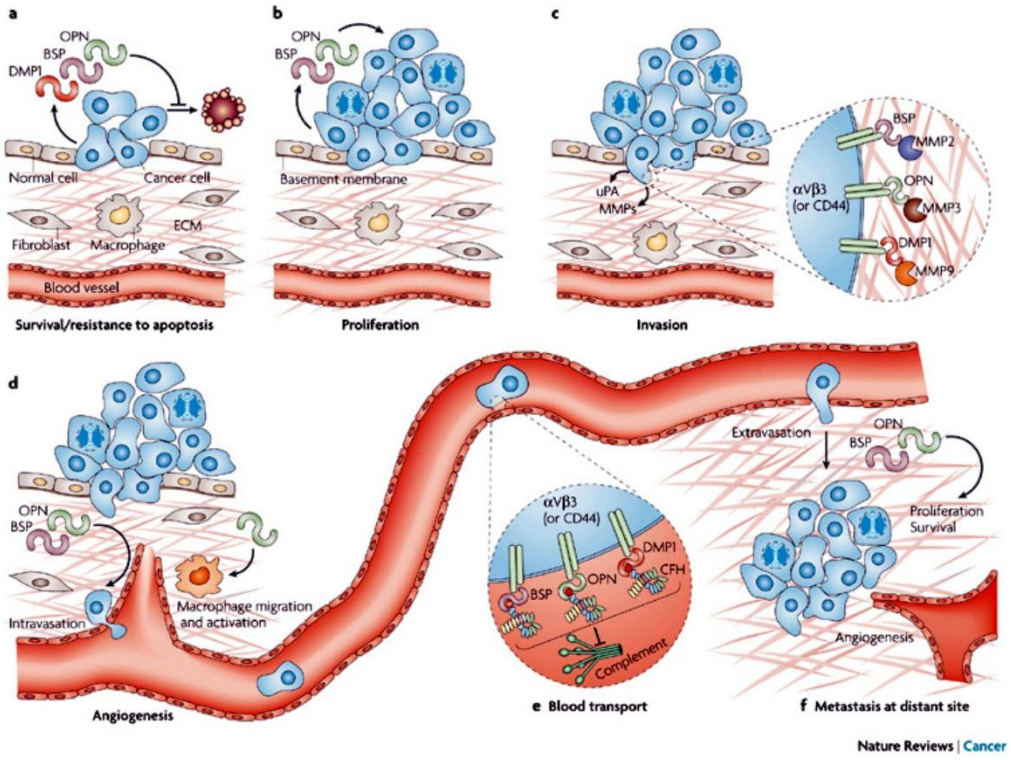

Figure 4.1 Illustration of cancer progression from survival from programmed death to metastasis at distant site. Along the progress, matrix metalloproteinases (MMPs) promote invasiveness of cancer cells and facilitate intra- and extravasation. (Adopted from Nature Review Cancer [116])

4.1.3 Limitation of current technology in single-CTC functional study

Despite the importance of CTCs in cancer progression, direct study on CTCs remained difficult because of their rarity. The number of CTCs is extremely low, comprising as few as one or two cells per 10^9 hematologic cells (mainly erythrocytes). Research has shown that CTCs are different from other hematologic cells in terms of surface molecule expression, size, stiffness and electrical property [52, 117-119]. Hundreds of microfluidic platforms have been developed to achieve accurate CTCs isolation from blood, leveraging their distinct tumor-specific surface markers and biophysical properties. Among those technologies, epithelial cell adhesion molecules (EpCAM)-based capture

and size-based sorting/filtration are the most popular approaches to enrich primary CTCs from blood sample [20].

Though microfluidic platforms can isolate CTCs from hematological cells at fast rate and with good accuracy, single-CTC functional assay still remains challenging. The assay efficiency is mainly restricted by low CTC count. In the previous chapter, we developed an integrated droplet device to encapsulate rare cells with high single-cell encapsulation efficiency. When we tried to apply this device on primary CTCs assay, we realized the developed device had some drawbacks to process the rare clinical sample.

First, the droplet size generated from the developed jetting device varies with cell size. Under jetting, the encapsulated cells are tightly packed in water and the size of cell-containing droplets depends heavily on cell size. As the droplet size varies, the amount of reagent loaded in every cell-containing droplet also differs, affecting downstream single-cell assay. This issue was subtle in the previous study because standard culture cell line has a more homogeneous size distribution. However, it became more serious for clinical samples, whose cell size is usually very heterogeneous compared with standard cultured cell lines. Secondly, droplets suffered from evaporation due to large surface-to-volume ratio. Cell-containing droplets produced under jetting was just 5 μm larger than the cells inside, so the total aqueous volume was small. As a result, cell-containing droplets evaporated fast and eventually collapsed during long-time observation (e.g. 1 to 2 hours). Based on these technical difficulties, we need to

find out a method to resolve the problems associated with low CTC count, droplet uniformity and droplet long-term stability.

4.1.4 Proposed technique and hypothesis

Here, a microfluidic droplet technology is purposed to study matrix metalloproteinase activity of individual cultured cancer cells, including cultured CTCs. In order to ensure the accuracy of functional assay, carefully-washed cancer cells are encapsulated with FRET-based MMP substrate into uniform droplets under drippling regime. Droplet size is large enough to sustain high cell viability and counter the evaporation issue for a long period. As cancer cells secrete active MMPs into the droplet environment, the fluorogenic substrate will be cleaved and produce increasing fluorescent signals, corresponding to the proteolytic activity of individual cancer cells. Tapered microwell device was applied to realize in-vitro expansion of circulating tumor cell for droplet-based assay [120]. In this way, the concentration of CTCs can be boosted to around 100 thousand per milliliter after 3-week culturing. The expanded CTC population could relieve the poor single-cell encapsulation problem. We hypothesized that we could observe brighter fluorescent signals for invasive and metastatic cancer cell lines due to their higher level of MMP activity. We then apply the developed system to study the MMP activity level of patient-derived circulating tumor cell samples to evaluate the potential of CTCs to extravasate from blood vessel and provide insights on disease status. The experimental

procedure of single cultured-CTC MMP assay is illustrated in the following figure 4.2.

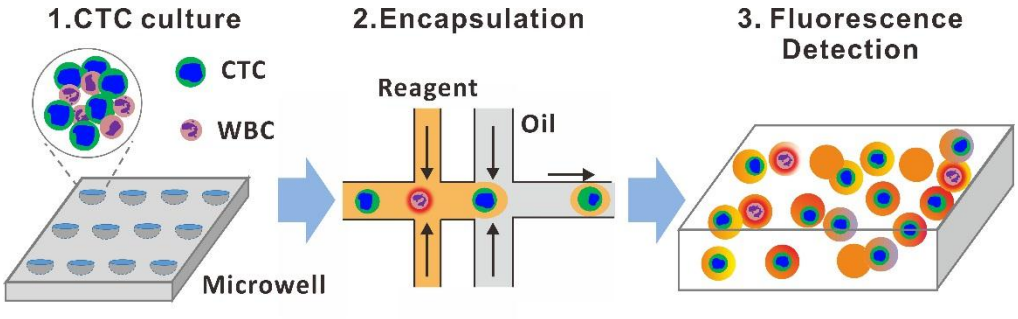

Figure 4.2 Schematics of droplet-based cultured-CTC MMP assay. Cultured CTCs are harvested from microwells and stained with CD-45 to distinguish WBC residues before they are encapsulated with MMP reagent into droplets. Fluorescence intensity of cell-containing droplets are measured after a certain period of incubation in an observation chamber.

4.2 Material and methods

4.2.1 Device design and fabrication

The main microfluidic device was a cross-flow droplet generator. It had three inlets for oil, cell solution and reagent, and one droplet outlet. The channel width and height were both 50 μm. Unlike the previous jetting project, droplets were produced under drippling mechanism. Therefore, the droplet size was similar to the channel dimension, about 50 to 60 μm. Droplet observation chamber was designed as a rectangular shape with 15mm length and 3 mm width and fabricated with a height of 50 μm. The total volume of the chamber was about 2.3 μL that may contain more than 2000 droplets as the volume of individual droplets was about 0.1 nL. Circular posts with 200 μm diameter were added

inside the observation chamber to prevent chamber collapse due to the low aspect ratio of chamber height to width. The device fabrication process was the same as described in Chapter 3, namely soft-lithography of polydimethylsiloxane (PDMS) using a SU-8 mold followed by an irreversible plasma bonding.

The tapered microwell design was used for circulating tumor cell (CTC) in-vitro culture. Each microwell had an elliptical opening of 250 × 150 μm. The slope profile was tapered to the microwell bottom. The microwell depth was about 150 μm. The 1st generation of the tapered microwell was fabricated on uncoated 60mm petri dishes (Becton Dickinson Corp, USA) using laser engraving/cutting system (VLS-2.3, Universal Laser System Inc, USA) [120]. The 2nd generation of microwell with better device uniformity and surface finishing was produced on PDMS with sophisticated soft-lithography technique [121]. The SU-8 mold was directly fabricated onto a chrome mask (Infinite Graphics, Singapore) with elliptical patterns. Firstly, a thick layer of SU-8 was coated on the chrome surface of the mask. Next, an opal diffusor glass (Edmund Optics Inc, USA) was attached to the other surface of the mask. UV shined through the opal diffusor glass and exposed onto the thick SU-8 layer. The diffused UV light created a hill-shape pattern with a slope on the SU-8 layer. After SU-8 development and hard-baking, the hill-shaped SU-8 mold can be used to produce PDMS microwell via soft-lithography. CTCs were directly cultured on the PDMS microwells under sterile condition.

4.2.2 Cancer cell line culture and preparation

Three commercially available human breast cell lines, MCF-7 (breast cancer cell), MCF-10A (normal breast epithelial cell) and MDA-MB-231 (breast cancer cell), were used to characterize device performance and protease activity of cultured cancer cells in this work. The MCF-7 cells (ATCC® HTB-22™, USA) and MDA-MB-231 cells (ATCC® HTB-22™, USA) were cultured in high-glucose Dulbecco's modified Eagle's medium (DMEM) (Invitrogen, USA) supplemented with 10% fetal bovine serum (FBS) (Invitrogen, USA) and 1% penicillin-streptomycin (Invitrogen, USA). The MCF-10A cells (ATCC® CRL-10317™, USA) were cultured in MEBM supplement with MEGM™ SingleQuot and cholera toxin (Lonza, Switzerland). The cells were cultured separately in T-25 flasks (ThermoFisher, USA) at 37 ℃ in a humidified atmosphere with 5% (v/v) CO_2 till 80% confluence. The cells were sub-cultivated two to three times a week with medium replaced every 48 hours. 0.01% trypsin and 5.3mM EDTA solution (Lonza, Switzerland) was used to harvest cells from culture flask. The trypsinization duration for MCF-7 and MDA-MB-231 was 5 minutes, but the duration for MCF-10A was 10 to 15 minutes because MCF-10A tended to attach flask surface more firmly.

For single-cell encapsulation experiment, the cultured cancer cells were diluted in 1x phosphate buffer saline (PBS) with 10% OptiPrep density gradient medium (Sigma, USA) to prevent cell precipitation during operation [66]. The

harvested cells were washed with PBS buffer thoroughly for 3 times to clean out contaminants in the cell solution or attached onto the cell membrane. For single-cell MMP assay experiment, cancer cells were synchronized using serum-free medium for at least 6 hours to minimize the fluctuation of MMP signal due to different cell cycles. Cell solution was always filtered using 40 μm stringer (Becton Dickinson, USA) to remove large cell clusters. The final cell concentration was adjusted to 1 million per ml with proper dilution. For cell viability evaluation, certain concentration of live/dead viability kit (ThermoFisher, USA) was added to cell solution according to the product instruction.

4.2.3 Circulating Tumor cell culture

Blood samples were obtained from different cancer patients. All patients gave their informed consent for inclusion in this study. The study of cultured CTCs was approved by our institutional review board and local ethics committee (DSRB reference 2012/00105, 2012/00979, 2010/00270 and 2010/00691). All blood specimens were collected in sterile EDTA-coated vacutainer tubes (Becton Dickinson, USA) and processed within 10 hours after blood withdrawal to reduce blood clotting and maintain cell viability. Whole blood was lysed with red blood cell (RBC) lysis buffer (Life Technologies, USA) for 5 minutes with gentle mixing, centrifuged to remove plasma and lyse RBC fragments, and then washed once with sterile PBS. All nucleated cells (CTC and white blood cells)

were re-suspended in fresh high-glucose DMEM with 10% FBS and 1% penicillin-streptomycin and seeded into the microwell device. The microwell device was rinsed and incubated with 70% ethanol for at least 15 minutes for sterilization before cell sample seeding.

Cells were kept at 37 ℃ in 5% CO_2 and 1% O_2 under humidified condition. The hypoxia condition was to mimic the realistic microenvironment of tumor niche [122].The culture medium was replaced every 2 to 3 days with minimum disturbance to the microwells to avoid cell loss. Cultured CTCs tended to form cluster during the culture process. Clusters were harvested and dissociated with pipetting for 3 minutes with 0.01% trypsin and 5.3mM EDTA.

As reported before, small population of residual leukocytes were found from the cultured CTC population [120]. Hence, cells harvested from microwell culture were stained with phycoerythrin (PE) conjugated CD45 antibody maker (1:10 ratio, Miltenyi Biotec Asia Pacific, Singapore) for 15 minutes on ice to differentiate leukocytes from cultured CTCs.

4.2.4 Device operation

In experiment, cell solution, reagent and oil (HFE-7500, 3M, USA) were pumped into the microfluidic droplet generator at different flow rates using syringe pumps (Harvard Apparatus, USA). The microfluidic device was mounted on an inverted phase contrast microscope (Olympus IX71, Japan) equipped with a high speed camera (Phantom, USA). The droplet generation

process was monitored and recorded using the high speed camera. The captured videos were later analyzed using ImageJ software (https://imagej.nih.gov/ij/, National Institute of Health, USA). Collected droplets could be incubated in fabricated observation chamber at room temperature. Fluorescent images of cell-containing droplets were captured by another epi-fluorescent microscope equipped with a 12-bit EMCCD camera (iXon^{EM} + 885, Andor Technology, USA). Matrix metalloproteinase activity were assayed using FRET-based substrate Pepdab010 (Biozyme Inc, USA), which is sensitive to MMP-9 and ADAM-17 [62]. The substrate was designed with a fluorescent quencher and a fluorophore at two different ends of a specially-sequenced peptide. The fluorescent images were acquired using Metamorph® software (Molecular Devices, USA) and analyzed using ImageJ (https://imagej.nih.gov/ij/, National Institute of Health, USA). The MMP signals of single cells were calculated by subtracting the average background intensity of empty droplets from the individual intensity of cell-containing droplets.

4.3 Results and discussion

4.3.1 Change in oil operation

In this project, droplet jetting was not required as the single-cell encapsulation efficiency for rare clinical sample was improved by in-vitro culture rather than size-based differentiation. Therefore, previously-used mineral oil was replaced by fluorocarbon oil HFE-7500, which was a more commonly-used oil in single-

cell study. Adopting new oil phase brought some changes on the droplet system due to distinct physical properties.

Firstly, the dynamic viscosity of HFE-7500 fluorocarbon oil is 7.7×10^{-4} Pa s [123], which is even lower than the dynamic viscosity of water. Such a low viscosity made the operation of microfluidic device relatively easy. Oil fluid could respond to flow rate adjustment almost spontaneously so that steady flow condition could be achieved quickly. However, low viscosity made droplet generation more difficult than before, as the friction force between water and fluorocarbon oil became weak. The weak interfacial friction force led to a reduced shearing effect on the water phase, which became less likely to be broken into mono-dispersed droplets. Therefore, the flow rate of fluorocarbon oil was always kept at least two times higher than the flow rate of water phase in order to have enough pinching effect at the cross-flow junction. Meanwhile, the surface wetting of the device was also important. The PDMS surface must recover its hydrophobicity after plasma bonding to effectively prevent water solution from sticking onto the device surface.

Secondly, the fluorocarbon oil has a low boiling temperature and a fast evaporation rate, compared with mineral oil. Oil phase evaporation could cause problems in long-term droplet signal detection because of droplet location shift, shape change, and coalescence. In order to slow the evaporation process down, once filled with droplets, the observation chamber was closed with double

clamps at inlet and outlet tubing. The connection ports were also sealed with liquid PDMS.

4.3.2 Fluorophore leaking prevention

Apart from change in oil operation, new problem of fluorescence leaking occurred in the static droplet detection process after using fluorocarbon oil. In preliminary test using diluted trypsin and MMP substrate, fluorescent signals leaked from water droplets into ambient oil after 40-minute stationary incubation in the observation chamber as shown in the figure 4.3(A). The fluorogenic MMP substrate we used in the new droplet system were the same as what we used for the previous project. Besides, the same fluorocarbon oil was successfully used for droplet-based fluorescent detection [124]. So the investigation was focused on the change of droplet configuration.

Soon, we found that the root cause of fluorescence leaking was the interaction between plasma treated PMDS layer and droplets. Unlike in the previous jetting project where droplets were small, the droplet size was about 60 μm. As the observation chamber height was 50 μm, all droplets were actually squeezed by the chamber ceiling and floor. As a result, each droplet had a large contact area with PDMS chamber surfaces. If the hydrophobicity of PDMS surface was not fully recovered from plasma treatment, fluorescent molecules could stick to the activated PMDS surface and then enter the surrounding oil phase.

Results from water contact angle tests later confirmed that overnight baking at 70 ℃, a protocol established from the previous project, could not fully recover the hydrophobicity of plasma-treated PDMS surface as a water drop spread out on the PDMS surface with a small contact angle. In order to accelerate the recovery process, the PDMS baking temperature was increased to 170 ℃ since higher temperature facilitated the diffusion of low molecular weight silicone fluid from the PDMS bulk to the PDMS surface to regain surface hydrophobicity [125]. The baking temperature should never exceed 250 ℃ because such high temperature could break the polymer bond of PDMS and cause cracks.

A verification test was conducted using the observation chamber prepared under overnight PDMS baking at 170 ℃. Two types of droplets were generated and mixed together in the observation chamber. The first type of droplets contained 0.1x trypsin and MMP substrate as positive control and the second type of droplets contained PBS and MMP substrate as negative control. Positive control droplets had high fluorescence intensity as trypsin molecules cleaved the substrate at very high rate. In contrast, negative control droplets had minimum fluorescence intensity. By monitoring the change of fluorescence intensity of positive and negative control droplets and oil background over time, we could clearly observe whether fluorophore leaking occurred among positive droplets, negative droplets and oil solution.

Over 70 minutes, we did not observe any signs of fluorophore leaking as shown in Figure 4.3(B). The quantified fluorescence intensity plotted in Figure 4.3(C) demonstrated the intensity of positive droplets decreased a bit over time while that of negative droplets and oil background did not increase. The reduction of fluorescence intensity of positive droplets might be caused by photo-bleaching, which was frequently observed other experiments before [126]. Based on this result, it was proved that baking the PDMS observation chamber at 170 ℃ for overnight could effectively prevent fluorophore leaking for long-term stationary fluorescence detection.

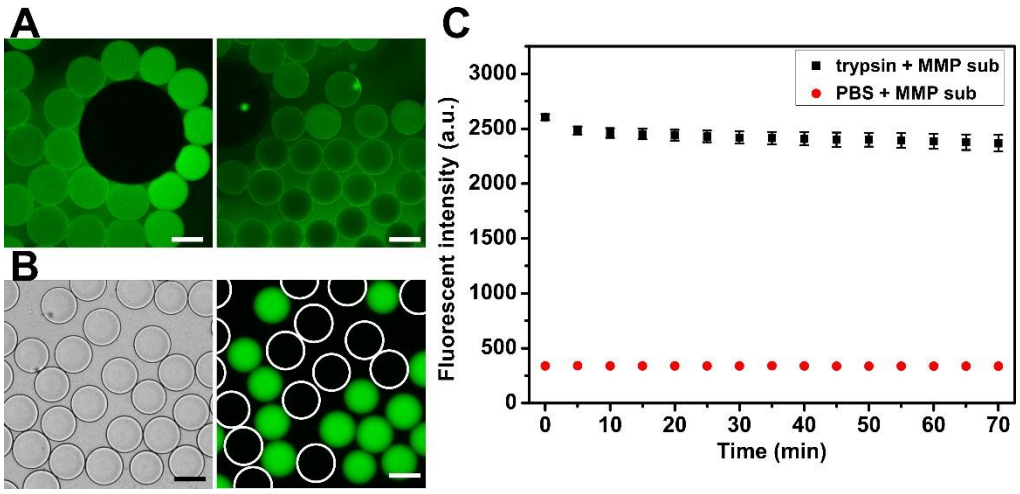

Figure 4.3 (A) Two fluorescent images showing fluorescent leaking where oil medium demonstrated fluorescence. (B) *left* brightfield image of both positive (trypsin + substrate) and negative (PBS + substrate) control droplets mixed together in an observation chamber that was baked at 170 ℃ overnight; *right* corresponding fluorescent image after 1-hour incubation showing only positive droplets had fluorescent signals. (C) Quantified fluorescence intensity of mixed positive and negative droplets over 70 minutes, proving no fluorescent leaking under the new device fabrication scheme. (Scale bars = 50 μm)

4.3.3 Single-cell encapsulation characterization

The single-cell encapsulation efficiency of the droplet generator was characterized using MDA-MB-231 cells. As no intervention was conducted to enhance the encapsulation efficiency, the single-cell encapsulation rate could be predicted using Poisson distribution as explained in Chapter 3. The size of droplets was 61 ±3.5 μm, corresponding to about 0.1 nL of volume. When the input cell concentration was 1 million per mL ($\lambda = 0.1$), the measured single cell encapsulation efficiency was about 7.8 ± 1.3%; when the input cell concentration was 4 million per mL ($\lambda = 0.4$), the measured single cell encapsulation efficiency increased to 19.8 ± 3.4%. The quantified single-cell rate based on experiment demonstrated a good agreement with Poisson model as shown in Figure 4.4. When cultured CTC sample was processed, the single-cell encapsulation efficiency ranged from 1 to 5% since the sample concentration varied from 100k to 500k cells per mL.

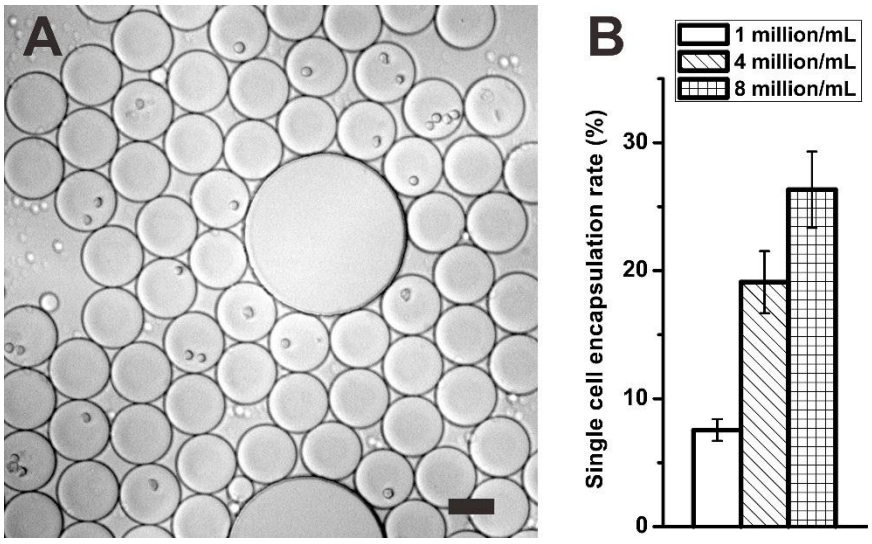

Figure 4.4 (A) Droplet encapsulation image of MDA-MB-231 cells with the concentration of 4 million per mL, where the majority of droplets are empty.

(Scale bar = 50 μm) (B) Measured single-cell encapsulation efficiency under three different cell concentrations. As no intervention is added to improve the encapsulation efficiency, the results simply follow Poisson distribution. (Sample size = 1102 droplets)

4.3.4 Viability characterization of cell in droplet

Viability test was conducted on freshly harvested MCF-7, MCF-10A and MDA-MB-231 cells to investigate the survival rate over 2 hours. The size of droplet generated under drippling was about 60 μm in diameter, which was much larger than the cell size. This large droplet volume provided a favorable environment to extend single-cell survival because the droplets carried a large number of nutrients. In addition, the accumulation of metabolites inside large droplets was slowed to have few adverse effects on cells. Moreover, as the oxygen solubility in fluorocarbon oil is much higher than mineral oil, the problem of lack of oxygen during cell incubation would not appear [127]. The single-cell viability across three cell lines are presented in figure 4.5. We could see the 1-hour survival rate was above 90% for all three cell lines. The survival rate reduced by 5 to 10% for one more hour of incubation. MCF-10A cells had the largest survival rate drop over the 2-hour monitoring. It could be because MCF-10A cells were less resilient than the two breast carcinoma cell lines and they needed to attach to a surface in order to survive for a longer time

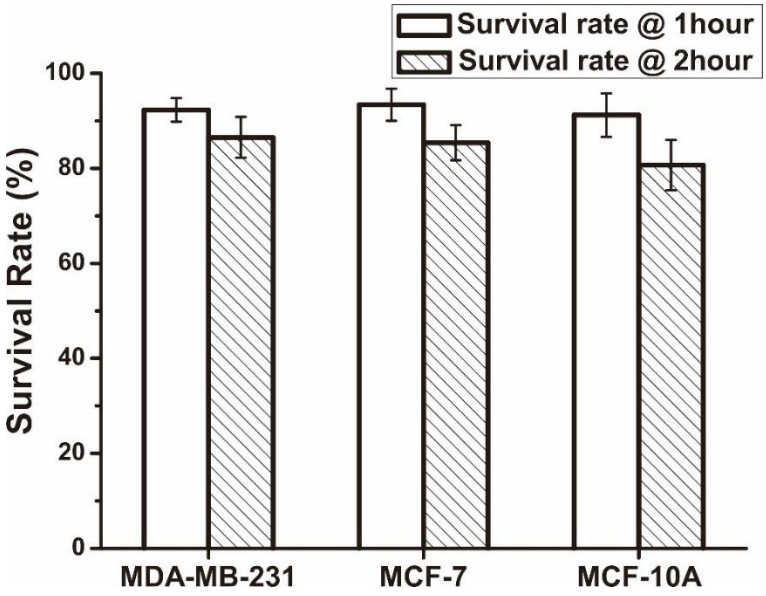

Figure 4.5 Survival rate of three breast epithelial cell lines in 50 μm droplets after 1-hour and 2-hour incubation. Approximately, over 90% cells remain viable for 1-hour incubation and the survival rate decreases by 5% for another 1-hour incubation. Total sample size = 346 cells.

4.3.5 Time-lapse MMP functional assay on single cells

MDA-MB-231 cells were used to investigate the dynamics of single-cell MMP activity over 1 hour. The harvested MDA-MB-231 cells were carefully washed with PBS to remove potential contaminants on the cell surface. Washed cells were encapsulated into droplets with 20 μM MMP substrate. As the protease produced by cancer cells cleaved the peptide bridge of fluorogenic substrate, the fluorophores were released from quenchers leading to an increase of fluorescence intensity.

The time-lapse single-cell assay results are presented in the Figure 4.6. The fluorescent signals of cell-containing droplets had an average increase of 270 a.u. for 70 min incubation with large standard deviation due to cell heterogeneity. In contrast, the signals of empty droplets had an average increase

of 50 a.u. with much smaller standard deviation. The increasing fluorescent signal of empty droplets were caused by hydrolysis of peptide bridge, which was much slower than the proteolytic cleavage by specific MMP.

During the time-lapse detection, it was found that the cells signal generated from cultured cancer cells did not reach the obvious plateau status, which was observed in the previous jetting project described in Chapter 3. This might be because the cell-friendly environment in the current droplet system did not impede the protease production of cancer cells within the observation period. Moreover, we did not observe any sudden onset of fluorescence intensity increase for cell-containing droplets, except for a small group of unhealthy cells that were undergoing apoptosis during observation. Once a cell underwent apoptosis, the membrane integrity would be compromised resulting in leaking intracellular proteases into ambient environment and abrupt increase of fluorescent signals.

Because of no saturation and sudden change of fluorescent signal, we found the fluorescent intensities of individual cells after 1-hour incubation correlated well with the increasing slope of individual signal profiles. Based on this observation, we decided to replace time-lapse detection with end-point detection for subsequent cell assays. This is because we can observe a large group of droplets at the same time without considering droplet movement in the observation chamber when doing 1-hour end-point detection. On the contrary, the time-lapse fluorescent detection was more difficult because droplets could move around

during the 1-hour observation which increased the difficulty in tracking the fluorescent change of individual droplets at every time point. In order to obtain distinguishable fluorescent signals from cell containing droplets, the incubation time was set 1 hour. At 1-hour time point, the signals from single cancer cells were high enough to be discriminated from the background signals of empty droplets while the majority of the cells still remained viable and healthy. In the subsequent experiment, the 1-hour fluorescent signals from cell-containing droplets were obtained by subtracting the individual intensity of cell-containing droplets by the average intensity of empty droplets.

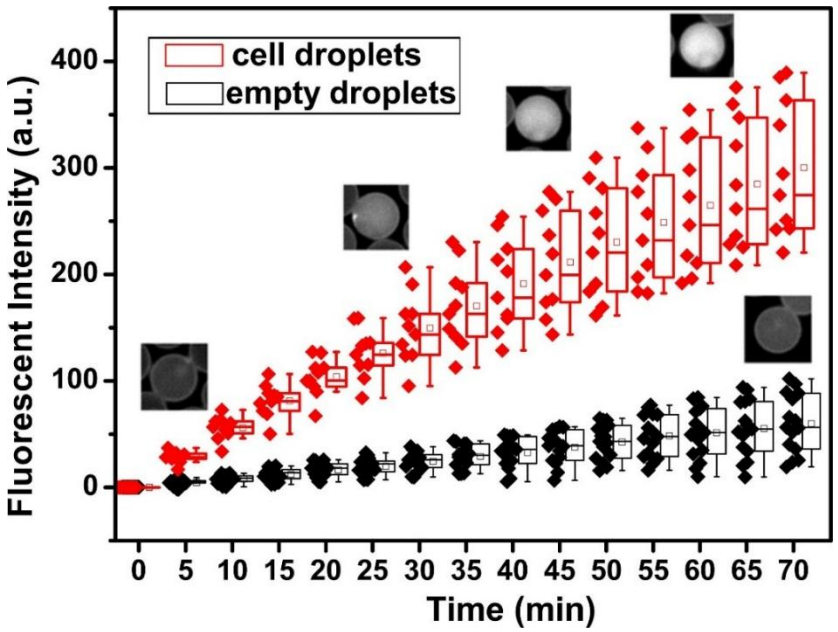

Figure 4.6 Time-lapse fluorescent signals from cell-containing droplets and empty droplets over 70 minutes. Cell-containing droplets have a large increase in the fluorescence intensity with a big standard deviation compared with empty droplets. Insets: fluorescent images of cell-containing and empty droplets at various time points.

4.3.6 End-point assay on various cell lines

All three cultured cell lines, MCF-7, MCF-10A and MDA-MB-231, were characterized using the single-cell protease assay platform. The end-point detection was carried out after 1-hour droplet incubation at room temperature. Based on the results shown in Figure 4.7, we can easily observe the inherent cell heterogeneity among the same types of cultured cell line. Even though those cells within one cell line were cultured under the same condition and synchronized before single-cell assay, their phenotypes in terms of protease activity still differed from each other.

As shown in Figure 4.7 (A), MDA-MB-231 cells had a signal intensity of 129.66 ± 52.40 a.u.; MCF-7 cells had a signal intensity of 65.02 ± 37.53 a.u. and MCF-10A cells had a signal intensity of 48.34 ± 23.51 a.u. Among all three cell lines, MDA-MB-231 had the greatest standard deviation of the fluorescent signals, suggesting that MDA-MB-231 breast cancer cells had the most diverse proteolytic activities at single-cell level. Some MDA-MB-231 cells had weak MMP secretion corresponding to the fluorescence intensity around 50 a.u., but some other cells had a much stronger MMP activity with the fluorescence intensity above 200 a.u. Provided MDA-MB-231 cell line was derived from an aggressive breast cancer tissue (triple-negative type) and had strong potential to metastasize [128], we speculated that aggressive cancer types are generally poorly-differentiated and have a highly heterogeneous cell behavior in terms of proteolytic activity.

Apart from the heterogeneity within a cell line, we also compared the overall fluorescent signals obtained from all three cell lines. Interestingly, the average fluorescence intensity had a decreasing trend, from MDA-MB-231 to MCF-7 and MCF-10A. T-tests results revealed that the intensity level of the metastatic MDA-MB-231 cells was significantly higher than that of the less invasive MCF-7 cells, which was also significantly higher than that of the breast epithelial MCF-10A cells as shown in Figure 4.7. As MMPs are essential enzymes to degrade basal membrane and promote angiogenesis, they have been demonstrated with elevated expression among invasive cancer cells and have been chosen as one of the biomarkers to indicate cancer invasiveness. High expression level of MMP also correlates low epithelial cell adhesion molecule (EpCAM) expression on the cell membrane since MMP could cleave EpCAM at the extracellular site transforming the cancer cells toward mesenchymal type. Previous studies have proven MDA-MB-231 cells generally have low EpCAM expression and undergo epithelial-mesenchymal transition (EMT) to become more mesenchymal-like cells [129].

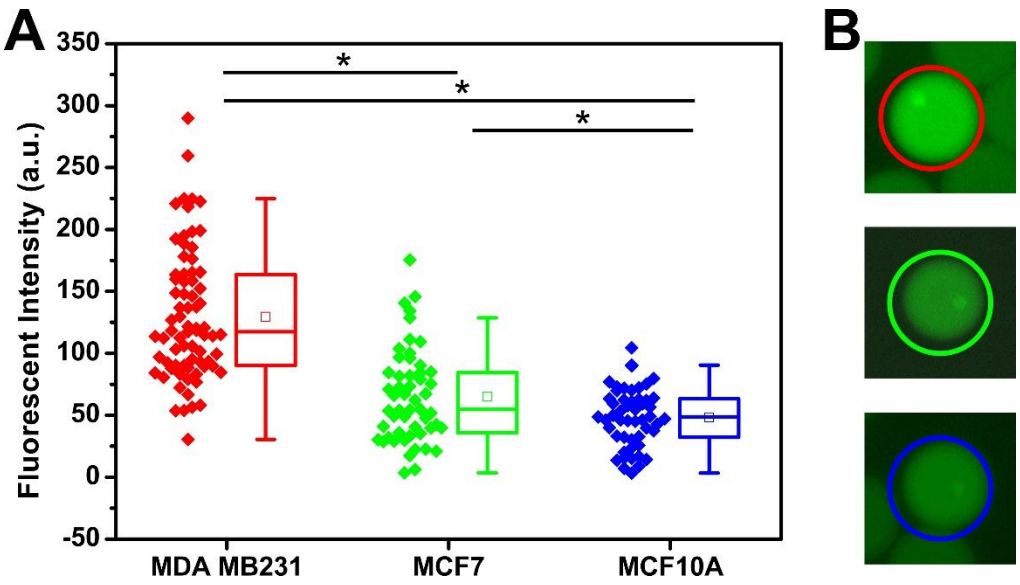

Figure 4.7 (A) Single-cell MMP assay results on MDA-MB-231, MCF-7 and MCF-10A cell lines obtained after 1-hour incubation. Three cultured cell lines are significant different from each other (asterisk refers to p-value <0.01) Total sample size = 178 cells. (B) Fluorescent images of different cultured cells in the droplets (red circle: MDA-MB-231; green circle: MCF-7 and blue circle: MCF-10A).

4.3.7 Single cultured CTC MMP functional assay

Next, we performed single-cell MMP functional assay on cultured CTC samples obtained from breast cancer patients. They were carefully characterized using nuclear-cytoplasmic ratio and immunostaining of cytokeratin (CK) and CD-45 as described in the previous work [120]. Clusters containing an increasing number of cytokeratin-positive (CK+) cells appeared after 2 weeks, while most blood cells disappeared with time. After culturing 2 to 3 weeks, CTC sample were harvested from the microwell culture device. Clusters of cultured CTCs were broken by repeated pipetting. As the harvested cancer cells were always present with some WBC residues, such as macrophages and monocytes, phycoerythrin (PE) conjugated CD45 antibody was used to distinguish the

residual WBCs from CTCs [130]. Only droplet signals from CD45-negative cells were considered as MMP activity of cultured CTCs.

Before performing end-point assay, we first conducted the time-lapse study on cultured CTCs to acquire the single-cell profile of MMP activities over 50 minutes. The measured results assured that no fluorescence saturation and sudden signal change happened during the detection period, similar to the results of cell lines, as shown in Figure 4.8(A). Therefore, the slope of individual MMP activity could be represented by the final intensity at 1-hour time point.

Then, the 1-hour end-time-point assay was performed on more than 300 cultured CTCs obtained from a breast cancer patient, who was at 2nd time point in the treatment course. We found the overall MMP activity level of single cultured CTCs demonstrated a spindle pattern with an average intensity of 59.2 a.u. and a standard deviation of 16.3 a.u. as shown in figure 4.8(B). About 3% of cultured CTCs had a fluorescence intensity over 100 a.u., which correlated with intensive MMP activity inside the droplets. Meanwhile, the co-existing WBCs in cultured CTC sample demonstrated an average fluorescence intensity of 47.2 a.u. and a standard deviation of 15.4 a.u. No cultured WBCs had a fluorescence intensity over 100 a.u. Most of MMP activities of WBC residues were below 80 a.u. The average fluorescence intensity of empty droplets as background signal was about 21.7 a.u.

Another batch of cultured CTCs was applied to the single-cell MMP assay. The CTCs were obtained from another breast cancer patient, who was also at 2nd

time point in the treatment course. The overall MMP activity level of single cultured CTCs also demonstrated a spindle pattern with an average intensity of 47.5 a.u. and a standard deviation of 20.4 a.u. as shown in figure 4.8(C). However, more cultured CTCs from this patient demonstrated low MMP activity level as 78% of the cultured CTCs had a fluorescence intensity below 60 a.u. This result may indicate this cancer patient responded quite well to the cancer treatment as the overall MMP secretion from CTCs was kept at low level. Very few cultured CTCs demonstrated high MMP activity with the fluorescence intensity over 100 a.u., which may be due to their resistance to the treatment. Meanwhile, the co-existing WBCs in this cultured CTC sample had an average fluorescence intensity of 34.9 a.u. and a standard deviation of 18.3 a.u. The average fluorescence intensity of empty droplets as background signal was about 18.4 a.u., which was comparable to the previous assay.

In addition, we studied the MMP activity level on a batch of cultured CTCs retrieved from a lung cancer patient. The pathological mechanisms of lung cancer and breast cancer are different, so are their MMP activity levels. The cultured lung CTCs displaced a low MMP activity level with an average intensity of 33.3 a.u. and a standard deviation of 9.6 a.u. as shown in Figure 4.8 (D). No cultured CTC had a fluorescence intensity above 100 a.u. Moreover, many leukocytes were found in the cultured sample, which had a very diverse MMP activities.

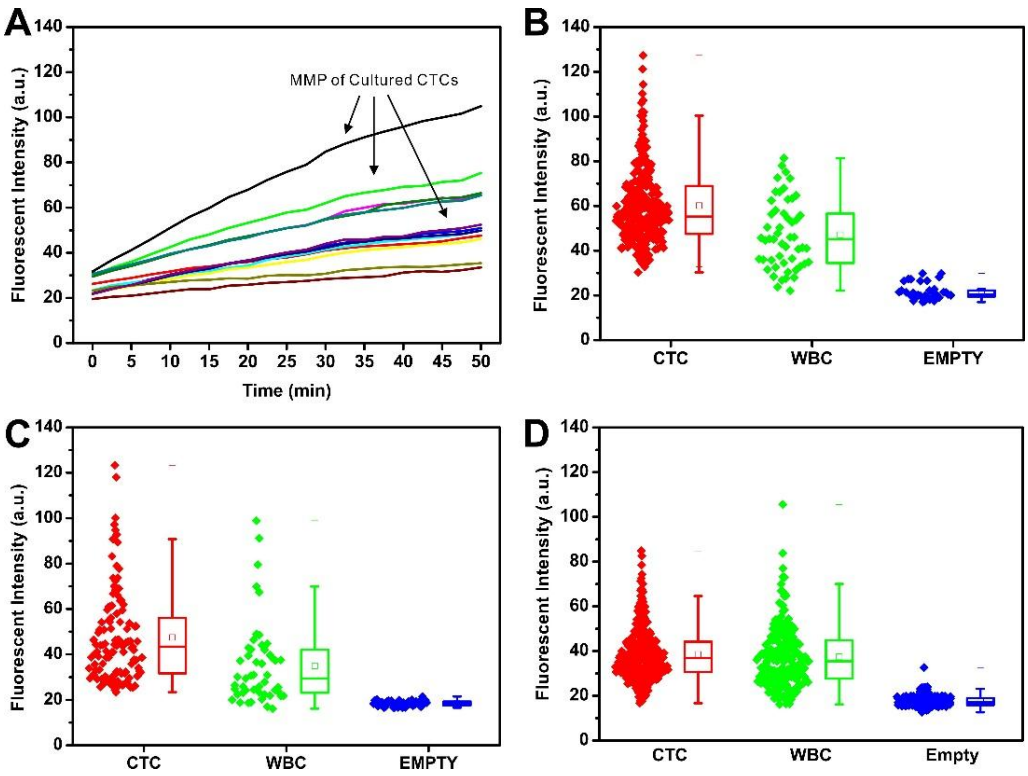

Figure 4.8 (A) Time-lapse MMP activity signals from 12 cultured breast CTCs over 50 minutes. (B) and (C) two profiles of end-point MMP activity signals from two cultured breast CTC samples after 1-hour incubation. Although both samples were retrieved from breast cancer patients at the same treatment stage, their MMP activity profiles were different due to distinct responses to treatment. (D) End-point MMP activity signals from a cultured lung CTC sample, demonstrating a low activity level from CTCs and the presence of a large number of leukocytes. (Total number of cultured CTCs = 634, total number of WBCs = 343)

4.4 Conclusions

In this chapter, we demonstrated the use of MMP functional assay on both cultured cell lines and cultured CTC samples using a droplet microfluidic device. The approach was capable of quantifying MMP activities of single viable cancer cells suspended in water-in-oil droplets rapidly and efficiently. The high sensitivity of the technique enabled the detection of distinct MMP activities among various cell sample. It was observed that highly metastatic cancer cells

(MDA-MB-231) have more intensive MMP activities than less invasive cells (MCF-7 and MCF-10A), suggesting MMP activity could be utilized to evaluate single-cell invasiveness. The single-cell MMP assay on cultured CTCs, obtained from cancer patients undergoing treatments, demonstrated diverse MMP profiles even though patients were at the same stage of treatments. The obtained single-cell MMP activity profile could shed insights on the functional heterogeneity among clinical CTC samples, and eventually provide treatment surveillance and guide development of personalized cancer treatment strategies.

Chapter 5. Single leukocyte protease study using integrated droplet platform

5.1 Introduction

In the single-cell functional assay of cultured circulating tumor cells (CTCs) described in Chapter 4, white blood cells (WBCs) were always found present in the cultured CTC samples as contaminants [120]. The proteolytic activity of WBCs was rather similar to cultured CTCs after two-week hypoxia culturing. Literatures have suggested that proteolytic activity, especially matrix metalloproteinase (MMP) activity, of WBCs are related to cell migration, inflammation response, immune defense and other diseases [131-133]. However, ensemble measurement of WBCs may be inaccurate because of the high cellular heterogeneity. Indeed, leukocyte heterogeneity has been reported critical to therapeutic outcomes [134]. Therefore, it would be of our interests to study the functional heterogeneity of WBCs at single cell level. In the following chapter, we will explore how to accurately study protease activity of single leukocytes using an integrated droplet microfluidic device.

5.1.1 Background of single leukocyte study

Leukocyte, also known as white blood cell, is an important component of hematological cells responsible to immune defense against foreign invaders. As reviewed in Chapter 2, leukocyte plays an important role in many acute and

chronic diseases, such as sepsis, asthma and cancer [135, 136]. Direct functional assay of leukocytes could offer rapid evaluation of patient's immune function and disease statues. However, it is rather difficult to achieve due to the highly heterogeneous nature of leukocytes.

The current analytical methods for leukocyte study includes peripheral blood smear and flow cytometry. They mainly measure morphological property and surface biomarker expression of individual leukocytes [137, 138]. These methods are insufficient to measure protein secretion of individual cells as well as investigate the functional heterogeneity of patients' immune capability.

Recently, microfluidic technologies have been widely applied to study single cells, including leukocytes. For example, individual leukocyte differentiation has been analyzed using single-cell impedance microfluidic cytometry [139, 140]. In addition, the measurement of cytokine production of single T lymphocytes was also achieved in gel particle with the help of ELISA-based bead assay [141]. However, measurement of comprehensive biochemical signals such as protease secretion still remains challenging.

5.1.2 Difficulty on single leukocyte functional study

Droplet microfluidics have recently emerged as a versatile tool for single-cell analysis as discussed in Chapter 2, 3 and 4. Although contamination across droplets could be greatly controlled by isolating cells within droplets, pre-

encapsulation contamination could still occur for highly secretion-active cells, such as leukocytes [142]. When leukocytes are stored in a syringe before encapsulation, a lot of soluble contaminant biomolecules are secreted into the solution and then compartmentalized into individual droplets randomly. These contaminant biomolecules unavoidably deteriorate the accuracy of downstream analysis as shown in Figure 5.1. Even worse, majority of leukocytes have a limited life time (e.g. two to three days). As a result, some leukocytes may die in the syringe and release significant number of intracellular biomolecules into the surrounding solution, limiting long-term robustness of droplet based single leukocyte analysis.

Dilution of cell solution might be helpful to reduce the contaminant concentration but this would inevitably reduce the cell concentration and decrease the single-cell encapsulation efficiency. Therefore, washing step before encapsulation becomes essential for single leukocyte study.

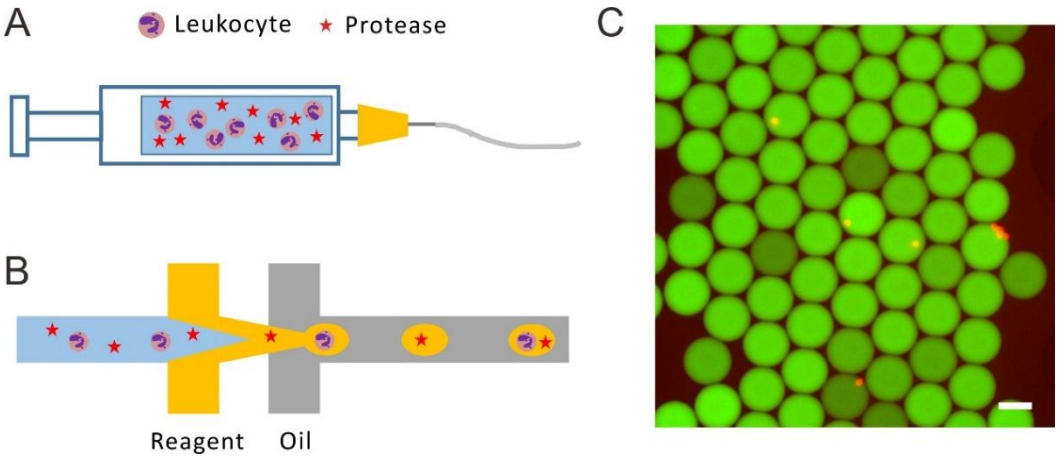

Figure 5.1 (A) and (B) Illustrations of a commonly-used cell injection method for cell encapsulation. Millions of cells continually release biomolecules into the mixed solution while storing in the syringe. These free biomolecules, as contaminants, are encapsulated into droplets randomly, affecting downstream

analysis. (C) Fluorescent image of droplets produced from leukocyte solution using the method described in (A) and (B). Due to the pre-encapsulation contamination, most of empty droplets became bright and undistinguishable from cell-containing droplets (green: matrix metalloproteinase signal; red: CD-45 stained WBC) (scale bar = 50 μm).

5.1.3 State-of-the-art for microfluidic cell washing

Conventional washing method requiring centrifugation and cell re-suspension is difficult to be achieved in microfluidics. Moreover, live leukocytes would still continually release various proteins and cause contamination even after washing. Hence, an in-situ microfluidic washing method is necessary for accurate and robust single leukocyte functional assay.

Inertial microfluidics has been widely deployed to purify cell samples from small debris [143-145]. More recently, Dudani demonstrated a rapid inertial solution exchange method to enrich microvesicles from acellular contaminants using antibody-coated polystyrene beads [146]. Essentially, the method was to separate large antibody-coated beads (20 μm) with captured exosomes and small acellular contaminants (<5 μm) by focusing them at different laminar positions. However, the inertial microfluidic methods are unable to resolve biomolecular contamination because the contaminant size is at nanometer scale.

Magnetic particle-based droplet washing has also been demonstrated to extract assay target from a contaminated droplet to a clean droplet for better detection resolution and immuno-staining [147]. Nevertheless, the dependence of antibody binding limits the downstream application as the binding could alter

the cell property and is irreversible. Furthermore, the usage of antibody largely increases the cost for each assay.

Chen and his colleagues proposed to use laminar flow and side-based sorting to achieve single leukocyte on-chip immune-staining [148]. Based on their measurement, the excessive antibody added in the system could be effectively washed away without contributing to the background fluorescence intensity. Similar design could be leveraged to achieve noise-free single leukocytes proteolytic assay.

5.1.4 Proposed technique and hypothesis

Here, an integrated droplet microfluidic device is proposed to study protease activity of individual leukocytes with solving the high pre-encapsulation contamination issue encountered in direct assay of fresh leukocytes. The microfluidic device consists of an upstream cell guiding array to purify leukocytes from a contaminated solution and a downstream droplet generator to compartmentalize individual purified cells into droplets for subsequent analysis. We hypothesize that we could suppress the pre-encapsulation contamination, reduce the false readouts and hereby improve the accuracy of cell-containing droplets using the developed device. We could apply the device to study functional heterogeneity among fresh leukocytes at naïve status and probe diverse response of individual leukocytes upon drug stimulation.

5.2 Materials and methods

5.2.1 Device design

The microfluidic device consisted of an upstream cell guiding array and a downstream cross-flow droplet generator as shown in Figure 5.2. Buffer and cell solution inlets were located at the same side of cell guiding array. The ratio of inlet width for buffer and cell solution was maintained at 1:1. The cell guiding array was 2.6 cm long and 800 μm wide with circular micropillars inside. The circular micropillars array was designed based on deterministic lateral displacement (DLD) design as discussed in Chapter 3. The pillar diameter and pillar gap was set 30 μm, which was sufficiently large for leukocytes to pass through. The row shift distance was set 1.5 μm. The resulting separation threshold was 10 μm approximately. Since the size of leukocyte is about 12 μm, the cells could be effectively deflected from original solution and enter clean buffer solution. At the end of DLD guiding array, the bifurcation point was set at 180 μm away from channel wall near the buffer solution side to prevent contaminant diffusing into droplet branch. The entrance width of waste channel is 620 μm. In this way, after passing through the cell guiding array, most of fluid would enter the waste outlet and only a small fraction of it would enter the droplet generator.

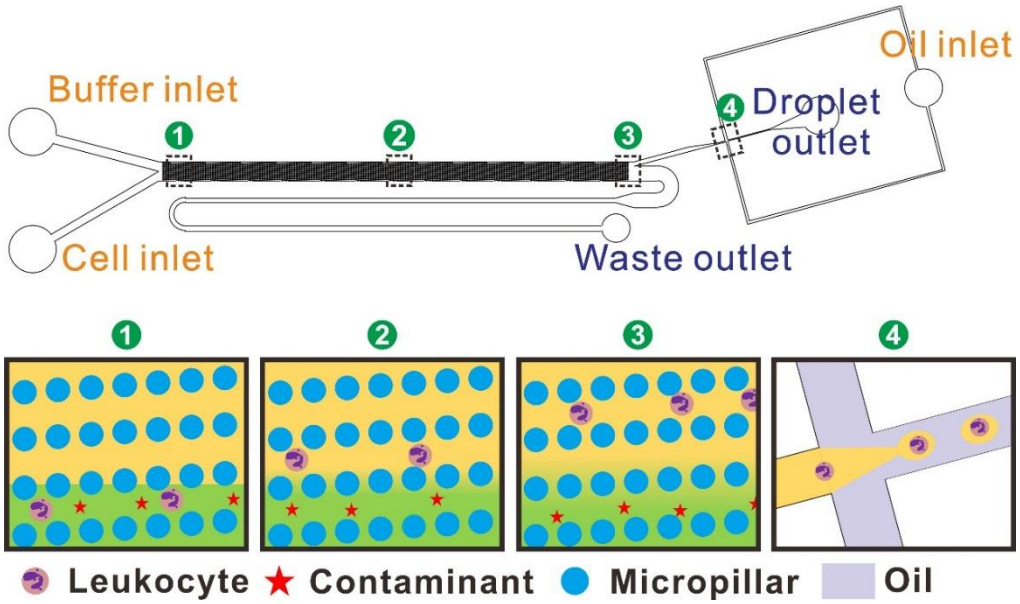

Figure 5.2 Device schematics showing an integration of a cell washing array and a droplet generator. Insets ① to ④ illustrate the flow conditions at the individual device positions. At ①, cells solution flows with buffer solution in parallel. At ② and ③, cells are gradually diverted away from the original cell solution while contaminants are still confined in the original solution due to laminar flow. At ④, washed cells are immediately encapsulated at the droplet generator with minimum level of contamination.

5.2.2 Device fabrication

The devices were fabricated in polydimethylsiloxane (PDMS) (Dow Corning, USA) using standard soft-lithographic microfabrication techniques described in previous chapters. In this work, cleaned PDMS device was irreversibly bonded to a PDMS sheet which was prepared by casting PDMS into a Petri dish. After plasma bonding, the device was baked at 170 ºC, instead of 70 ºC, on a hotplate for overnight. The reason to incubate the device at such a high temperature is to recover the hydrophobicity of fabricated device, especially near the droplet generator [125]. Otherwise, buffer solution flushed from the cell guiding array would stick to the channel wall at the droplet generation junction and could not

be compartmentalized by oil solution to form monodispersed droplets.

5.2.3 WBC retrieval from whole blood

Fresh leukocytes were retrieved from whole blood of healthy donors via red blood cell (RBC) lysis [149]. Whole blood was firstly added to pre-warmed RBC lysis buffer (eBioscience, USA) with a volume ratio of 1:9 and then incubated in water bath at 37 ºC for 5 minutes. The lysed blood was centrifuged at 1200 rpm for 5 minutes. The resulting cell pellet, consisting of leukocytes and some RBC debris, was washed once with PBS carefully. The washed cells were then re-suspended in a buffer solution containing 1% bovine serum albumin (BSA) (ThermoFisher Scientific, USA), 0.1% Poloxamer 188 (Sigma Aldrich, USA) and 20% OptiPrep density gradient medium (Sigma Aldrich, USA). The addition of Poloxamer was to prevent leukocytes from sticking to microfluidic device or tubing during experiment [150] and the addition of density gradient was to avoid cell sedimentation due to gravitational force [73]. For cell washing experiment, leukocytes were stained with Hoechst nucleus stain (ThermoFisher Scientific, USA) for cell visualization under high speed camera. For leukocyte viability test and MMP secretion assay, propidium iodide (PI) dead stain (ThermoFisher Scientific, USA) was applied on fresh leukocytes to indicate viability of individual cells. Before cell encapsulation experiment, the stained leukocyte solution was always filtered with 20 μm stringer (Becton Dickinson, USA) to remove large cell aggregation and fibronectin clots formed

during storage. The concentration of stained leukocytes was diluted below 500 k/mL before injecting cells into microfluidic device. Higher cell concentration was likely to cause device clogging.

5.2.4 Device operation

Before testing, the microfluidic device was primed with 70% ethanol for 1 minute in order to make sure no air bubble was trapped in the channel. Next, the device was flashed with complete buffer solution (with BSA, Poloxamer and OptiPrep) for 5 minutes. After washing, the cell solution, PBS buffer and fluorocarbon oil (HFE-7500) (3M, USA) were pumped into the microfluidic device using syringe pump (Harvard Apparatus, USA). The PBS buffer was changed into MMP substrate solution in single leukocyte functional assay experiment. The initial flow rate of oil solution was kept low compared with the cell and buffer solutions. This was to prevent oil from back-flowing into the cell guiding array. The microfluidic devices were mounted on an inverted microscope (Olympus IX81, Japan) equipped with a high speed camera (Phantom, USA) for flow investigation. The droplets stored in observation chamber were imaged under another epi-fluorescent microscope (Olympus IX83, Japan) equipped with a CCD camera (Retiga 2000R, QImaging, Canada). High speed videos and fluorescent images captured from the integrated device and observation chamber were then analyzed using ImageJ® software (https://imagej.nih.gov/ij/, National Institute of Health, USA). For viability

evaluation, the fluorescent images of nucleus staining (blue) and dead staining (red) was converted into binary images by thresholding with Otsu filter. The resulting images was then counted using the "analyze particle" function of ImageJ® with pre-defined cell size range. The numbers of particles obtained from nucleus and dead staining images were regarded as total cell number and dead cell number.

5.2.5 Immunofluorescence staining and FACS analysis

Leukocytes extraction efficiency of the device and composition of retrieved leukocytes were measured using flow cytometer (Accuri C6, Becton Dickinson, USA) on the collected samples. Oil solution was not used in all FACS-related experiment. Washed leukocytes directly exited the microfluidic device from droplet outlet and the debris and contaminants exited from the waste outlet. Before experiment, freshly retrieved leukocytes were incubated with phycoerythrin (PE) conjugated CD45 antibody (1:10, Miltenyi Biotec Asia Pacific, Singapore) for 15 minutes, followed by washing to remove unbound antibody. Immunofluorescence staining allowed discrimination of leukocytes from other debris and enumeration of the number of leukocytes from collected samples. Together with side scattering (SSC) signals, granulocytes and agranulocytes could be distinguished effectively based on their different cell granularity. During FACS analysis, leukocytes were gated based on CD45 signals and side scattering signals.

5.2.6 Droplet-based MMP assay

The protease detection experiment was done by encapsulating leukocyte together with MMP substrate, the same as described in the chapter 4. Matrix metalloproteinase activity were assayed using FRET-based substrate Pepdab010 (Biozyme Inc, USA), which is sensitive to MMP-9 and ADAM-17. The concentration of the substrate solution was 20 μM. Fluorescent signal of cell-containing droplets was collected after 1-hour droplet incubation.

5.3 Results and discussion

5.3.1 Laminar flow verification

Fluorescein isothiocyanate (FITC) dye was used to validate laminar flow condition in the cell washing channel. 100nM FITC solution was injected in the device together with PBS buffer. The flow profile was monitored by measuring the fluorescence intensity across the microchannel at three different locations (inlet, middle of channel and outlet bifurcation) as shown in Figure 5.5. The fluorescent images in Figure 5.5 (B) and the quantified fluorescence intensity shown in Figure 5.5(C) demonstrated that fluorescent dye solution was well confined to one side of microchannel throughout the whole washing section. The presence of micropillars did not affect the laminar flow consistency. It was observed that the slope of fluorescence intensity profile across the channel width had a decreasing trend due to diffusion.

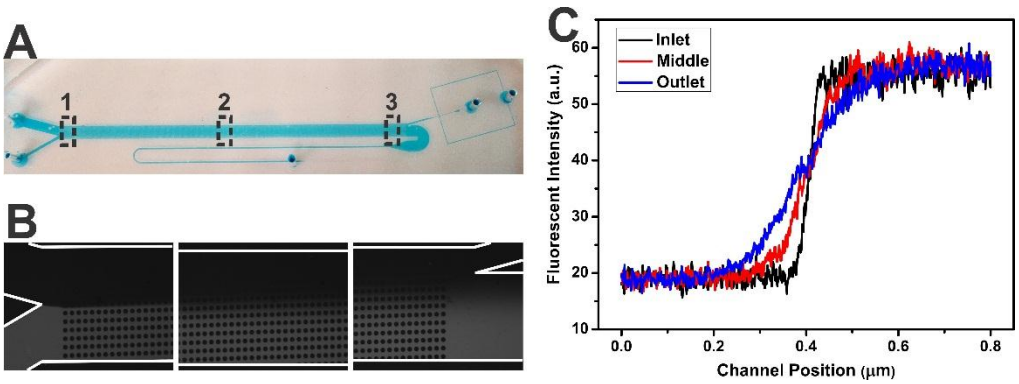

Figure 5.3 (A) Device image with dye injected into the microchannel. (B) FITC dye (100 nM) flowing in the channel parallel with PBS buffer at 1) inlet, 2) middle section and 3) bifurcation point. (C) Measured fluorescence intensity at 3 channel locations as shown in (B).

5.3.2 Diffusion characterization on enzyme and substrate

After validating with fluorescent dye, the diffusion of biomolecular contaminants was further characterized using MMP substrate and trypsin, which could cleave the MMP substrate at high reaction rate [101]. Trypsin has a molecular weight of 23.3kDa, which is closer to matrix metalloproteinases compared with FITC dye. In the microchannel, trypsin and substrate diffused against each other and reacted at once when they were in close proximity. When the substrate was cleaved by trypsin, fluorophores would be released to form a bright band along with flow direction. As the cleavage rate of trypsin against substrate is very high, the rate limiting factor of the overall fluorogenic reaction was the diffusion of trypsin and substrate molecules. Hence, the diffusion zone of trypsin and substrate molecules could be identified by monitoring the bright fluorescent band in the microdevice.

Two sets of experiments were conducted to investigate the diffusion effect. First,

the flow ratio of trypsin and substrate was fixed at 1:1 while their flow rate was scaled up gradually. Based on the fluorescent images in Figure 5.6 (A) to (C), it was observed that higher flow rate resulted in narrower fluorescent band, indicating the smaller diffusion occurred in the microchannel due to shorter diffusion time. Based on the quantified result shown in Figure 5.6(D), the width of fluorescent band at 150 a.u. shrank from 275.8 to 116.0 μm as the total flow rate decreased from 16 to 2 μL/min.

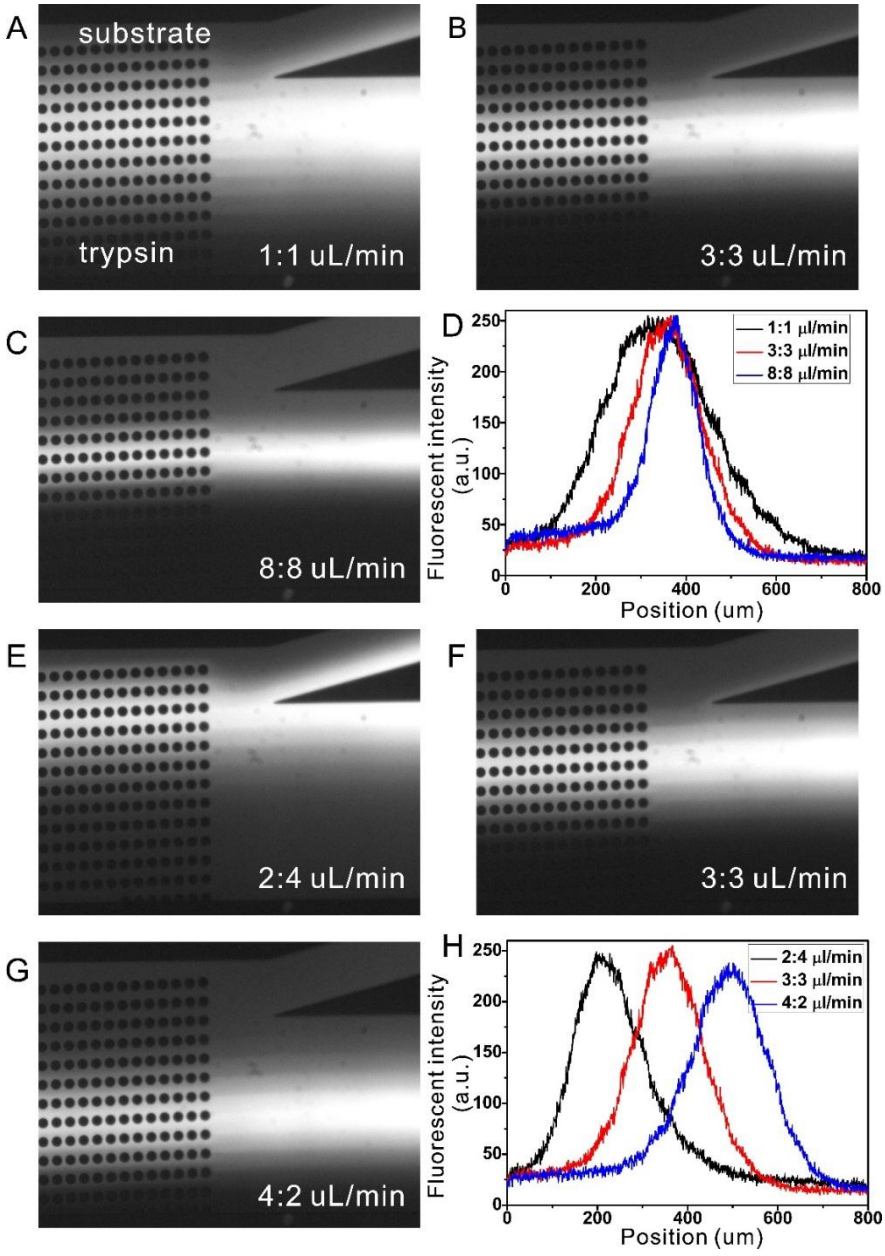

Figure 5.4 (A) (B) (C) Fluorescent images of flowing trypsin and fluorogenic substrate at 1:1 flow ratio near the bifurcation point. Higher total flow rate corresponds to dimmer and narrower fluorescent band, suggesting less diffusion occurred. (D) Quantified fluorescence intensity of three flow conditions with 1:1 flow ratio. (E)(F)(G) Fluorescent images of flowing trypsin and fluorogenic substrate at differential flow rates near the bifurcation point. The location of fluorescent band can be adjusted by the differential flow rates. (H) Quantified fluorescence intensity of three conditions with differential flow rates.

Different flow rates were also applied to investigate how diffusion zone could be shifted based on differential flow ratio. Based on the experiment results, it was observed that the position of fluorescent peak could be easily adjusted by controlling the flow rate as shown in Figure 5.6(E) to (G). High flow rate of the substrate solution shifted the fluorescent peak towards the trypsin solution and far away from the bifurcation point as shown in Figure 5.6(H). Therefore, high flow rate of washing buffer, compared with cell solution, was deployed in the single leukocyte study project in order to stop contaminants diffusing into the droplet generator

5.3.3 Leukocyte viability characterization

After diffusion characterization, it seemed high flow was desirable for diffusion suppression. However, high flow could make leukocytes subject to high shear rate and heavy collision impact with guiding micropillar, which may affect leukocyte viability. Hence, we conducted a cell viability test to investigate the relationship between cell survival rate and flow rate. The viability of cell was monitored at two time points, 1) right after the cells exited the washing channel

2) after 1-hour incubation at the room temperature to mimic the duration of the functional assay. The viability test was conducted in the normal buffer solution without droplet formation. Because of large droplet size and good oxygen solubility in the fluorocarbon oil [127], the viability measured in the buffer environment was a reasonable estimation of the real viability inside water-in-oil droplet for short period of time.

The immediate viability of fresh leukocytes after passing through the DLD-based washing channel remained around 90% for all flow conditions as shown in Figure 5.7. However, after 1-hour incubation the unwashed leukocytes in the control group demonstrated an overall viability of 89.9%. The measured viability of cells flowed at 5 μL/min was 91.2%. Nevertheless, the overall viability under 10, 20 and 40 μL/min flow rates reduced to 85.1%, 82.7% and 82.2%, respectively. This decreasing viability with increasing flow rate indicated that the high shear force and fierce collision with micropillar under high flow rate did compromise the survival rate of fresh leukocytes, which could inevitably affect the accuracy of the following single-cell functional assay. In order to ensure that cells remained their original status as much as possible after washing, the flow rate for the subsequent functional assay was controlled below 10 μL/min.

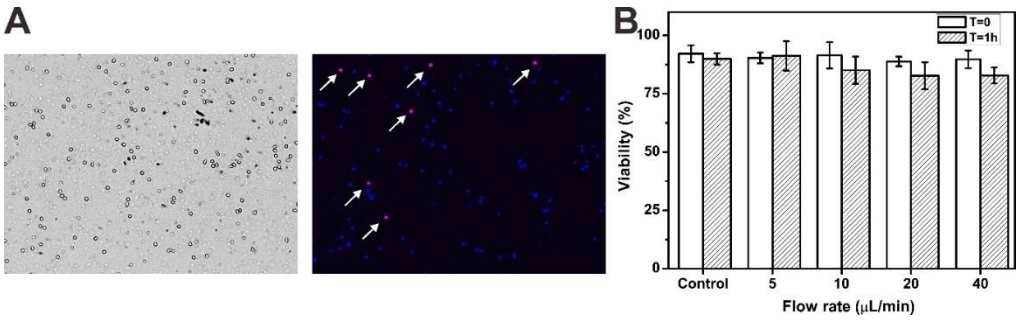

Figure 5.5 (A) Brightfield and fluorescent images (blue: nucleus stain; red: dead stain) of leukocytes after passing through the washing channel at 5 μL per minute. (B) Quantified viability rate of cells at t=0 and t=1-hour after passing the device at different flow rates.

5.3.4 Washing channel design and beads test

DLD has been well studied to separate particle from based on the size difference. Two formulae have been derived to calculate the critical separation dimension. The first one is the analytical formula that has been discussed in Chapter 3 [100]. The second version is known as empirical formula based on separation results obtained from more than 20 devices with varying channel design [151]. The empirical formula, unlike the analytical formula, does not contain a correction factor. The empirical formula has been proved to generate a more accurate predication of critical separation dimension of DLD array than the analytical model [152]. Its separation cut-off dimension depends on the array slant angle and lateral gap size between pillars in the same row as shown below,

$$D_c = 1.4g\varepsilon^{0.48} \quad (5.1)$$

Where Dc is the critical dimension of particle for DLD separation, g is the lateral gap size and ε is the row shift fraction (ε = tanθ = Δλ/λ, where θ is the array

slant angle, $\Delta\lambda$ is the row shift distance and λ is the center-to-center lateral distance between micropillars) [151]. For this project, the empirical formula was adopted into the device design.

In order to effectively retrieve fresh leukocytes from RBC-lysed blood, the separation threshold dimension was set 10 μm given the fact that average size of leukocytes is about 12 μm. In the first design, the pillar dimension and lateral pillar gap (g) was set 30 μm. The row shift distance was set 2.4 μm, resulting in row shift fraction (ε) equal to 0.04. The empirical cut-off separation dimension would be 8.96 μm. However, when testing with polystyrene beads, the cell washing device could only divert beads over 15 μm from the original solution into the washing solution. This DLD design had no influence on the trajectory of 10 μm beads as they were still refined in the original solution.

At first, it was believed that microfabrication error led to sorting failure. The measured diameter of micropillar was 27.21 $\pm$1.37 μm rather than 30 μm, because of UV overexposure. As a result of shrinking micropillar diameter, the effective gap size would expand and increase the separation cut-off dimension. In order to have better tolerance of microfabrication error, the row shift distance was adjusted to 1.5 μm with empirical cut-off dimension equal to 7.1 μm in the second design. However, 10 μm beads still moved directly into the waste outlet without deflection in the adjusted design. Although the microfabrication error could cause 5 to 10 % increase of gap size, this error was unable to increase the separation cut-off dimension by 3 μm. Hence, the empirical formula was not

accurate for Dc ≤ 10 μm.

The critical separation dimension must be reduced further in order to effectively deflect 10 μm polystyrene bead and white blood cell. To achieve this, either the gap size (g) or the row shift distance (Δλ) must be reduced based on the empirical model. However, neither of them was favorable. On one hand, reduced gap size could make the DLD-based cell washing array vulnerable to clogging due to bead/cell cluster. On the other hand, decreased row shift distance could unavoidably increase the channel length because of the reduced slant angle. Additionally, such a small row shift distance could pose challenges on the precision of microfabrication. Since neither gap size nor row shift distance could be reduced further with the consideration of device operation and fabrication, new parameter that was not covered in analytical and empirical formulae must be exploited to decrease the cut-off dimension.

In fact, the distance between neighboring columns of micropillar (λ_v) is always assumed to be identical to the lateral distance (λ) between micropillars in the same column in both DLD analytical and empirical model, as shown in Figure 5.8(A)-middle. Nevertheless, the asymmetric micropillar array with unmatched λ_v and λ could have different critical separation dimension deviating from the existing models. In general, when λ_v becomes smaller than λ, the critical cut-off dimension for separation reduces and vice versa. In the extreme scenario, when λ_v reaches 0, the DLD array effectively becomes into an array of closed channels where particles of any size would be definitely diverted from one side to the

other; and when λ_v is too large, the DLD array would have no sorting effect on particles no matter of their size, because particles could recover to their original trajectory after bumping to micropillars. Some DLD-based platforms have exploited the relationship of λ_v and Dc to achieve optimal sorting efficiency [153, 154]. Therefore, beads sorting experiment was conducted with new DLD design of reduced λ_v. Eventually, it was observed that 10 μm beads could be effectively diverted when λ_v was reduced to 15 μm with λ, g and Δλ remaining as 60, 30 and 1.5 μm, respectively. As shown in the figure 5.8(B), it was clearly observed that both 10 and 15 μm polystyrene beads could be successfully directed from the original solution (lower stream) into washing solution (upper stream) and 7 μm beads kept moving straight into waste outlet.

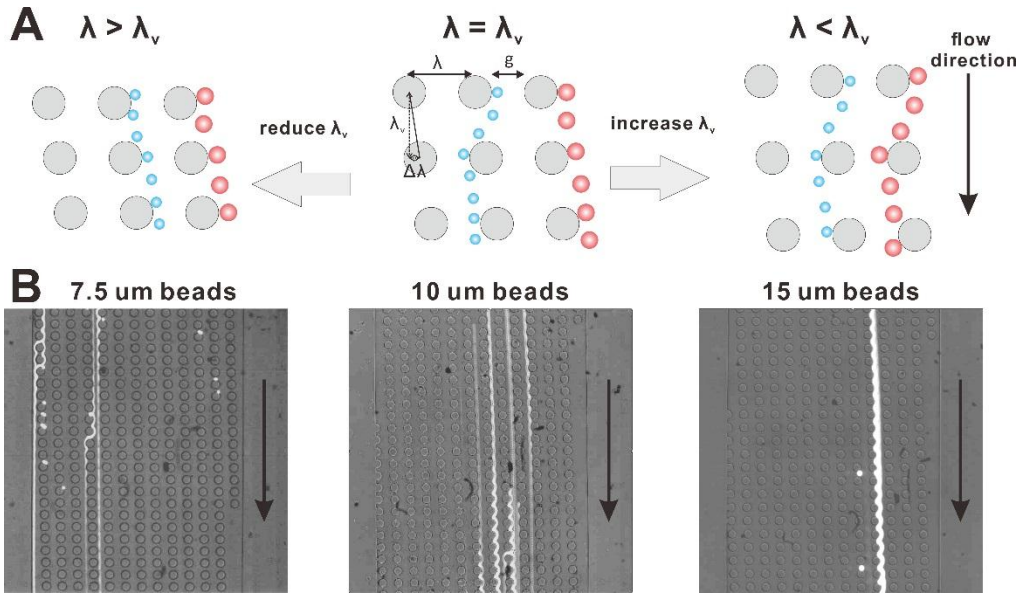

Figure 5.6 (A) Schematics showing the relationship between vertical pillar distance (λ_v) and critical separation dimension (D_C). D_C is positive correlated with λ_v as increasing λ_v leads to increasing D_C. (B) Overlaid images of polystyrene beads moving in the DLD-based cell washing channel: *left* 7.5 μm beads demonstrated no deflection and remained in the lower stream; *middle and right* 10 and 15.5 μm beads demonstrated a lateral migration toward upper stream as they kept bumped with micropillars.

5.3.5 Leukocyte flow test and FACS characterization post-washing

Next, freshly harvested leukocytes were tested using the optimal device design. Figure 5.9 illustrates the moving trajectory of fluorescent-labelled leukocytes at different locations in the cell washing channel. Leukocytes, like 10 μm polystyrene beads, kept bumping to circular micropillars in the microchannel and were forced to leave the original cell solution, enter the clean buffer solution and be encapsulated into droplets. Meanwhile, RBC debris and other molecular contaminants were still confined in the original cell solution and eventually exited the device from waste outlet.

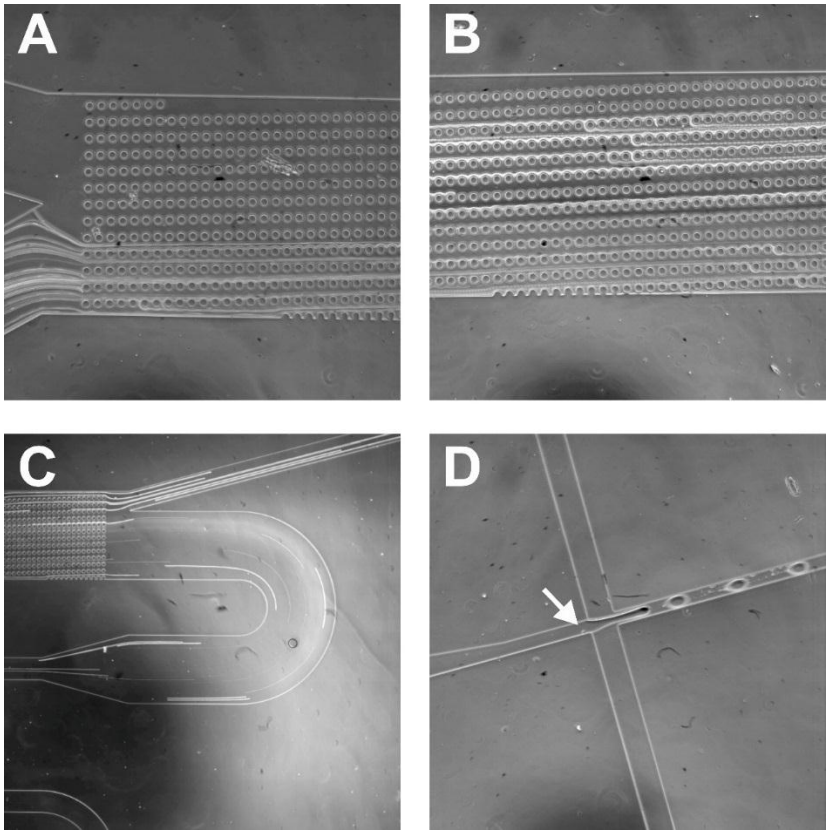

Figure 5.7 Phase contrast images of leukocytes in the microfluidic device (A) Labeled leukocytes entered the cell washing array at one inlet. (B) Leukocytes started to migrate into the clean buffer solution as they passed through the cell washing channel. (C) Most of leukocytes entered the droplet branch after

washing while some small cells and debris escaped into the waste outlet. (D) A washed leukocyte was encapsulated into droplet with clean buffer.

The cell solution and waste solution were collected for cell count and FACS analysis to investigate leukocyte extraction efficiency and cell composition. According to the cell concentration and volume of the solutions collected at droplet and waste outlets, the leukocyte recovery rate was calculated as 82.7% when flow rates of buffer and cell solution were set 5 and 4 μL/min, respectively. The average leukocyte recovery rate was about 80% at various flow rate as shown in figure 5.10(A). The main reason of cell loss might be because some leukocytes, like lymphocytes, was unable to be guided into buffer solution due to their small size [155].

In order to verify this hypothesis, FACS analysis was performed to investigate the cell composition of the samples collected from both outlets. Due to the different cellular structure of nucleus and presence of granules, granulocytes (mainly neutrophils with small number of eosinophils and basophils) generate a higher side-scattering (SSC) signal than lymphocytes and monocytes under FACS scan [156]. Figure 5.10 (C) and (D) demonstrate the FACS scan results obtained from cell and waste outlet. Gate P1 indicated the granulocytes population since the cells carried positive CD45 and high SSC signals. Gate P2 indicated the lymphocytes and monocytes population since the cells falling in this gate had positive CD45 but low SSC signals. Based on the FACS results, it was confirmed that the majority of cell population extracted from the cell

washing channel were granulocytes. The granulocytes-to-agranulocytes ratio of unsorted control sample was about 2.15:1. The ratio of sample collected from the cell outlet was about 2.81:1 while it decreased to 0.57: 1 for sample obtained from the waste outlet (Figure 5.10(B)). Thereof, the developed device owned a selectivity of granulocytes over agranulocytes due to the size-based sorting (granulocytes: 12~17 μm, monocytes: 15~30 μm, lymphocyte: 7~13 μm). Many lymphocytes escaped into the waste outlet because of their small size. An even better granulocyte purity could be achieved if increasing the critical separation dimension of the cell washing channel with the risk of losing more small cells.

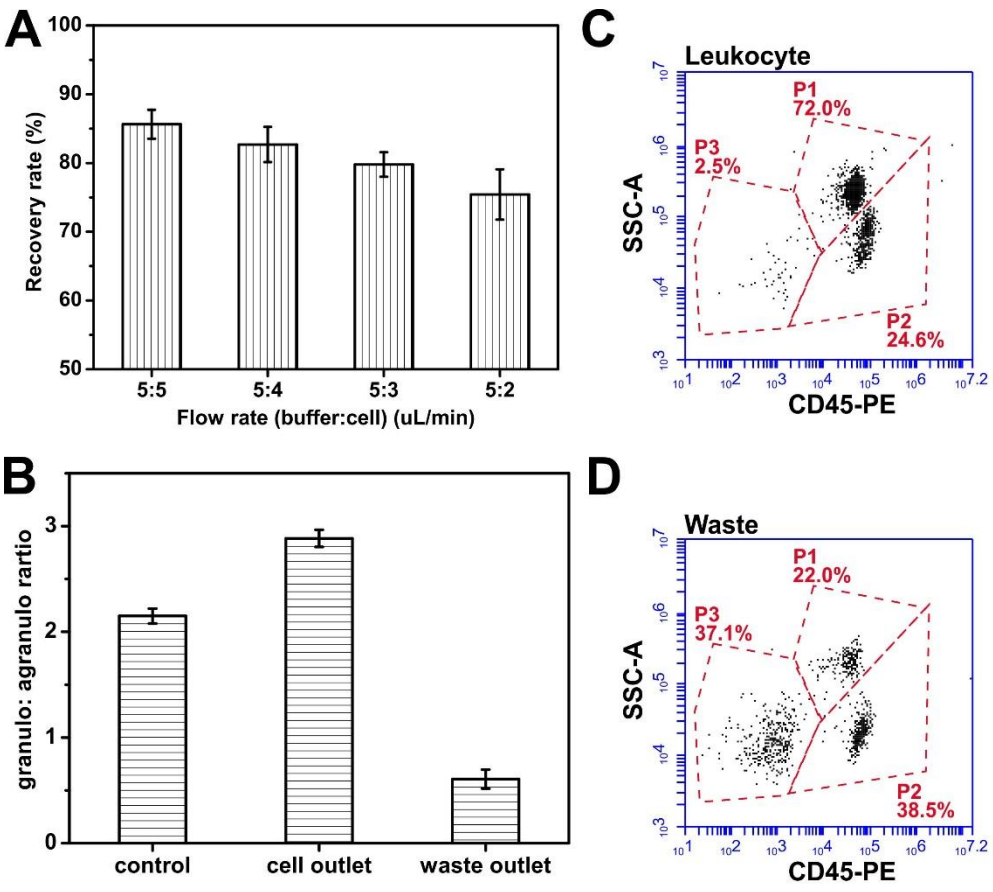

Figure 5.8 (A) Leukocyte recovery rate at different flow ratios. An average recovery rate of 80% was obtained, with about 20% leukocytes loss. (B) Measured granulocytes-to-agranulocytes ratio of samples collected from different device outlets, suggesting an enhancement of granulocytes due to size-based sorting. (C) and (D) Flow cytometry results of cell collected from both droplet outlet (C) and waste outlet (D). P1 gate indicated the granulocyte population; P2 gate indicated the monocyte and lymphocyte population; and P3 gate indicated the cell debris and other acellular contaminant.

5.3.6 Protease assay of single leukocytes

Matrix metalloproteinase (MMP) activity of individual live leukocytes was analyzed using the developed device, which was difficult to measure with conventional droplet technology due to pre-encapsulation contamination. As shown in Figure 5.1 (C), the fluorescence intensities of empty and leukocyte-containing droplets were very close (difference was less than 20 a.u.). With the spontaneous cell washing mechanism, the functionality level of single leukocytes could be accurately assayed in the individual water-in-oil droplets. As a proof-of-concept, MMP substrate was pumped into the microfluidic device as the washing buffer with leukocyte solution.

We first studied the MMP activity level of single leukocytes at naïve status. Leukocyte-containing droplets with different fluorescent intensities (Figure 5.11(A)) showed the cells had a diverse level proteolytic activity at naïve status. The quantified results shown in Figure 5.11(B) showed the heterogeneous proteolytic profile with a mean fluorescence intensity of 136.3 a.u. and standard deviation of 54.6 a.u. The two clusters (around 60 a.u. and 175 a.u.) in the fluorescence intensity were identified from the scattered plot of a population of

leukocytes, which may be contributed by two different subpopulations of leukocytes (i.e. granulocytes and agranulocytes). Monocytes have been demonstrated with low MMP expression and activity level at naïve status in previous studies [157]. Excitingly, we also found the fluorescence intensity level of empty droplets was largely reduced from 96.9 ± 6.7 a.u. to 23.4 ± 4.9 a.u. due to the washing function integrated before cell encapsulation as shown in Figure 5.11(C). The reduced noise signal made empty droplets easily distinguishable from leukocyte-encapsulated droplets.

Next, 1 μM of phorbol 12-myristate 13-acetate (PMA) was introduced into the MMP substrate to study the MMP activity level of fresh leukocytes under PMA stimulation. In previous literature, PMA has been proved to boost the MMP activity on cultured cancer cells [62]. Before single-cell experiment, viability test on 1 μM PMA mediated leukocytes was conducted to ensure that PMA did not have an adverse effect on cell survival rate for 1-hour incubation. In the single leukocytes experiment, we observed the elevated MMP activity after incubating single leukocytes with 1 μM PMA in droplets for 1 hour. The mean fluorescence intensity increased to 416.8 a.u., which was 2-fold higher than the mean intensity obtained at naïve condition. Meanwhile, the standard deviation of fluorescence intensity also increased by 1 fold to 104.7 a.u., suggesting the heterogeneity of MMP activity level of single leukocytes was intensified after PMA stimulation. This intensified heterogeneity of single-cell profile under PMA mediation was originally difficult to be captured by average-based

ensemble measurement. In addition, it became difficult to identify 2 signals clusters after PMA stimulation, which may suggest the effect of MMP elevation was greater on monocytes than on granulocytes, resulting in overlapped MMP signal intensity.

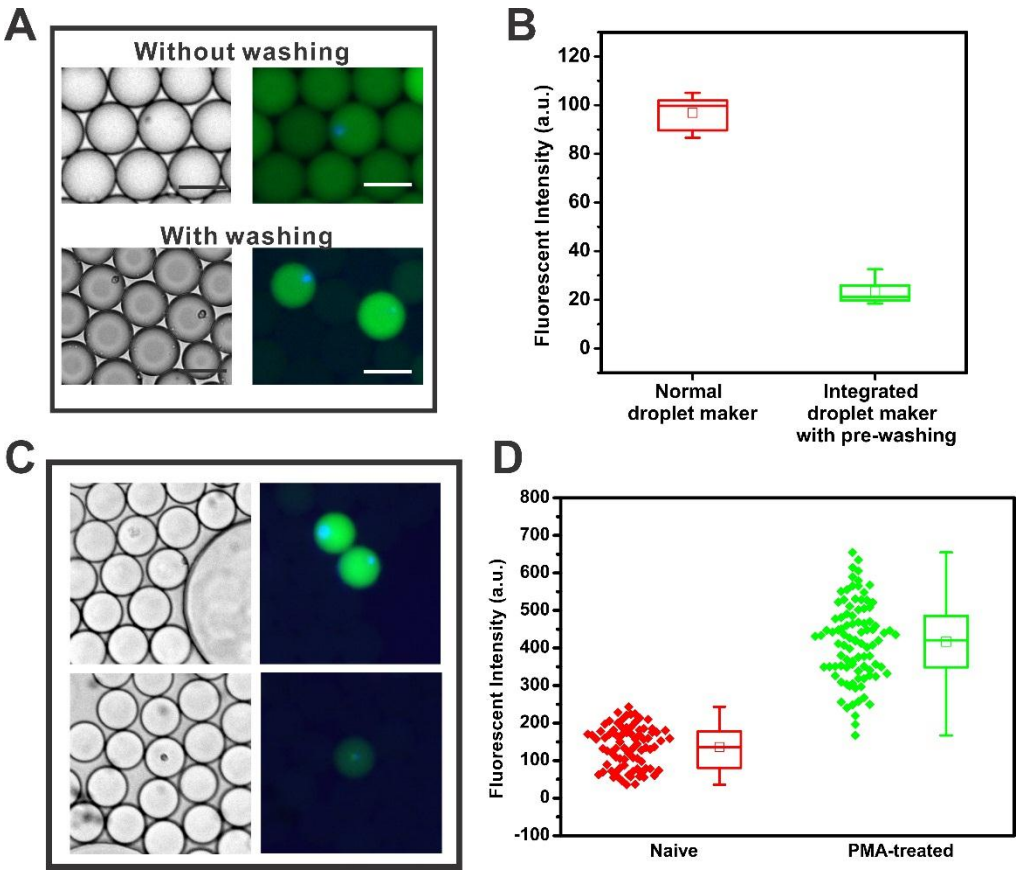

Figure 5.9 (A) Brightfield and fluorescent images of leukocyte-containing and empty droplets produced by normal droplet generator and developed device. Empty droplets have different fluorescent signals under two scheme (B) Comparison of fluorescence intensity of empty droplets generated from normal droplet generator and the developed device with washing function. The intensity of empty droplet was reduced by 4 times due to the implementation of pre-encapsulation washing. (C) Brightfield and fluorescent images of single leukocyte-containing droplets under naïve status. Different fluorescent intensities can be clearly observed at the single leukocyte level. (D) Quantified fluorescence intensity for single leukocyte-containing droplets under both naïve and 1 μM PMA-mediated condition. PMA treatment apparently lifted the MMP activity of leukocytes.

5.4 Conclusions

An integrated microfluidic device combining cell washing section and droplet generator was developed for single leukocyte functional study. The DLD-based washing channel could divert leukocytes from cross-contaminated solution to clean buffer solution and guide the washed leukocytes to enter droplet generator while directing contaminants and debris to the waste outlet. The flow condition was carefully characterized in order to minimize the diffusion of molecular contaminants and the viability loss of fresh leukocytes. The developed device demonstrated around 80% leukocyte recovery rate with a selectivity of granulocytes over monocytes and lymphocytes. The MMP activity of individual leukocytes was measured by detecting the fluorescent signal generated from cell-containing droplets. At the naïve status, the MMP profile revealed a heterogeneous activity level with two clusters that may be contributed by different subpopulations of leukocytes. PMA-mediated MMP activity was also successfully measured at single leukocyte level. After 1-hour incubation with 1 μM PMA in the droplet environment, the MMP activity was intensified with 2-fold increase in the average fluorescence intensity and diversified with 1-fold increase in the spread. We believe the developed single cell assay platform is ideal for the functional analysis of highly active cells from an impure and cross-contaminated solution due to the washing-immediately-before-encapsulation function. With further development, the microfluidic device can be used for

quick evaluation of patient immunity and immune response to different drugs in the clinical context.

Chapter 6. Conclusions and future work

6.1 Conclusions

No two cells are exactly alike. Each cell has its distinct phenotype, behavior and function even when compared to other cells from the same lineage or sharing the same gene. However, conventional biological assays, such as western blot and ELISA, adopt a simplistic method to extract the average prevalent cell signals from non-homogeneous cell population. The average behavior of a cell population is summarized by a mean value, without considering cell-to-cell differences. Today more scientific evidences have pointed out cellular heterogeneity can have functional consequences and a population average can generate misleading assay outcomes because of neglecting critical details of individual cells.

Single-cell assay is essential in order to enable scientists to capture cell-to-cell variance beneath population average of seemingly identical cells. In general, conventional macro-scale single-cell analytical approaches are seriously constrained by high system cost, low assay throughput, low detection sensitivity and heavy sample/reagent consumption. In contrast, microfluidics offers a simple but versatile approach to perform single-cell analysis. Individual cells are isolated from each other in the single-cell compartments for various downstream applications. Among all microfluidic single-cell approaches, droplet microfluidics is most suitable for metabolism and biomolecule secretion

assay.

In this dissertation, we focused on the development of droplet microfluidic platform for single-cell proteolytic assay. Proteolytic activity at single-cell level provides important insights of cellular heterogeneity which in turn aids in accurate cell behavior evaluation and precise personalized medicine in cancer and immune disorder.

We first developed an integrated droplet platform combining jetting and passive sorting. We used this novel platform to improve the poor single-cell efficiency of random encapsulation process. The achieved single-cell encapsulation efficiency was consistently above 70% for various cell concentrations, which beat the Poisson prediction. The enhanced encapsulation efficiency could largely facilitate the downstream assay, particularly for low input cell concentration. The entire process was label-free so the original cell status could be successfully preserved to the maximum extent. Single-cell proteolytic assay and drug test were performed on cultured cell lines using the developed platform.

Next, we further developed the droplet platform to make it more reliable and accurate. Combined with in vitro circulating tumor cell (CTC) culture, the droplet platform could realize single-cell proteolytic assay on cultured CTCs, which were expanded from cancer patients. In the system characterization, we studied 3 breast cell lines and found that the metastatic cancer cell line possessed an elevated level of matrix metalloproteinase (MMP) activity, compared with the non-metastatic cancer cell line and the normal epithelial cell line. Then we

applied the assay method on cultured CTC sample. The results revealed cultured CTCs were very heterogeneous in MMP activity and different batches of cultured CTCs had distinct MMP profiles even through the CTC donors were in the same stage of cancer treatment.

While studying cultured CTCs, we found leukocyte residue was always present in the culture sample. Hence, we decided to perform a comprehensive study on single leukocytes. Unlike cancer cell, leukocytes are highly active in protease secretion due to their responsibility in host defense. In order to prevent pre-encapsulation contamination, we developed a droplet generator with cell washing function. Freshly-retrieved leukocytes were diverted into a clean buffer solution from the impure cell solution in the washing channel and immediately encapsulated into droplets. Using this developed platform, the background signal in empty droplets was largely suppressed and the proteolytic assay accuracy was significantly improved. We successfully applied this platform to study MMP activity of leukocytes at naïve and PMA-mediated conditions, finding PMA treatment not only intensified the single-cell MMP activity but also stimulated the cell-to-cell variance.

In conclusion, we have shown that functional assay of matrix metalloproteinase produced by single cancer cells and leukocytes can be achieved using droplet microfluidics. Compared with other single-cell analytical methods, the droplet microfluidic systems possess high detection sensitivity, low cross-contamination, minimum interference on cells and scale-up potential. With

further development, we believe that the droplet technologies presented in this work could be applied in the clinical practice to evaluate patient and disease status, and eventually benefit the medical community.

6.2 Future work

The future work for single-cell proteolytic functional assay can be expanded in three directions: improvement on fluorescent detection, multiplexed signal detection and clinical application on diseased cell characterization.

The scheme of fluorescent detection can be modified to handle large volume of sample with relatively high throughput. Current detection was conducted under a stationary condition, which limited the detection throughout by the microscopic observation window. Continuous high-throughput droplet detection has been reported long ago [158]. By adopting this detection method, it will be easy to study hundreds of thousands of droplets to generate clinical conclusions within a short duration. Apart from throughput, a more rigorous calibration on fluorescent measurement can be helpful to produce more consistent single-cell proteolytic assay results. As fluorescent based detection is sensitive to environmental and other factors, such as ambient brightness and intensity fluctuation of fluorescent light source, a fluorescent calibration before droplet detection using some reference subjects (e.g. dye solution or fluorescent bead) can ensure experimental condition is coherent across different sets of

experiments.

Secondly, only one MMP substrate has been used to detect single-cell proteolytic activity in this PhD project. As mentioned before, the MMP substrate is not specific to any kind of MMPs. A more accurate and specific detection could be realized based on multiplexed MMP assay, where multiple substrates are injected into droplets and different signals are acquired at the same time [68]. By de-convoluting the multiplexed signals, the activity level of specific types of MMPs could be derived correctly with great biological significance.

Lastly, more clinical samples can be studied using the developed droplet platform. In this work, we only emphasized on cancer cells and leukocytes. Single-cell proteolytic activity has a broad clinical implication. Hence, it will be meaningful to expand the application beyond the current scope. Definitely, the detection targets can include other biomarkers (e.g. metabolism) to form multiplexed single-cell droplet assays. These aspects of future work require various multidisciplinary collaboration for fruitful research. But I firmly believe much on-going research is working towards this direction.

References

1. López-Otín, C. and L.M. Matrisian, *Emerging roles of proteases in tumour suppression.* Nature Reviews Cancer, 2007. **7**(10): p. 800-808.
2. Janeway Jr, C.A. and R. Medzhitov, *Innate immune recognition.* Annual review of immunology, 2002. **20**(1): p. 197-216.
3. Walling, M.A. and J.R. Shepard, *Cellular heterogeneity and live cell arrays.* Chemical Society Reviews, 2011. **40**(7): p. 4049-4076.
4. Altschuler, S.J. and L.F. Wu, *Cellular heterogeneity: do differences make a difference?* Cell, 2010. **141**(4): p. 559-563.
5. Spudich, J.L. and D. Koshland Jr, *Non-genetic individuality: chance in the single cell.* Nature, 1976. **262**(5568): p. 467-471.
6. Jackowski, S., *Cell cycle regulation of membrane phospholipid metabolism.* Journal of Biological Chemistry, 1996. **271**(34): p. 20219-20222.
7. van den Heuvel, S., *Cell-cycle regulation.* 2005.
8. Harbour, J.W. and D.C. Dean, *Rb function in cell-cycle regulation and apoptosis.* Nature cell biology, 2000. **2**(4): p. E65-E67.
9. Hedrick, P.W., *Genetic polymorphism in heterogeneous environments: a decade later.* Annual review of ecology and systematics, 1986: p. 535-566.
10. Cedar, H. and Y. Bergman, *Linking DNA methylation and histone modification: patterns and paradigms.* Nature Reviews Genetics, 2009. **10**(5): p. 295-304.
11. Elowitz, M.B., et al., *Stochastic gene expression in a single cell.* Science, 2002. **297**(5584): p. 1183-1186.
12. Newman, J.R., et al., *Single-cell proteomic analysis of S. cerevisiae reveals the architecture of biological noise.* Nature, 2006. **441**(7095): p. 840-846.
13. Stewart, P.S. and J.W. Costerton, *Antibiotic resistance of bacteria in biofilms.* The lancet, 2001. **358**(9276): p. 135-138.
14. Fillmore, C.M. and C. Kuperwasser, *Human breast cancer cell lines contain stem-like cells that self-renew, give rise to phenotypically diverse progeny and survive chemotherapy.* Breast Cancer Research, 2008. **10**(2): p. 1.
15. Powell, A.A., et al., *Single cell profiling of circulating tumor cells: transcriptional heterogeneity and diversity from breast cancer cell lines.* PloS one, 2012. **7**(5): p. e33788.
16. Chattopadhyay, P.K., et al., *Single-cell technologies for monitoring immune systems.* Nature immunology, 2014. **15**(2): p. 128-135.
17. Rubakhin, S.S., et al., *Profiling metabolites and peptides in single cells.* Nat Meth, 2011. **8**(4s): p. S20-S29.
18. Ferlay, J., et al., *Cancer incidence and mortality worldwide: sources, methods and major patterns in GLOBOCAN 2012.* International journal of cancer, 2015. **136**(5): p. E359-E386.
19. Siegel, R.L., K.D. Miller, and A. Jemal, *Cancer statistics, 2015.* CA: a cancer journal for clinicians, 2015. **65**(1): p. 5-29.
20. Chaudhuri, P.K., et al., *Microfluidics for research and applications in oncology.* Analyst, 2016. **141**(2): p. 504-524.

21. Khoo, B.L., et al., *Single‐cell profiling approaches to probing tumor heterogeneity.* International journal of cancer, 2016.
22. Fidler, I.J., *The pathogenesis of cancer metastasis: the'seed and soil'hypothesis revisited.* Nature Reviews Cancer, 2003. **3**(6): p. 453-458.
23. Yu, Z., et al., *Cancer stem cells.* The international journal of biochemistry & cell biology, 2012. **44**(12): p. 2144-2151.
24. Niederst, M.J. and J.A. Engelman, *Bypass mechanisms of resistance to receptor tyrosine kinase inhibition in lung cancer.* Science signaling, 2013. **6**(294).
25. Dahlén, S.-E., et al., *Leukotrienes promote plasma leakage and leukocyte adhesion in postcapillary venules: in vivo effects with relevance to the acute inflammatory response.* Proceedings of the National Academy of Sciences, 1981. **78**(6): p. 3887-3891.
26. Badenhoop, K., et al., *Susceptibility and resistance alleles of human leukocyte antigen (HLA) DQA1 and HLA DQB1 are shared in endocrine autoimmune disease.* The Journal of Clinical Endocrinology & Metabolism, 1995. **80**(7): p. 2112-2117.
27. DeNardo, D.G., et al., *Leukocyte complexity predicts breast cancer survival and functionally regulates response to chemotherapy.* Cancer discovery, 2011. **1**(1): p. 54-67.
28. Elbim, C., et al., *Differential priming effects of proinflammatory cytokines on human neutrophil oxidative burst in response to bacterial N-formyl peptides.* Infection and immunity, 1994. **62**(6): p. 2195-2201.
29. Eggleton, P., et al., *Differences in oxidative response of subpopulations of neutrophils from healthy subjects and patients with rheumatoid arthritis.* Annals of the rheumatic diseases, 1995. **54**(11): p. 916-923.
30. Fridlender, Z.G., et al., *Polarization of tumor-associated neutrophil phenotype by TGF-β:"N1" versus "N2" TAN.* Cancer cell, 2009. **16**(3): p. 183-194.
31. Van den Steen, P.E., et al., *Gelatinase B/MMP-9 and neutrophil collagenase/MMP-8 process the chemokines human GCP-2/CXCL6, ENA-78/CXCL5 and mouse GCP-2/LIX and modulate their physiological activities.* European Journal of Biochemistry, 2003. **270**(18): p. 3739-3749.
32. Spiegel, A., et al., *Neutrophils Suppress Intraluminal NK Cell–Mediated Tumor Cell Clearance and Enhance Extravasation of Disseminated Carcinoma Cells.* Cancer discovery, 2016. **6**(6): p. 630-649.
33. Ohno, I., et al., *Eosinophils as a source of matrix metalloproteinase-9 in asthmatic airway inflammation.* American journal of respiratory cell and molecular biology, 1997. **16**(3): p. 212-219.
34. Wright, H.L., R.J. Moots, and S.W. Edwards, *The multifactorial role of neutrophils in rheumatoid arthritis.* Nature Reviews Rheumatology, 2014. **10**(10): p. 593-601.
35. de Oliveira, S., E.E. Rosowski, and A. Huttenlocher, *Neutrophil migration in infection and wound repair: going forward in reverse.* Nat Rev Immunol, 2016. **16**(6): p. 378-391.
36. Laerum, O.D. and T. Farsund, *Clinical application of flow cytometry: a review.* Cytometry, 1981. **2**(1): p. 1-13.
37. Owens, T.W. and M.J. Naylor, *Breast cancer stem cells.* Advances in Systems

Immunology and Cancer, 2014: p. 7.
38. Pillay, J., et al., *A subset of neutrophils in human systemic inflammation inhibits T cell responses through Mac-1.* The Journal of clinical investigation, 2012. **122**(1): p. 327-336.
39. Dettmer, K., P.A. Aronov, and B.D. Hammock, *Mass spectrometry ‐based metabolomics.* Mass spectrometry reviews, 2007. **26**(1): p. 51-78.
40. Onjiko, R.M., S.A. Moody, and P. Nemes, *Single-cell mass spectrometry reveals small molecules that affect cell fates in the 16-cell embryo.* Proceedings of the National Academy of Sciences, 2015. **112**(21): p. 6545-6550.
41. Fujii, T., et al., *Direct metabolomics for plant cells by live single-cell mass spectrometry.* Nature protocols, 2015. **10**(9): p. 1445-1456.
42. Lombard ‐ Banek, C., S.A. Moody, and P. Nemes, *Single ‐Cell Mass Spectrometry for Discovery Proteomics: Quantifying Translational Cell Heterogeneity in the 16 ‐Cell Frog (Xenopus) Embryo.* Angewandte Chemie International Edition, 2016. **55**(7): p. 2454-2458.
43. Ornatsky, O., et al., *Highly multiparametric analysis by mass cytometry.* Journal of immunological methods, 2010. **361**(1): p. 1-20.
44. Bendall, S.C., et al., *Single-cell mass cytometry of differential immune and drug responses across a human hematopoietic continuum.* Science, 2011. **332**(6030): p. 687-696.
45. Giesen, C., et al., *Highly multiplexed imaging of tumor tissues with subcellular resolution by mass cytometry.* Nature methods, 2014. **11**(4): p. 417-422.
46. Beckham, Y., et al., *Arp2/3 inhibition induces amoeboid-like protrusions in MCF10A epithelial cells by reduced cytoskeletal-membrane coupling and focal adhesion assembly.* PloS one, 2014. **9**(6): p. e100943.
47. Zhang, H. and K.-K. Liu, *Optical tweezers for single cells.* Journal of The Royal Society Interface, 2008. **5**(24): p. 671-690.
48. García-Cardeña, G., et al., *Biomechanical activation of vascular endothelium as a determinant of its functional phenotype.* Proceedings of the National Academy of Sciences, 2001. **98**(8): p. 4478-4485.
49. Xu, W., et al., *Cell stiffness is a biomarker of the metastatic potential of ovarian cancer cells.* PloS one, 2012. **7**(10): p. e46609.
50. Lee, G.Y. and C.T. Lim, *Biomechanics approaches to studying human diseases.* Trends in biotechnology, 2007. **25**(3): p. 111-118.
51. Barbee, K.A., P.F. Davies, and R. Lal, *Shear stress-induced reorganization of the surface topography of living endothelial cells imaged by atomic force microscopy.* Circulation Research, 1994. **74**(1): p. 163-171.
52. Cross, S.E., et al., *AFM-based analysis of human metastatic cancer cells.* Nanotechnology, 2008. **19**(38): p. 384003.
53. Grier, D.G., *A revolution in optical manipulation.* Nature, 2003. **424**(6950): p. 810-816.
54. Zare, R.N. and S. Kim, *Microfluidic platforms for single-cell analysis.* Annual review of biomedical engineering, 2010. **12**: p. 187-201.
55. Carlo, D.D., L.Y. Wu, and L.P. Lee, *Dynamic single cell culture array.* Lab on a Chip,

2006. **6**(11): p. 1445-1449.
56. Kobel, S.A., et al., *Automated analysis of single stem cells in microfluidic traps.* Lab on a Chip, 2012. **12**(16): p. 2843-2849.
57. Lee, L.M. and A.P. Liu, *A microfluidic pipette array for mechanophenotyping of cancer cells and mechanical gating of mechanosensitive channels.* Lab on a Chip, 2015. **15**(1): p. 264-273.
58. Dura, B., et al., *Profiling lymphocyte interactions at the single-cell level by microfluidic cell pairing.* Nat Commun, 2015. **6**.
59. Rettig, J.R. and A. Folch, *Large-Scale Single-Cell Trapping And Imaging Using Microwell Arrays.* Analytical Chemistry, 2005. **77**(17): p. 5628-5634.
60. Hong, J.W., et al., *A nanoliter-scale nucleic acid processor with parallel architecture.* Nature biotechnology, 2004. **22**(4): p. 435-439.
61. Park, M.C., et al., *High-throughput single-cell quantification using simple microwell-based cell docking and programmable time-course live-cell imaging.* Lab on a Chip, 2011. **11**(1): p. 79-86.
62. Wu, L., et al., *High-throughput protease activity cytometry reveals dose-dependent heterogeneity in PMA-mediated ADAM17 activation.* Integrative Biology, 2015. **7**(5): p. 513-524.
63. Marcus, J.S., W.F. Anderson, and S.R. Quake, *Microfluidic single-cell mRNA isolation and analysis.* Analytical Chemistry, 2006. **78**(9): p. 3084-3089.
64. Zhong, J.F., et al., *A microfluidic processor for gene expression profiling of single human embryonic stem cells.* Lab on a Chip, 2008. **8**(1): p. 68-74.
65. White, A.K., et al., *High-throughput microfluidic single-cell RT-qPCR.* Proceedings of the National Academy of Sciences, 2011. **108**(34): p. 13999-14004.
66. Teh, S.-Y., et al., *Droplet microfluidics.* Lab on a Chip, 2008. **8**(2): p. 198-220.
67. Koster, S., et al., *Drop-based microfluidic devices for encapsulation of single cells.* Lab on a Chip, 2008. **8**(7): p. 1110-1115.
68. Ng, E.X., et al., *Single cell multiplexed assay for proteolytic activity using droplet microfluidics.* Biosensors and Bioelectronics, 2016. **81**: p. 408-414.
69. Brouzes, E., et al., *Droplet microfluidic technology for single-cell high-throughput screening.* Proceedings of the National Academy of Sciences, 2009. **106**(34): p. 14195-14200.
70. Ramji, R., et al., *Single cell kinase signaling assay using pinched flow coupled droplet microfluidics.* Biomicrofluidics, 2014. **8**(3): p. 034104.
71. Leng, X., et al., *Agarose droplet microfluidics for highly parallel and efficient single molecule emulsion PCR.* Lab on a Chip, 2010. **10**(21): p. 2841-2843.
72. Wang, B.L., et al., *Microfluidic high-throughput culturing of single cells for selection based on extracellular metabolite production or consumption.* Nat Biotech, 2014. **32**(5): p. 473-478.
73. Mazutis, L., et al., *Single-cell analysis and sorting using droplet-based microfluidics.* Nature protocols, 2013. **8**(5): p. 870-891.
74. Shemesh, J., et al., *Stationary nanoliter droplet array with a substrate of choice for single adherent/nonadherent cell incubation and analysis.* Proceedings of the National Academy of Sciences, 2014. **111**(31): p. 11293-11298.

75. Frey, O., et al., *Reconfigurable microfluidic hanging drop network for multi-tissue interaction and analysis.* Nat Commun, 2014. **5**.
76. Abate, A.R., et al., *High-throughput injection with microfluidics using picoinjectors.* Proceedings of the National Academy of Sciences, 2010. **107**(45): p. 19163-19166.
77. Ng, A.H., et al., *Digital microfluidic magnetic separation for particle-based immunoassays.* Analytical Chemistry, 2012. **84**(20): p. 8805-8812.
78. Konry, T., et al., *Droplet-based microfluidic platforms for single T cell secretion analysis of IL-10 cytokine.* Biosensors and Bioelectronics, 2011. **26**(5): p. 2707-2710.
79. Edd, J.F., et al., *Controlled encapsulation of single-cells into monodisperse picolitre drops.* Lab on a Chip, 2008. **8**(8): p. 1262-1264.
80. Kemna, E.W.M., et al., *High-yield cell ordering and deterministic cell-in-droplet encapsulation using Dean flow in a curved microchannel.* Lab on a Chip, 2012. **12**(16): p. 2881-2887.
81. Lagus, T.P. and J.F. Edd, *High Throughput Single-cell and Multiple-cell Micro-encapsulation.* Journal of Visualized Experiments, 2012(64): p. e4096.
82. Abate, A.R. and D.A. Weitz, *Single-layer membrane valves for elastomeric microfluidic devices.* Applied Physics Letters, 2008. **92**(24): p. 243509.
83. Baret, J.-C., et al., *Fluorescence-activated droplet sorting (FADS): efficient microfluidic cell sorting based on enzymatic activity.* Lab on a Chip, 2009. **9**(13): p. 1850-1858.
84. Franke, T., et al., *Surface acoustic wave (SAW) directed droplet flow in microfluidics for PDMS devices.* Lab on a Chip, 2009. **9**(18): p. 2625-2627.
85. Terazono, H., et al., *Labelling of live cells using fluorescent aptamers: binding reversal with DNA nucleases.* Journal of Nanobiotechnology, 2010. **8**(1): p. 8.
86. Winzen, S., et al., *Fluorescence labels may significantly affect the protein adsorption on hydrophilic nanomaterials.* Colloids and Surfaces B: Biointerfaces, 2016. **147**: p. 124-128.
87. Yan, Y., et al., *Continuous-flow C. elegans fluorescence expression analysis with real-time image processing through microfluidics.* Biosensors and Bioelectronics, 2016. **77**: p. 428-434.
88. Chabert, M. and J.-L. Viovy, *Microfluidic high-throughput encapsulation and hydrodynamic self-sorting of single cells.* Proceedings of the National Academy of Sciences, 2008. **105**(9): p. 3191-3196.
89. Utada, A., et al., *Dripping, jetting, drops, and wetting: the magic of microfluidics.* Mrs Bulletin, 2007. **32**(09): p. 702-708.
90. Huang, L.R., et al., *Continuous Particle Separation Through Deterministic Lateral Displacement.* Science, 2004. **304**(5673): p. 987-990.
91. Hou, H.W., et al., *Isolation and retrieval of circulating tumor cells using centrifugal forces.* Scientific reports, 2013. **3**: p. 1259.
92. Hanemaaijer, R., et al., *Inhibition of MMP Synthesis by Doxycycline and Chemically Modified Tetracyclines (CMTs) in Human Endothelial Cells.* Advances in Dental Research, 1998. **12**(1): p. 114-118.
93. Manning, M.W., L.A. Cassis, and A. Daugherty, *Differential Effects of Doxycycline, a Broad-Spectrum Matrix Metalloproteinase Inhibitor, on Angiotensin II–Induced*

Atherosclerosis and Abdominal Aortic Aneurysms. Arteriosclerosis, Thrombosis, and Vascular Biology, 2003. **23**(3): p. 483-488.

94. Utada, A.S., et al., *Absolute Instability of a Liquid Jet in a Coflowing Stream.* Physical Review Letters, 2008. **100**(1): p. 014502.
95. Utada, A.S., et al., *Dripping to Jetting Transitions in Coflowing Liquid Streams.* Physical Review Letters, 2007. **99**(9): p. 094502.
96. Baret, J.-C., *Surfactants in droplet-based microfluidics.* Lab on a Chip, 2012. **12**(3): p. 422-433.
97. Kaltenbach, M., S.R.A. Devenish, and F. Hollfelder, *A simple method to evaluate the biochemical compatibility of oil/surfactant mixtures for experiments in microdroplets.* Lab on a Chip, 2012. **12**(20): p. 4185-4192.
98. Joensson, H.N., M. Uhlen, and H.A. Svahn, *Droplet size based separation by deterministic lateral displacement-separating droplets by cell-induced shrinking.* Lab on a Chip, 2011. **11**(7): p. 1305-1310.
99. Di Carlo, D., *Inertial microfluidics.* Lab on a Chip, 2009. **9**(21): p. 3038-3046.
100. Inglis, D.W., et al., *Critical particle size for fractionation by deterministic lateral displacement.* Lab on a Chip, 2006. **6**(5): p. 655-658.
101. Miller, M.A., et al., *Proteolytic Activity Matrix Analysis (PrAMA) for simultaneous determination of multiple protease activities.* Integrative Biology, 2011. **3**(4): p. 422-438.
102. Chen, C.-H., et al., *Enhancing Protease Activity Assay in Droplet-Based Microfluidics Using a Biomolecule Concentrator.* Journal of the American Chemical Society, 2011. **133**(27): p. 10368-10371.
103. Gialeli, C., A.D. Theocharis, and N.K. Karamanos, *Roles of matrix metalloproteinases in cancer progression and their pharmacological targeting.* FEBS Journal, 2011. **278**(1): p. 16-27.
104. Roomi, M., et al., *Patterns of MMP-2 and MMP-9 expression in human cancer cell lines.* Oncology reports, 2009. **21**(5): p. 1323.
105. Mehlen, P. and A. Puisieux, *Metastasis: a question of life or death.* Nat Rev Cancer, 2006. **6**(6): p. 449-458.
106. Cristofanilli, M., et al., *Circulating tumor cells, disease progression, and survival in metastatic breast cancer.* New England Journal of Medicine, 2004. **351**(8): p. 781-791.
107. Wittekind, C. and M. Neid, *Cancer invasion and metastasis.* Oncology, 2005. **69**(Suppl. 1): p. 14-16.
108. Ignatiadis, M., et al., *Different prognostic value of cytokeratin-19 mrna–positive circulating tumor cells according to estrogen receptor and HER2 status in early-stage breast cancer.* Journal of Clinical Oncology, 2007. **25**(33): p. 5194-5202.
109. de Bono, J.S., et al., *Circulating tumor cells predict survival benefit from treatment in metastatic castration-resistant prostate cancer.* Clinical Cancer Research, 2008. **14**(19): p. 6302-6309.
110. Cristofanilli, M., et al., *Circulating tumor cells: a novel prognostic factor for newly diagnosed metastatic breast cancer.* Journal of Clinical Oncology, 2005. **23**(7): p. 1420-1430.

111. Lu, P., et al., *Extracellular matrix degradation and remodeling in development and disease.* Cold Spring Harbor perspectives in biology, 2011. **3**(12): p. a005058.
112. Rundhaug, J.E., *Matrix Metalloproteinases, Angiogenesis, and Cancer Commentary re: AC Lockhart et al., Reduction of Wound Angiogenesis in Patients Treated with BMS-275291, a Broad Spectrum Matrix Metalloproteinase Inhibitor. Clin. Cancer Res., 9: 00–00, 2003.* Clinical Cancer Research, 2003. **9**(2): p. 551-554.
113. Egeblad, M. and Z. Werb, *New functions for the matrix metalloproteinases in cancer progression.* Nat Rev Cancer, 2002. **2**(3): p. 161-174.
114. Coussens, L.M. and Z. Werb, *Inflammation and cancer.* Nature, 2002. **420**(6917): p. 860-867.
115. Liu, Y., *Epithelial to mesenchymal transition in renal fibrogenesis: pathologic significance, molecular mechanism, and therapeutic intervention.* Journal of the American Society of Nephrology, 2004. **15**(1): p. 1-12.
116. Bellahcene, A., et al., *Small integrin-binding ligand N-linked glycoproteins (SIBLINGs): multifunctional proteins in cancer.* Nat Rev Cancer, 2008. **8**(3): p. 212-226.
117. Osta, W.A., et al., *EpCAM is overexpressed in breast cancer and is a potential target for breast cancer gene therapy.* Cancer research, 2004. **64**(16): p. 5818-5824.
118. Vona, G., et al., *Isolation by size of epithelial tumor cells: a new method for the immunomorphological and molecular characterization of circulating tumor cells.* The American journal of pathology, 2000. **156**(1): p. 57-63.
119. Hyun, K.A. and H.I. Jung, *Microfluidic devices for the isolation of circulating rare cells: A focus on affinity‐based, dielectrophoresis, and hydrophoresis.* Electrophoresis, 2013. **34**(7): p. 1028-1041.
120. Khoo, B.L., et al., *Short-term expansion of breast circulating cancer cells predicts response to anti-cancer therapy.* Oncotarget, 2015. **6**(17): p. 15578-15593.
121. Khoo, B.L., et al., *Liquid biopsy and therapeutic response: Circulating tumor cell cultures for evaluation of anticancer treatment.* Science Advances, 2016. **2**(7).
122. Whiteside, T., *The tumor microenvironment and its role in promoting tumor growth.* Oncogene, 2008. **27**(45): p. 5904-5912.
123. Abate, A.R., J. Thiele, and D.A. Weitz, *One-step formation of multiple emulsions in microfluidics.* Lab on a Chip, 2011. **11**(2): p. 253-258.
124. Agresti, J.J., et al., *Ultrahigh-throughput screening in drop-based microfluidics for directed evolution.* Proceedings of the National Academy of Sciences, 2010. **107**(9): p. 4004-4009.
125. Kim, J., M.K. Chaudhury, and M.J. Owen, *Hydrophobic recovery of polydimethylsiloxane elastomer exposed to partial electrical discharge.* Journal of Colloid and Interface Science, 2000. **226**(2): p. 231-236.
126. Barnes, M.D., W.B. Whitten, and J.M. Ramsay, *Detecting single molecules in liquids.* Analytical Chemistry, 1995. **67**(13): p. 418A-423A.
127. Holtze, C., et al., *Biocompatible surfactants for water-in-fluorocarbon emulsions.* Lab on a Chip, 2008. **8**(10): p. 1632-1639.
128. Neve, R.M., et al., *A collection of breast cancer cell lines for the study of functionally distinct cancer subtypes.* Cancer cell, 2006. **10**(6): p. 515-527.
129. Gorges, T.M., et al., *Circulating tumour cells escape from EpCAM-based detection*

due to epithelial-to-mesenchymal transition. BMC cancer, 2012. **12**(1): p. 178.

130. Warkiani, M.E., et al., *Slanted spiral microfluidics for the ultra-fast, label-free isolation of circulating tumor cells.* Lab on a Chip, 2014. **14**(1): p. 128-137.
131. Brundula, V., et al., *Targeting leukocyte MMPs and transmigration.* Brain, 2002. **125**(6): p. 1297-1308.
132. Van den Steen, P.E., et al., *Gelatinase B/MMP‐9 and neutrophil collagenase/MMP‐8 process the chemokines human GCP‐2/CXCL6, ENA‐78/CXCL5 and mouse GCP‐2/LIX and modulate their physiological activities.* European Journal of Biochemistry, 2003. **270**(18): p. 3739-3749.
133. Provatopoulou, X., et al., *Circulating levels of matrix metalloproteinase-9 (MMP-9), neutrophil gelatinase-associated lipocalin (NGAL) and their complex MMP-9/NGAL in breast cancer disease.* BMC cancer, 2009. **9**(1): p. 390.
134. Hallett, R.M. and T. Chew, *Immune cell transcript modules reveal leukocyte heterogeneity in synovial biopsies of seronegative spondylarthropathy patients.* BMC musculoskeletal disorders, 2014. **15**(1): p. 446.
135. Shamamian, P., et al., *Activation of progelatinase A (MMP‐2) by neutrophil elastase, cathepsin G, and proteinase‐3: A role for inflammatory cells in tumor invasion and angiogenesis.* Journal of cellular physiology, 2001. **189**(2): p. 197-206.
136. Beyrau, M., J.V. Bodkin, and S. Nourshargh, *Neutrophil heterogeneity in health and disease: a revitalized avenue in inflammation and immunity.* Open biology, 2012. **2**(11): p. 120134.
137. Bain, B.J., *Diagnosis from the blood smear.* New England Journal of Medicine, 2005. **353**(5): p. 498-507.
138. Siena, S., et al., *Flow cytometry for clinical estimation of circulating hematopoietic progenitors for autologous transplantation in cancer patients.* Blood, 1991. **77**(2): p. 400-409.
139. Holmes, D., et al., *Leukocyte analysis and differentiation using high speed microfluidic single cell impedance cytometry.* Lab on a Chip, 2009. **9**(20): p. 2881-2889.
140. Han, X., et al., *Microfluidic Lysis of Human Blood for Leukocyte Analysis Using Single Cell Impedance Cytometry.* Analytical Chemistry, 2012. **84**(2): p. 1070-1075.
141. Chokkalingam, V., et al., *Probing cellular heterogeneity in cytokine-secreting immune cells using droplet-based microfluidics.* Lab on a Chip, 2013. **13**(24): p. 4740-4744.
142. Owen, C.A. and E.J. Campbell, *The cell biology of leukocyte-mediated proteolysis.* Journal of Leukocyte Biology, 1999. **65**(2): p. 137-150.
143. Bhagat, A.A.S., S.S. Kuntaegowdanahalli, and I. Papautsky, *Inertial microfluidics for continuous particle filtration and extraction.* Microfluidics and Nanofluidics, 2009. **7**(2): p. 217-226.
144. Mach, A.J. and D. Di Carlo, *Continuous scalable blood filtration device using inertial microfluidics.* Biotechnology and Bioengineering, 2010. **107**(2): p. 302-311.
145. Mach, A.J., et al., *Automated cellular sample preparation using a Centrifuge-on-a-Chip.* Lab on a Chip, 2011. **11**(17): p. 2827-2834.
146. Dudani, J.S., et al., *Rapid inertial solution exchange for enrichment and flow cytometric detection of microvesicles.* Biomicrofluidics, 2015. **9**(1): p. 014112.

147. Lee, H., L. Xu, and K.W. Oh, *Droplet-based microfluidic washing module for magnetic particle-based assays.* Biomicrofluidics, 2014. **8**(4): p. 044113.
148. Chen, Y., et al., *Microfluidic chemical processing with on-chip washing by deterministic lateral displacement arrays with separator walls.* Biomicrofluidics, 2015. **9**(5): p. 054105.
149. Khoo, B.L., et al., *Clinical validation of an ultra high-throughput spiral microfluidics for the detection and enrichment of viable circulating tumor cells.* PloS one, 2014. **9**(7): p. e99409.
150. Hunter, R.L., et al., *Poloxamer 188 inhibition of ischemia/reperfusion injury: evidence for a novel anti-adhesive mechanism.* Annals of Clinical & Laboratory Science, 2010. **40**(2): p. 115-125.
151. McGrath, J., M. Jimenez, and H. Bridle, *Deterministic lateral displacement for particle separation: a review.* Lab on a Chip, 2014. **14**(21): p. 4139-4158.
152. Zeming, K.K., S. Ranjan, and Y. Zhang, *Rotational separation of non-spherical bioparticles using I-shaped pillar arrays in a microfluidic device.* Nature communications, 2013. **4**: p. 1625.
153. Zeming, K.K., et al., *Asymmetrical Deterministic Lateral Displacement Gaps for Dual Functions of Enhanced Separation and Throughput of Red Blood Cells.* Scientific reports, 2016. **6**.
154. Karabacak, N.M., et al., *Microfluidic, marker-free isolation of circulating tumor cells from blood samples.* Nature protocols, 2014. **9**(3): p. 694-710.
155. Downey, G.P., et al., *Retention of leukocytes in capillaries: role of cell size and deformability.* Journal of Applied Physiology, 1990. **69**(5): p. 1767-1778.
156. Brown, M. and C. Wittwer, *Flow cytometry: principles and clinical applications in hematology.* Clinical chemistry, 2000. **46**(8): p. 1221-1229.
157. Prikk, K., et al., *In vivo collagenase‐2 (MMP‐8) expression by human bronchial epithelial cells and monocytes/macrophages in bronchiectasis.* The Journal of pathology, 2001. **194**(2): p. 232-238.
158. Kang, D.-K., et al., *Rapid detection of single bacteria in unprocessed blood using Integrated Comprehensive Droplet Digital Detection.* Nat Commun, 2014. **5**.